XUROGRAPHIC MICROWIRE INTEGRATION TECHNIQUE FOR LAB ON CHIP APPLICATIONS

XUROGRAPHIC MICROWIRE INTEGRATION TECHNIQUE FOR LAB ON CHIP APPLICATIONS

By JUNCONG LIU

B.Eng. (Xi'an Jiaotong University, Shaanxi, P.R. China)

A Thesis Submitted to the School of Graduate Studies in Partial Fulfilment of the Requirements for the Degree Master of Applied Science

McMaster University	MASTER OF APPLIED SCIENCE (2016)
Hamilton, Ontario (History)	Mechanical Engineering
TITLE:	XUROGRAPHIC MICROWIRE INTEGRATION TECHNIQUE FOR LAB ON CHIP APPLICATIONS
AUTHOR:	JUNCONG LIU, B.Eng.
Supervisor	Professor P. R. Selvaganapathy Department of Mechanical Engineering
NUMBER OF PAGES	xviii, 141

ABSTRACT

Many functions in a lab-on-a-chip device such as heating, electrochemical sensing and electrophoresis require integration of microelectrodes. However, conventional techniques for microelectrode integration are either requiring expensive facilities, cleanroom environment or insufficient in resolution and microelectrode thickness. Microwires have also been integrated into LOC devices as microelectrodes. They are commercially available in a diversity of material. and diameter, with industrial production standard and mechanical strength comparable to bulk metal, which make them ideal candidate for microelectrode. Nonetheless a technique to integrate these microwires into complicated microelectrode patterns has not yet been developed. In this thesis, two microwire integration techniques based on xurography are developed for elastomer and rigid polymer. Copper, silver, platinum, carbon and Ni-Cr alloy microwires down to 15 μm with minimum spacing of 150 μm and controllable position in the height direction are successfully integrated. The microwire electrode can also be suspended in the middle of the microchannel with desired length and angle. Various applications are presented to demonstrate the versatility of the xurographic microwire integration process.

ACKNOWLEDGEMENT

First, I would like to appreciate my supervisor Professor Ponnambalam Ravi Selvaganapathy, for his trust and support throughout these 2 years. He encouraged me to come up with my own research idea, and unconditionally supported me with his expertise. He generously spared his time for discussion about this research, gave me enough freedom to try new ideas and offered advices whenever I needed. It is his professional and inspiring guidance that made it possible for me to complete this research.

I also want to thank Professor James B. Mahony for supporting this research and sparing time in his busy schedule to set up meeting with us. Dr. Chan Y. Ching who give me support and suggestions and pushing me forward with his sense of humor also deserve my appreciation. My appreciation also goes to all the committee members: Dr. Howlader, Dr. Mahony and Dr. Ravi for their valuable time, especially in the busy end of the year.

I thank my fellow labmates in Center for Advanced Micro-Electro-Fluidics: Dr. Leo Hsu, Dr. Dingsheng Liu, Dr. Kamrul Russel, Dr. Aditya Aryasomayajula, Reza, Jun Yang, Ali, Rana, Shubham, Pankaj, Aliakbar, Harpreet, Sondos, Shayan, Mohammadhossein, Michael, Melizeth, Celine. They are all very nice friends who gave me many advices and help with this research and my life. A very special thanks goes to Dr. Leo Hsu, who helped me with the electrochemical experiments with his expertise in electrochemistry and introduced me with many of his friends in different departments to help me with other problems I met.

I must also acknowledge Professor Jun Yang in Western University, Professor Feng Xu and Dr. Guoyou Huang in Xi'an Jiaotong University. My past research experience under their supervision sure contributes to the successful completion of this research. Their patient guidance is and will always be a treasure for my lifetime.

Last but not least, I have to thank my wife, the love of my life, Zhongwen Zhou, who sacrificed so much to come to Canada to be with me. Her unconditionally support and love are the inner power that have been driving me to go forward. Her accompany made my life in these 2 years beautiful and memorable. I am very grateful for the perfect gift she gave me: the lovely boy Peyton. The little new member brings so much joy and happiness to the family. My sincere gratitude also goes to my parents who support me to pursue my dream far away from them. This thesis is dedicated to my wife, my son and my parents, for their unconditional love for me.

TABLE OF CONTENTS

LIST OF FIGURES

LIST OF TABLES

LIST OF ALL ABBREVIATIONS

AC	alternating current
DI water	deionized water
LOC	lab on a chip
ICEO	induced charged electro-osmosis
ITO	indium tin oxide
LED	light-emitting diode
PC	polycarbonate
PCR	polymerase chain reaction
PDMS	polydimethylsiloxane
PE	polyethylene
PET	polyethylene terephthalate
PMMA	poly (methyl methacrylate)

PSA	pressure sensitive adhesive
PVD	physical vapor deposition
SEM	scanning electron microscope
TAS	total analysis system

Chapter 1: Introduction

1.1 Motivation

Lab-on-a-chip (LOC) technology was developed in 1970s with the aim to miniaturized chemical and biological analytical assays [1, 2]. A complete analytical assay normally involves many different functions such as temperature control, transportation, separation, extraction, mixing, detection, etc. Electrodes plays an important role in many of these functions, e.g. electrical heater and electrochemical cells. Miniaturization of these analytical assays also necessitates the integration of microelectrodes into the miniaturized LOC devices. However, existing microelectrode fabrication processes are either expensive, time-consuming, labor intensive, low resolution, or deposit thick films. Many of these techniques also require photolithography to pattern the microelectrode. These problems can be overcome if a technique is developed that is capable of integrating microwires as microelectrodes. Microwires are commercially available in various material and ultrafine dimension with industrial production standard. Successful integration of these microwires can eliminate the necessity to fabricate the microelectrodes, i.e. no expensive deposition and lithography process is needed. However, conventional techniques can only control the position of a straight microwire electrode in a LOC device and the integration process is tricky [3-5]. In this thesis, two different integration techniques based on xurography were developed that could efficiently integrate these microwire electrodes into LOC devices made of different polymer materials. The first integration technique was designed for an elastomer such as Polydimethylsiloxane (PDMS). The second integration technique is more general and applicable to most of the polymer materials. Microelectrodes down to 15 μm in diameter has been integrated successfully with positional resolution up to 150 μm using a low-cost cutting plotter. The microwire electrodes can also be suspended in the microchannel, which can bring advantageous features that other microelectrode integration techniques are lack of.

1.2 Organization

This thesis is organized as follows:

Chapter 2 covers the history of LOC, the role of microelectrodes and the current methods used for LOC microelectrode fabrication. The microelectrode fabrication techniques are classified as physical methods and chemical methods according to whether the metal is deposited physically or chemically. The history and applications of xurography is also briefly reviewed.

Chapter 3 describes a xurographic process for microwire electrode integration into elastomers. Characterization of the integration process is presented together with several application examples. Advantages and disadvantages of this process are discussed.

Chapter 4 introduces another xurographic process for microwire integration for most of the polymer materials based on adhesive bonding. Characterization and application examples are included.

Chapter 5 concludes the thesis with a brief discussion on the contribution made in this thesis and a summary of the main results. The advantages of the microwire integration techniques developed here over existing methods are highlighted. Their limitations are pointed out together with aspects to be improved.

1.3 Contributions

The contributions made in this thesis are as follows:

1.3.1 Establishment of low-cost microelectrode integration process

Most of the microelectrode integration techniques include deposition of metal microstructures by either physical vapor deposition (PVD), nanoparticle sintering, chemically reduction of metal cations, etc. These processes require extra equipment or chemicals and some of these process are not compatible with some polymers. Microwire electrodes, in contrast, can be implemented directly into the LOC devices. Neither pretreatment or metal deposition process is needed.

Fabrication of microelectrodes with feature size within 100 μm normally relies on photolithography or other high precision machining techniques, e.g. laser scanning. These techniques require either cleanroom working condition or costly equipment. Microwires of various diameters are commercially available. Microwires as small as about 12 micrometers in diameter can be acquired from the market (e.g. from Alfa Aesar Co., Inc.). Direct implementation of these ultrafine microwires also avoids the necessity of these microfabrication techniques.

1.3.2 All-in-one xurographic process

Xurography was developed for low-cost microfabrication of polymeric LOC devices by mechanical cutting [6-9]. The microwire integration process developed in this thesis makes it possible to fabricate polymeric LOC devices with integrated microelectrodes with a low-cost cutting plotter. With these modified xurographic techniques, LOC technology can be more affordable and accessible to all the laboratories.

1.3.3 Suspended microelectrode

Integration of suspended microelectrodes in microchannel has been demonstrated for the first time. Most of the microelectrode integration techniques are to fabricate microelectrodes at the bottom or on the side wall of the microchannel. The integration of suspended microelectrodes goes beyond these two formats and can be very useful for some LOC applications, e.g. electrokinetic mixing, cell capture.

Chapter 2: LITERATURE REVIEW

2.1 Lab on a chip

In a chemical laboratory, a typical chemical analysis consists of a series of necessary steps such as sampling, sample transport, mixing, dilution, separation, filtration, chemical reactions, staining and detection. These steps were conventionally operated by a qualified technician with many stand alone apparatus. Even though accurate and reproducible, these steps are time-consuming and labor-intensive. The total volume of the equipment used is also considerable.

Total analysis system (TAS) is a device that automates all the analytical steps in a continuous flow stream. Continuous analysis is important for many applications such as environmental monitoring [10] and clinical diagnostics [11]. However, the large volume of the system, slow sample transportation, insufficient separation efficiency and considerable consumption of reagents of TAS necessitate the miniaturization of these systems.

The first practice of miniaturization of TAS was a gas chromatographic air analyzer with thermal conductivity sensor fabricated on silicon in 1975 [1, 2]. However, these early silicon chip analyzers didn't capture the attention and interest of the research community and industry immediately. Instead, it stimulated research on the miniaturization of components such as micropumps [12] and microvalves [13] on silicon. It was only in the early 1990's that a similar chip based total analysis system for liquid chromatography was also miniaturized on silicon [14]. this development also led to the establishment of the concept of "miniaturized total chemical analysis system" [15], which is also called LOC.

The early LOC devices were fabricated on silicon and glass by standard lithographic and micromachining techniques used in semiconductor manufacturing. The fabrication process for these materials is costly, slow and tedious, involving cleanroom facilities and complicated bonding techniques. Subsequently, polymers were investigated as alternative materials as they are lower in cost, come with a wide variety of chemical properties and have been used in many biochemical assays. The early polymeric LOC devices were created by wire imprinting [16], laser machining [17] and injection molding [18] and casting [19]. Among the wide variety of polymers investigated, PDMS has many attractive features such as low-cost, elasticity, high optical transparency, gas permeability and biocompatibility. For a long time PDMS was mainly used to replicate microstructures for soft lithography [20]. Not until 1997 was it used for the first time to replicate microchannels from an etched silicon wafer master [19]. The PDMS slabs were simply stacked together with weak bonding. A year later, an rapid prototyping technique for PDMS microfluidic devices was developed to replicate microfluidic channels from photoresist master mold [21]. The PDMS slabs were irreversibly bonded together to a robust microfluidic device by plasma oxidation. The technique was widely used in many applications because of its easy and fast fabrication process and is still widely used today.

Besides the fabrication of the microfluidic channels, integrated metallic components are also indispensable for many LOC applications. For instance, metallic components has been integrated as heating elements for temperature control [22], electrodes for capillary electrophoresis [18, 19, 23] or electrodes for on-chip detection [14, 24, 25].

Microelectrodes in the early silicon/glass devices were normally deposited by thin film technologies such as PVD [1, 2] and plating [26, 27], which are conventionally used in semiconductor manufacturing. However, expensive equipment, tedious process and long deposition time are required for PVD. Electroplating and electroless plating, in contrast, require simple or no equipment to deposit metals. However, electroplating cannot be used to deposit metal directly on polymer substrate and high resolution lithography techniques such as photolithography in cleanroom facilities are needed to selectively deposit metal layer [28] or catalytic layer [29] for plating. Alternatively, microelectrodes can be formed on polymer substrate by sintering selectively deposited conductive nanoparticles [30, 31]. They are less expensive but the resolution of microelectrode pattern and the thickness is too low. These planar microelectrodes are also fragile and can be easily cracked. Microelectrode with good mechanical property can be formed by casting low melting point alloy and conductive polymer composite in fabricated microchannel [32-35] but material choices are limited. Photolithography is also required. Microwires are promising candidates for microelectrode integration which can be used directly without additional fabrication process [24, 36]. The performance of these microwires are also strictly controlled under industrial standard. However, an efficient technique to integrate these microwires into polymer LOC devices is still needed.

2.2 Microelectrode fabrication techniques

2.2.1 Physical vapor deposition (PVD)

PVD is a vacuum deposition technique used to fabricate thin films. The PVD process is shown in Figure 2.1. The target (source material) is sputtered or evaporated to gas phase (Figure 2.1a), transported to the substrate (Figure 2.1b) and then deposited on the substrate (Figure 2.1c). The thickness of the thin film microelectrode can be as thin as several nanometer [37] to several micrometers [38]. Together with photolithography, the minimum feature size of the microelectrode pattern can reach 1 μm. In principle, any material, including chemical elements such as gold, silver, platinum, alloys such as Ni-Cr and compounds such as indium tin oxide can be deposited on any substrate.

Physical vapor deposition has been used in the early LOC device to deposit, for instance, a nickel film resistor sensor on silicon wafer [2]. The nickel film electrode was exposed to a gas sample to measure the thermal conductivity of the gas for gas chromatography. Other application examples include microheaters for on-chip Polymerase chain reaction (PCR) [39] thermally responsive polymer microvalve [22], electrochemical sensors for pathogen DNA detection [40], nitrate detection in freshwater [41] and cell culture monitoring [42], electrokinetic micropumps [43], acoustic micropumps [44].

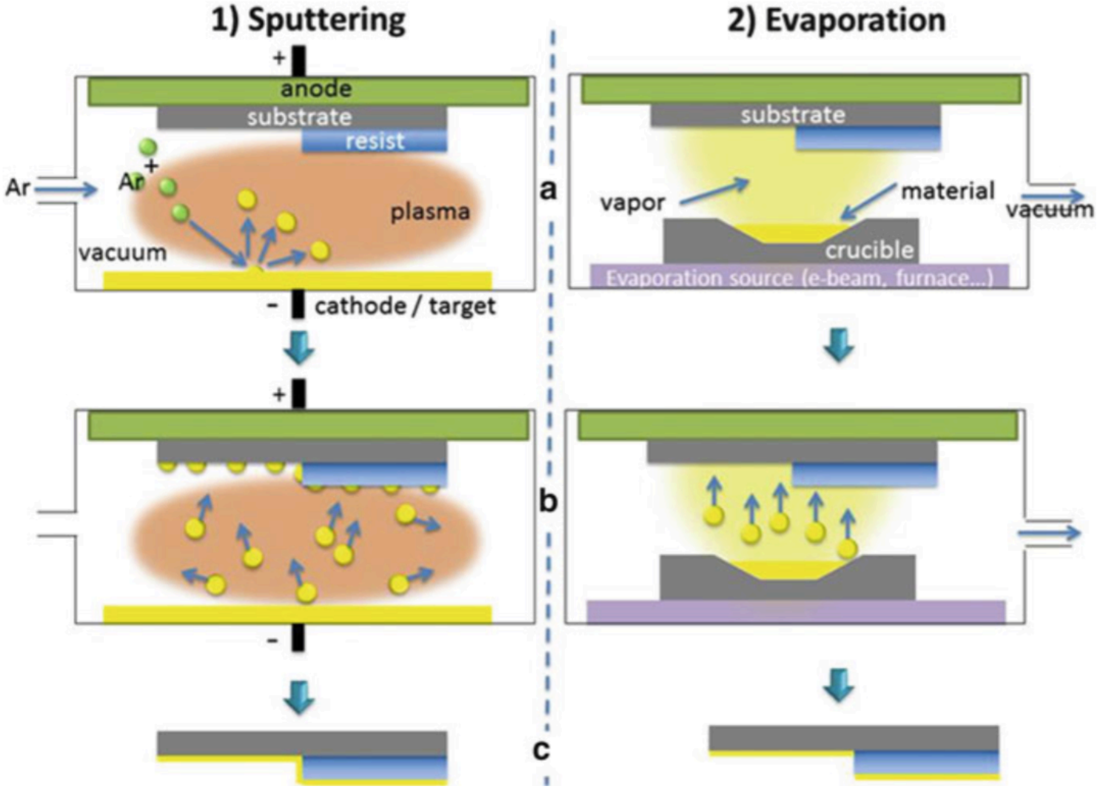

Figure 2.1 Schematic of physical vapor deposition process 1) Sputtering. 2) Evaporation. [45]

Advantages of PVD combined with lithography include its capacity to deposit ultrathin films and high resolution microelectrode pattern. A variety of materials can be deposited with high purity and uniform thickness. The PVD process is also clean compared to plating.

The most significant disadvantage of PVD, however, is the expensive equipment containing high energy source for heating or sputtering the target, vacuum chamber and turbopump for high vacuum. The deposition process is also time-consuming, tedious and experienced operation is required to ensure the repeatable thickness of the deposited metal films.

Besides, the microelectrodes are normally patterned by photolithography, which requires cleanroom facilities. Moreover, utilization of PVD for microelectrode fabrication on polymers is limited by the low adhesion between polymer and metal as well as the incompatibility of photolithography with some polymers due to solvents and temperatures used in the photolithographic process. Microstenciling (shadow masking) [46] and microstamping [47] are alternative techniques to pattern microelectrode deposited though PVD but the fabrication of the stencil and stamp is expensive and complicated. Photomask can also be xurographically patterned [6] but the resolution of xurography is much lower than photolithography. The deposited thin film is also brittle and can be easily buckled or cracked.

2.2.2 Electroplating

Electroplating is an electrochemical process in the electrolysis process used to coat metal on objects driven by external direct current. The substrate is usually made as the cathode and driven by external direct current, metal cations in the precursor are reduced and deposited on the cathode. An example of electroplating used in microelectrode fabrication is shown in Figure 2.2. The glass was first patterned with a base platinum layer by PVD combined with photolithography (Figure 2.2.a) Then resist layers was laminated (Figure

2.2.b) on top and patterned (Figure 2.2.c) to form microstructures and the channel walls. A silver microelectrode layer was then electroplated on the platinum layer in a silver-plating bath (Figure 2.2.d). The device with integrated microelectrode was then sealed with another glass wafer (Figure 2.2.e) and diced (Figure 2.2.f). Thin film of thickness of tens of nm can be plated by correctly controlling the electroplating parameters. For electrical application, electroplating is mainly used to deposit metallic films with thickness from several hundreds of nm to 100 μm [48]. The resolution of the microelectrode can also be patterned by photolithography with feature size down to 1 μm. Up to 31 metals and their alloys can be electroplated on conductive substrate [49]. It was used to deposit thick microelectrodes such as sidewall electrodes for cell lysis [26], dielectrophoresis [28], permalloy for magnetic bead separation [50] and microcoils for magnetic particle trapping[51].

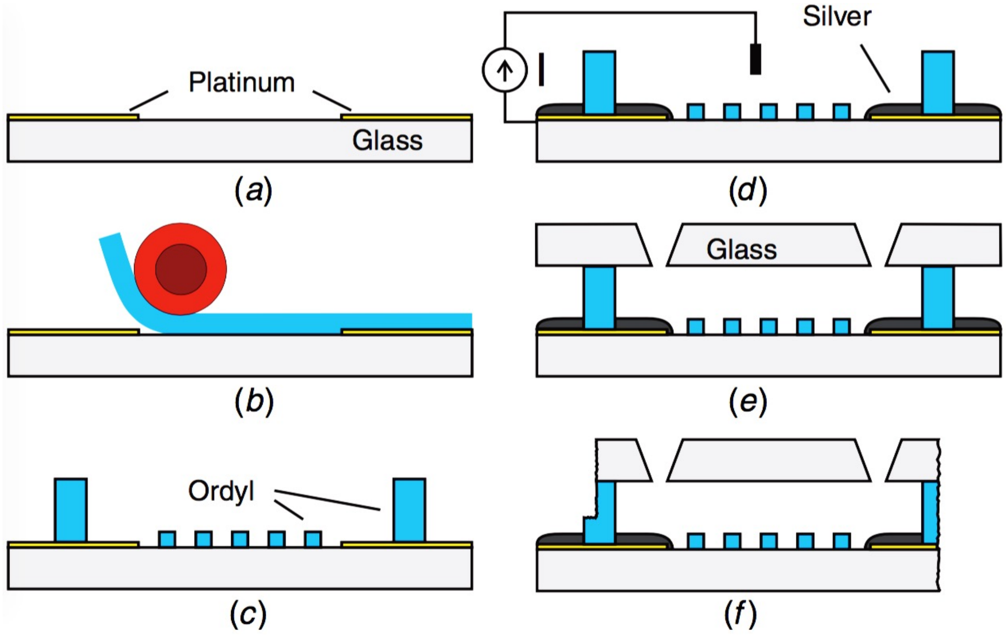

Figure 2.2 An example of electroplating microelectrodes for microfluidic chips. [52]

The main advantages of electroplating are the low cost and high deposition rate. The only equipment required for electroplating is the external power source and electrodes, compared to the expensive facilities required for PVD. The deposition rate of electroplating is also higher than PVD, therefore it is usually used to deposit thick microelectrodes.

However, the object to be electroplated has to be conductive while most of the materials used for LOC devices are nonconductive. To electroplate microelectrode on polymers, a thin conductive layer has to be coated on the object by PVD or electroless plating is performed first, therefore electroplating alone cannot be used to deposit microelectrodes for LOC devices. It should also be noted that when multiple microelectrodes are to be fabricated on the same substrate, all the microelectrodes have to be connected to the cathode which would require complicated network of electrical contacts. Moreover, the thickness of the electroplated microelectrodes is influenced by the resist pattern. The current density tends to be higher in regions densely coated with photoresist which results in thicker electrodeposit. Finally, the electroplating waste containing heavy metals, acids, cyanides and nitrides would also cause severe pollution to the environment [53].

2.2.3 Electroless plating

Electroless plating is another plating technology that deposit metallic films through an autocatalytic reaction. The electroless plating is first initialized by the catalytic layer coated on the object. Once the metal start to be deposited on the object, the electroless plating is catalyzed by the deposited metal itself. Thin film of thickness of tens of nm can be plated by correctly controlling the electroplating parameters. For electrical application, electroplating is mainly used to deposit metallic films with thickness from about hundreds of nm to 100 μm [48]. The minimum feature size is dependent on the lithography used, which can be 1 μm with photolithography. Electroless plating has been applied to fabrication of microelectrodes for electrochemical sensing [54-56], electrowetting [57], microthermocouple [58] and dielectrophoresis [59].

Compared to the PVD and electroplating, electroless plating is simple without external power, electrical contact and any other special equipment. Moreover, metal microelectrodes can be electroless plated on nonconductive materials, i.e. glass and polymers which cannot be electroplated directly. The thickness of the electroless-plated microelectrode is also more uniform than that of electroplated microelectrodes, regardless of the geometry of the object to be plated.

However, electroless plating also comes with many drawbacks. First, the nonconductive material has to be coated with a catalytic layer to initialize the plating process. The catalytic layer can be either palladium or poly (dopamine) [60]. Secondly, the catalytic layer has to be patterned by high resolution lithography methods. Thirdly, numerous parameters need be carefully controlled (e.g. plating time, temperature, electroless plating bath composition) to obtain uniform outcome. The deposition rate is also slow compared to electroplating. A comparison of deposition rate, pressure and temperature between PVD, electroplating and electroless plating is listed in Table 1.

Table 1 Comparison of physical vapor deposition and plating

Deposition technique	Pressure (Torr)	Substrate temperature (°C)	Deposition rate (µm/min)
Evaporation	10^{-7} - 10^{-5}	50-100	0.006-0.12
Sputtering	10^{-3} - 10^{-1}	~200	~0.6
Electroplating	Ambient	10-100	0.4-180
Electroless plating	ambient	15-100	0.5-2

2.2.4 Nanoparticle sintering

Nanoparticle sintering includes all the techniques that form microelectrodes by sintering nanoparticles deposited on the substrate. The melting point of these nanoparticles is reduced greatly with the decreased particle size [61]. The nanoparticles were prepared in a solvent that prevents them from aggregation. These prepared nanoparticle inks were selectively patterned on the substrate by drop-on-demand inkjet printing [62, 63] or screen printing [64, 65]. The deposited ink was then dried and sintered by oven/hot-plate [31], microwave [66], laser [67], high intensity flash light [68], plasma [69], direct current [70], or chemical destabilizer [71]. A micrograph of inkjet printed silver lines on PDMS surface is shown in Figure 2.3. Microelectrodes with thickness from several micrometer to hundreds of micrometers can be deposited. Different types of conductive inks are commercially available including gold, silver, copper, platinum, indium tin oxide (ITO), titanium dioxide, zin dioxide, carbon nanotube, graphene. Application examples are electrochemical electrodes for immunoassay [65] and glucose sensing, heaters for microreactor [72], piezoelectric actuator for micropumps [73], dielectrophoresis for cell separation [74] and microbead manipulation [75, 76], etc.

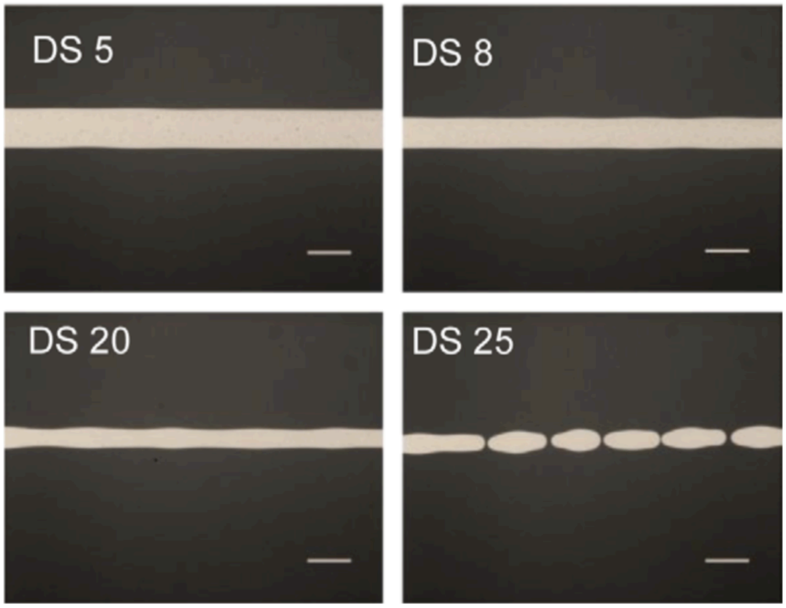

Figure 2.3 Silver line printed on PDMS with different droplet spacing (DS). Scale bar = 100 µm. [75]

An obvious advantage of this technique is the fast fabrication process compared to PVD, electroplating and electroless plating. Inkjet printers and screen printing machines are also more affordable than PVD machines and cleanroom facilities. Furthermore, the nanoparticles can be sintered on polymer surface directly by special sintering process developed to reduced the heat dissipated to the bulk material microwave or lower the sintering temperature [66-71]. The conductivity of these microelectrodes can reach up to 41% of the conductivity of bulk metal [77]. The usage of material is also more efficient.

However, the resolution of these printed microelectrodes is typically around 100 μm. The minimum thickness of several μm of these microelectrodes also make it difficult to be bonded to other polymeric substrate reliably. Moreover, the microelectrode film sintered on polymeric substrate are easily cracked due to the thermal expansion of polymer (Figure 2.4) or bending. The diversity of nanoparticles inks is limited. There is also a growing concern about the environmental and health impact of nanoparticles.

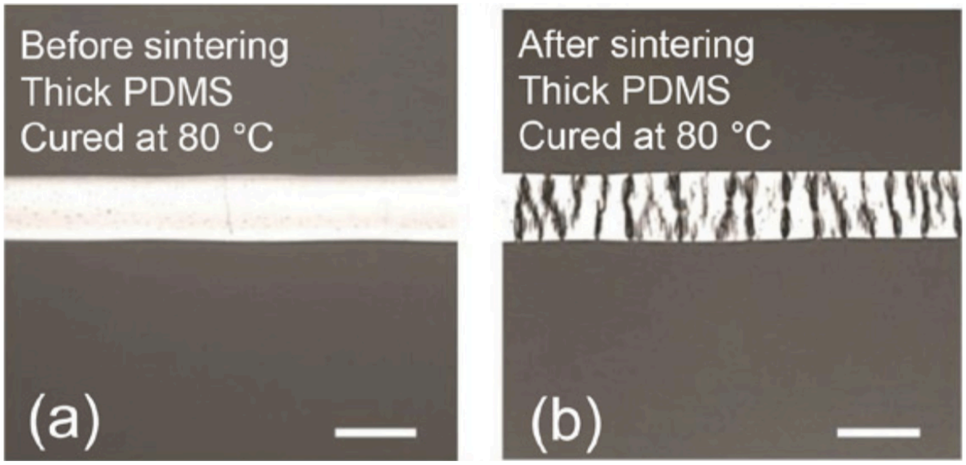

Figure 2.4 Cracking of printed silver microelectrode on PDMS due to thermal expansion of PDMS. Scale bar = 100 μm. [75]

2.2.5 Low melting point alloy casting

The melting point of some alloys containing gallium and indium are lower than 200 °C. The melt alloy can be easily injected or casted. The fabrication of microelectrodes by low melting point alloy casting includes fabrication of electrode microchannel, injection of melted low melting point alloy into the microchannel. The injected low melting point metal is then casted by cooling down or stabilized by formation of an oxide layer. A typical fabrication process is shown in Figure 2.5. The photoresist master mold with the designed microelectrode pattern was fabricated on silicon wafer by standard photolithography. The microelectrode patterned was then replicated to PDMS microchannel and inlet/outlet holes were punched on it. A closed microelectrode channel was form after plasma bonding the

PDMS microchannel to another flat PDMS plate. The microelectrode was fabricated by injecting melted solder (low melting point alloy) into the closed microelectrode channel and cooled down. It can be used to fabricate microelectrodes with feature size as small as 10 μm, depending on the dimension of the microchannel. It has been used to fabricate electromagnets for manipulation of superparamagnetic beads [32], dielectrophoresis device for droplet microfluidics [78-80] and particle sorting [81], micro-oulter counter for particle counting [82], electrical stimulation and response recording of neuron [83] and electrohydrodynamic mixer [84].

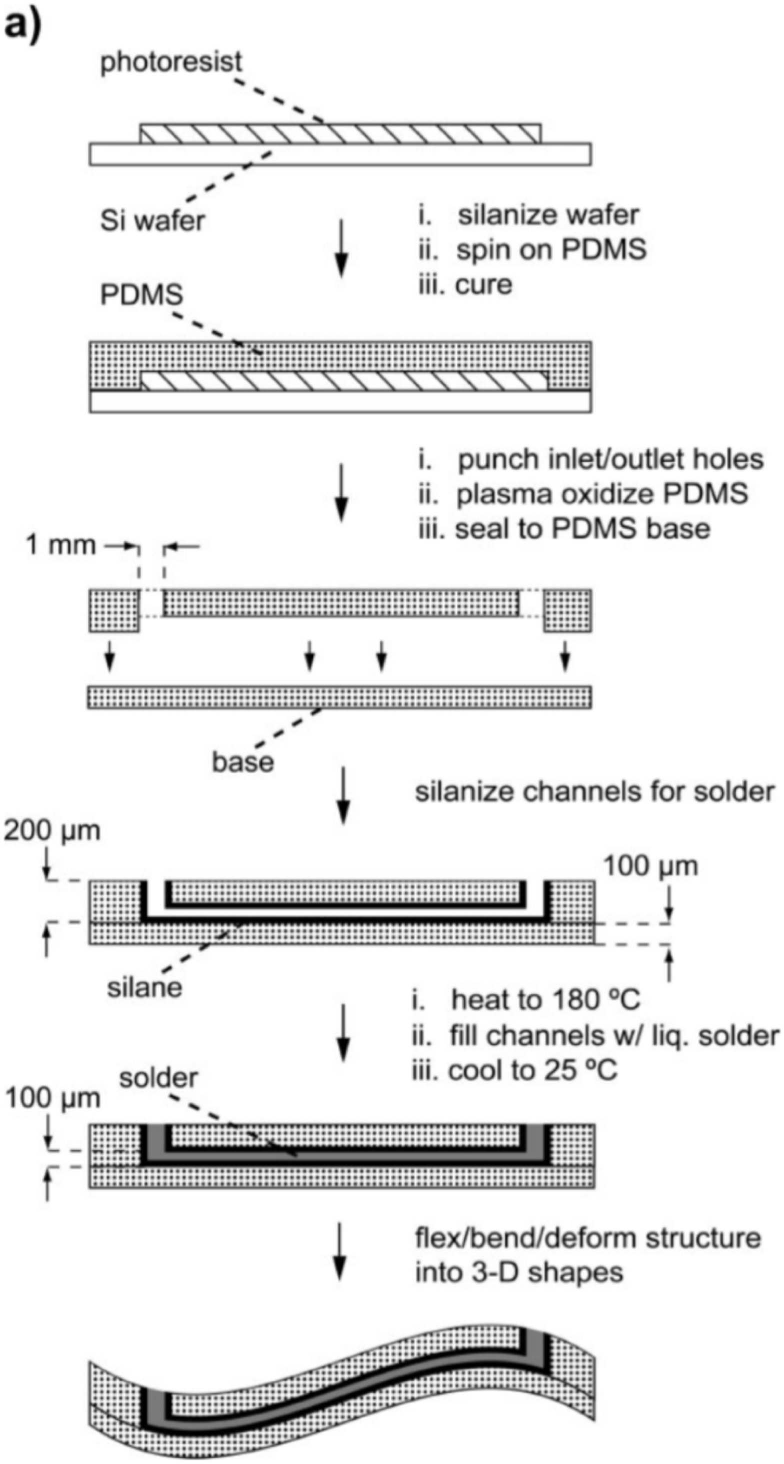

Figure 2.5 Microelectrode fabrication process by low melting point alloy casting

The most significant advantage of this technique is the capability to integrate complicated 3D metallic microelectrodes by injecting low melting point alloys into 3D microfluidic channels. As the electrode microchannel was fabricated together with the fluidic microchannel, the microelectrode is pre-aligned with the fluidic microchannel. Sidewall microelectrodes can be easily integrated even for microchannel with height of several hundred micrometers, which would be difficult or impossible for other microelectrode integration techniques.

However, most of the low melting point alloys are alloy of gallium and indium and common materials such as gold, silver, platinum cannot be integrated with this technique. The casted low melting point microelectrodes are not suitable for application under temperature higher than their melting point. Moreover, the thickness of the microelectrode is normally the same with the fluidic channel and it is integrated into the sidewall of the fluidic channel and the dimension of the microelectrode pattern relies on photolithography. In addition, low melting point alloy casting is a post processing technique and the injection of alloy is completed manually, which is not a scalable process.

2.2.6 Conductive polymer nanocomposite

Conductive polymer composite is polymer that is mixed with conductive filler. These composites are conductive once the concentration of the filler reaches the percolation threshold [85]. These composites can be integrated into polymeric LOC devices by similar technique with low melting point alloy casting [86], photolithography [87] or microcontact printing [88]. Dimension of the microelectrode pattern can be as small as 10 μm for PDMS-based composite patterned by photolithography and 3D microelectrode can also be fabricated [89]. Carbon black, carbon nanotube, silver nanoparticles are commonly used as fillers. It has been used to fabricate microelectrodes for electrokinetic manipulation of particles/cells [87], electrochemical sensing [35, 90], electrical stimulation on cells [86], pressure sensors [88, 91].

One of the attractive advantages of conductive polymer nanocomposite is its mechanical property. The film microelectrodes fabricated in other methods are fragile and cracked easily, especially considering the different mechanical property between the bulk polymer and the integrated metallic film. The conductive polymer nanocomposite maintains the good mechanical property of the polymer, making these microelectrodes more robust. Even elastic microelectrodes can be made by filling conductive nanoparticles into PDMS.

However, the microelectrode material is limited to polymer with several available fillers and the conductivity of these conductive polymer composites is much lower than the bulk conductive material. Moreover, photolithography is needed to pattern these conductive polymer nanocomposites.

2.2.7 Microwire integration

Microwires had been used as microelectrode in LOC devices for a long time. The microwires were first used directly by simply immersed into the reservoir (Figure 2.6). Alternatively, an electrode microchannel with the same size with the microwire was prefabricated together with the microfluidic channels to better position the microwire electrode in the LOC devices, (Figure 2.7). The microwire electrode was then fitted into the electrode microchannel followed by device bonding. These microwires are commercially available with diameter down to 4 μm. Various materials are available in microwire form, including gold, silver, copper, platinum, aluminum, stainless steel, palladium, Ni-Cr alloy, to name but a few (Table 2). These microwire electrodes has been used for dielectrophoresis [19], electrochemical detection [3-5, 25, 92-95], electroporation [96], etc.

Table 2 List of some suppliers for microwire products

Supplier	Products
Alfa Aesar	A wide range of microwires of different element, alloy, carbon, etc. Diameter ranges from 10 µm to 2 mm.
Luma Metall	Tungsten, rhenium, molybdenum, gold, silver, brass, stainless steel bare and plated microwires. Diameters ranges from 4 µm to 500 µm.
CALIFORNIA FINE WIRE CO.	A wide range of round, flat, electroplated, insulated microwires of pure elements or alloys. Diameter ranges from 10 µm to 1 mm. Flat microwire with thickness from 5 µm to 1.27 mm and width from 50 µm to 2.54 mm.
Ulbrich Stainless Steels & Special Metals, Inc.	Round, square and flat shaped microwires of stainless steel, titanium, nickel, cobalt, nitinol, carbon steel, brass, bronze, aluminum, etc. Round microwire diameter ranges from 19 µm to 10 mm. Flat microwire with thickness from 5 µm to 5 mm and width from 50 µm to 50 mm.
Heraeus Electronics	Gold, silver, aluminum, copper, palladium, platinum microwires for wire bonding. Diameter up to 15 µm.

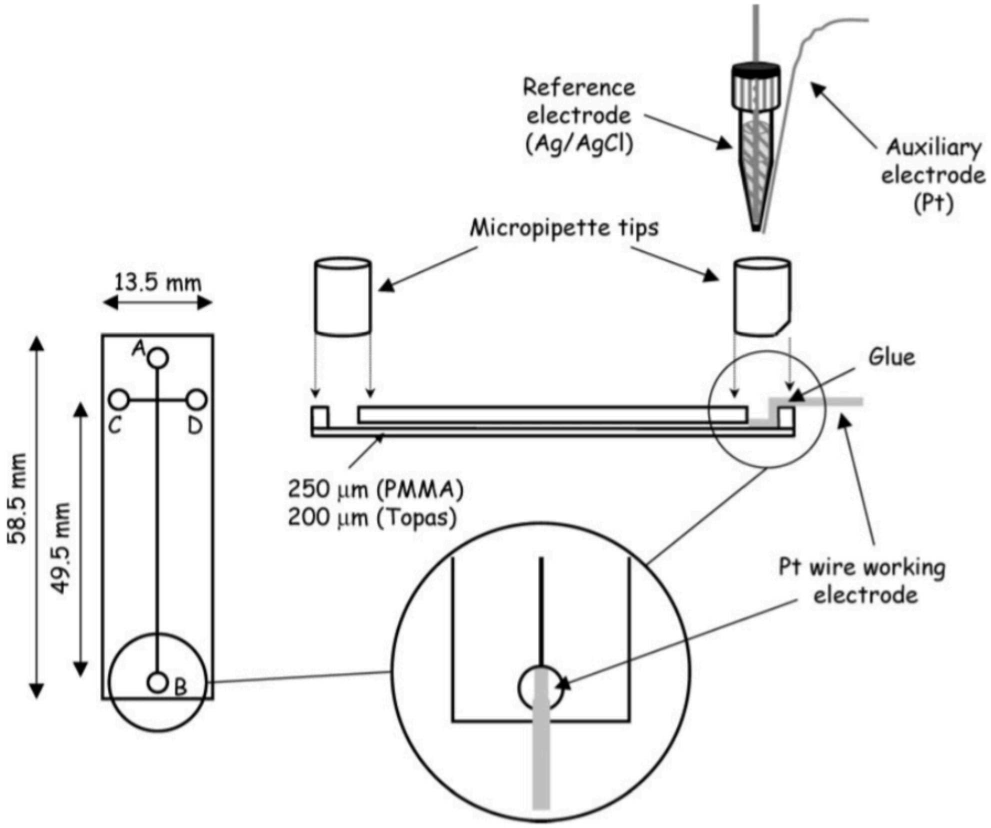

Figure 2.6 A capillary electrophoresis microchip with integrated microwire electrochemical sensor. [92]

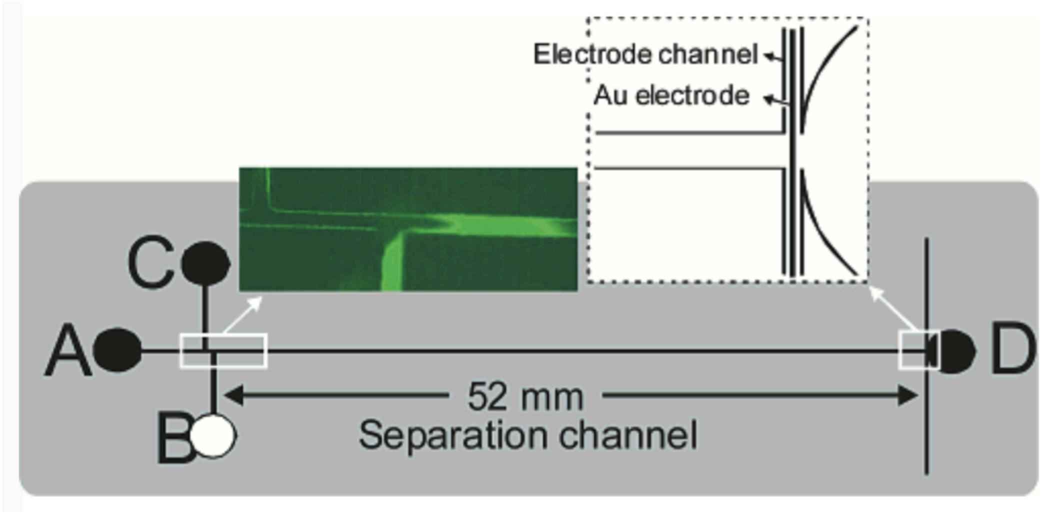

Figure 2.7 A capillary electrophoresis chip with integrated microwire electrode in an electrode channel. [4]

Implementation of microwires as microelectrodes for LOC application has a number of advantages. Firstly, these microwires are commonly used to build interconnection between semiconductor devices and integrated circuits by wire bonding. To ensure high quality of the interconnection, the diameter of these microwires is tightly controlled. For example, the production tolerance of gold microwire diameter is +/-3% [97]. Moreover, these microwires are manufactured by wire drawing followed by annealing and their tensile strength is comparable to the bulk metal. Secondly, microwires from 12 μm to several hundred micrometers, with numerous material choices are commercially available. Thirdly, by direct implementation of these high quality microwires, no other microfabrication technique is required and greatly reduce the cost for microelectrode integration.

However, an efficient microwire electrode integration method is still needed. The position of the microwire electrode has been precisely controlled by fitting the microwire into prefabricated electrode microchannel as previously described. However, the fitting of the microwire electrode into the electrode microchannel is manual and difficult because of the small size of the microwire and the microchannel. Moreover, it is not a scalable process and integration of multiple electrodes with curves or bends will be difficult as the wires tend to pop out of the channels/grooves when bent.

2.3 Xurography: low-cost rapid prototyping

Xurography, is also called razor cutting, is a rapid prototyping technique using cutting plotters [6]. A typical xurographic process for microfabrication is shown in Figure 2.8: 1) First, adhesive films are patterned by the cutting plotter. 2) Next, the unwanted areas are removed. 3) Subsequently, application tape is applied on the remaining pattern. 4) The remaining pattern is then peeled off by the application tape. 5) Next, the pattern on the application tape is transferred to the desired substrate. 6) Finally, the the application tape is removed leaving the pattern on the substrate. The cutting plotter was used to fabricate microfluidic channel on polymer film [6-9], bulk polymer [98, 99], glass [100] and heat-shrink film [101]. Minimum feature size that can be obtained from xurographically patterned polymer film is 18 μm [6]. Xurography has been used to fabricate polymer diffusion-based gradient generator [9, 102], cell culture devices [9, 99], centrifugal solid extraction devices [103], centrifugal PCR devices [104], electrophoresis chip [100], etc.

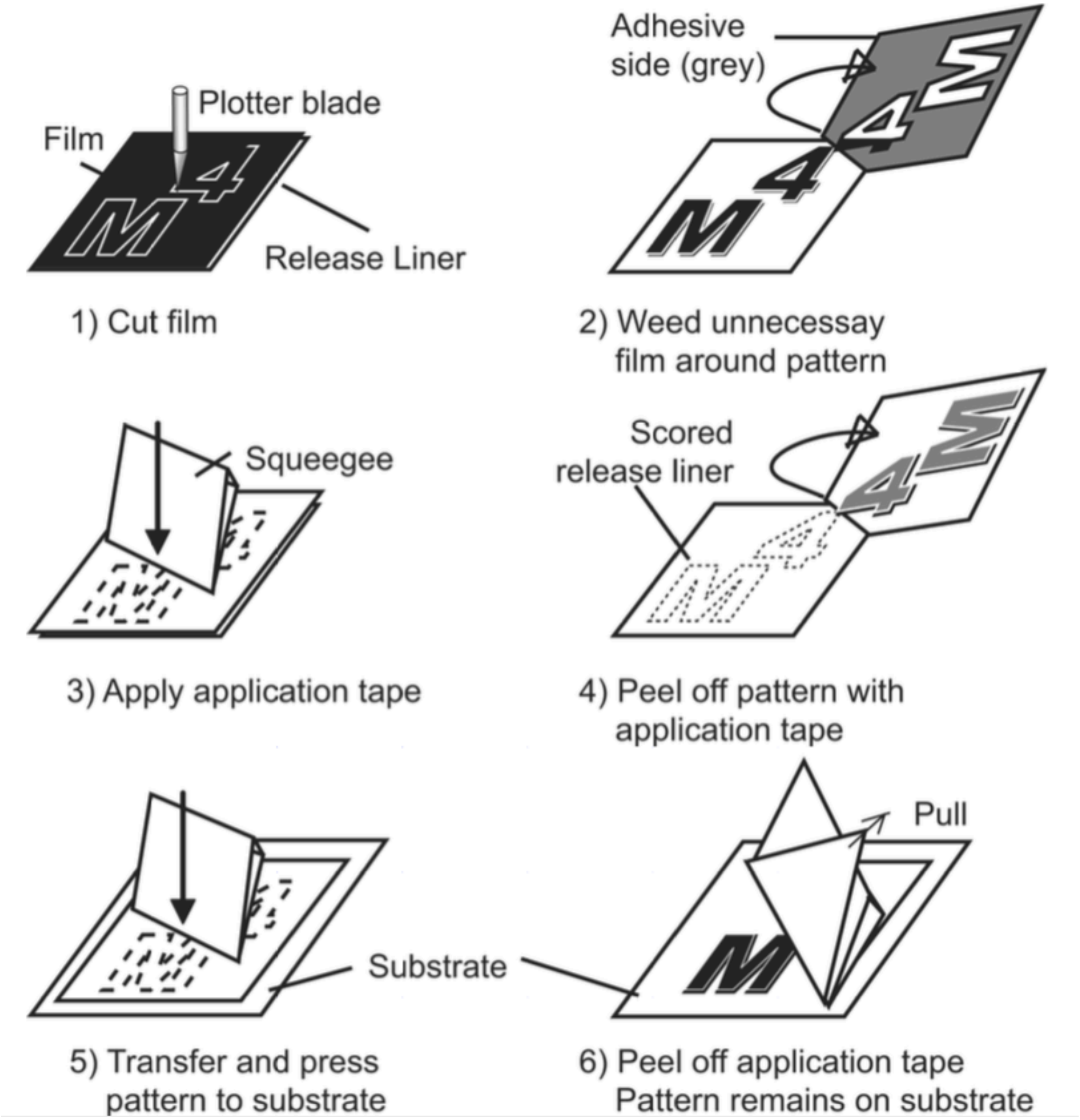

Figure 2.8 Xurographic microfabrication process. [6]

Cost of xurography is much lower than other forms of microfabrication, which is the most significant advantage of xurography over other techniques. Cost for a cutting plotters can be as low as 200 USD but high resolution cutting plotter for about 4000 USD is also available. The resolution of these cutting plotters are lower than other microfabrication techniques but sufficient for many LOC applications. Films of various materials such as polyester, vinyl, vinyl foam, rubber, nitrocellulose，aluminum [6], polyolefin shrink film [101], cyclic olefin [105], polyimide [106] have been tested for prototyping with xurography. 3D microfluidic structures can also be fabricated by assembling multilayer polymer films [6]. These multilayer microfluidic layers could be made of different materials to meet different requirements [107]. 3D complicated features on microchannel wall for surface tension flow guide to avoid bubbles and slant grooves to enhance mixing can also be introduced by cutting scratches on these films with low pressure. [105].

However, xurography has only been used to fabricate microchannels. It has also been used to pattern shallow mask for sputtering [6], but has not been employed directly to integrate electrodes into microchannels. Plotters has been used to cutting, writing, embossing, debossing complicated patterns. It can also potentially be used to integrate and pattern microwire electrodes to complicated patterns. The combination of microwire electrodes and plotting techniques can reduce the cost for both microchannel fabrication and microelectrodes integration.

2.4 Summary

In this chapter the existing microelectrode fabrication techniques were reviewed. Techniques used in semiconductor manufacturing, i.e. PVD require expensive equipment and clean environment. Many of the microfabrication techniques rely on high resolution but expensive lithography techniques, such as photolithography to pattern the microelectrodes. Cleanroom working condition is needed to use photolithography and the photolithography process is not compatible with many polymers. Moreover, the deposition process for PVD, electroplating, electroless plating is long, especially for thick microelectrodes. Alternative patterning methods such as inkjet printing and screen printing together with nanoparticle-based conductive inks lower the cost of the fabrication equipment and accelerate the process for microelectrode fabrication. However, the thick film microelectrodes are difficult to be integrated into polymeric LOC device and the resolution of these microelectrode patterns is low. Moreover, mechanical properties of these film microelectrodes are also poor. Microelectrodes fabricated by low melting point alloy casting and conductive polymer nanocomposite have better mechanical performance but choices for the microelectrode material are limited and photolithography is also needed to pattern these microelectrodes. Compared to these microfabrication techniques, microwires are commercially available with uniform diameter as small as 12.5 µm. Most of the commonly used materials are available in microwire form. No expensive microelectrode deposition equipment and high resolution lithography technique is needed to implementing these microwires as microelectrodes but the microwire can only be integrated straightly with the current techniques. A comparison between these microelectrode fabrication techniques is listed in

Table 3.

Table 3 Comparison of microelectrode fabrication techniques

Fabrication technique	**Resolution**	**Minimum Thickness**	**Mechanical property**	**Fabrication speed**
PVD	~ 1 µm	1 nm	Poor	Low
Electroplating	~ 1 µm	~500 nm	Poor	Medium
Electroless plating	~ 1 µm	~100 nm	Poor	Low
Nanoparticle sintering	~ 100 µm	~ 2-3	Poor	Fast
Low melting point alloy casting	~ 50 µm	10 µm	Good	Fast
Conductive polymer nanocomposite	~ 50 µm	10 µm	Good	Fast
Microwire	12.5 µm	12.5	Good	Fast

Table 3 Continued

Fabrication technique	**Photolithography required**	**Equipment cost**	**Material choices**	**Material waste**
PVD	Yes	High	Numerous	High
Electroplating	Yes	Low	Numerous	High
Electroless plating	Yes	Low	Numerous	High
Nanoparticle sintering	No	Low	Limited	Low
Low melting point alloy casting	Yes	Low	Limited	Low
Conductive polymer nanocomposite	Yes	Low	Limited	Low
Microwire	Yes	Low	Numerous	Low

Microwire is an optimal candidate for microelectrodes integration into LOC devices but an efficient technique to integrate these microwires into complicated patterns is needed. Xurography is a recently developed technique for rapid and low-cost microchannel fabrication but has not be used for microwire electrode integration. In chapter 3, a modified xurographic process is described to integrate microwire electrodes into PDMS elastomer with a cutting plotter. Combination of xurography and microwire electrodes reduces the fabrication cost for microelectrode-integrated LOC devices.

Chapter 3: Xurographic microwire electrode integration for PDMS

As discussed in chapter 2, integrating microelectrodes into LOC devices remains challenging and the current techniques for microelectrode fabrication are either expensive, time-consuming, low resolution, or limited in material choices. Integrating microwire electrode can be effective in integrating high quality materials at low-cost. However, an efficient technique to integrate microwires into complicated patterns is needed.

In this chapter, xurography is investigated as a cost effective and versatile technique to integrate microwire electrodes into PDMS LOC devices. PDMS is one of the most popular material used in laboratories because of its low-cost, elasticity, high optical transparency, gas permeability, biocompatibility. However, due to the poor adhesion between PDMS and metal, integrating leak-free microelectrodes into PDMS LOC devices is quite difficult. Moreover, film electrodes deposited onto PDMS fail easily due to fracture cause by the difference of mechanical properties between the elastic PDMS and metal. In this chapter, a xurographic microwire integration process is proposed to overcome this problem. The mechanism and process of the xurographic microwire electrode integration into PDMS are discussed and the parameters involved in the process are characterized. Finally, the xurographic microwire integration process has been used to demonstrate some applications in fabrication of components for PDMS LOC devices.

3.1 Mechanism

The microwire electrodes are ultrathin and flexible. To integrate these ultrathin microwires into microelectrode patterns, a guiding path is required. In the conventional methods [3, 4, 95] discussed in 2.2.7, the microwire electrodes were fixed into prefabricated electrode channels with dimensions that the same as the diameter of the microwire. In this case, the microwire electrodes are only in gentle contact with the electrode channel walls and can be pulled out of the channel easily due to any force on the electrode wires themselves. In order to integrate the microwire electrodes into more complicated patterns, a better guiding path that can hold the microwire in place is needed.

One way to achieve good insertion of microwires into PDMS is to open a guiding slit in PDMS with a syringe needle. The sharp tip allows cutting of a guiding slit in PDMS and its hollow structure enables insertion of microwire into the slit as shown in Figure 3.1. First, the microwire was threaded into the lumen of the syringe needle (Figure 3.1a). The tip of the microwire was dragged out of the needle tip to keep in contact with PDMS. The needle with microwire was then inserted into a PDMS substrate (Figure 3.1b). These syringe needles were designed with beveled sharp end to penetrate skin easily in their medical application. In a similar fashion, the sharp needle cut a slit in the PDMS without removing any material. The syringe needle was subsequently withdrawn from the PDMS but the microwire in contact with PDMS remained in the resulting PDMS slit closing on the protruding wire as the needle is withdrawn. As no material was removed during the process, the compressed PDMS around the microwire provided sufficient friction to prevent the microwire from being dragged out of the slit (Figure 3.1c).

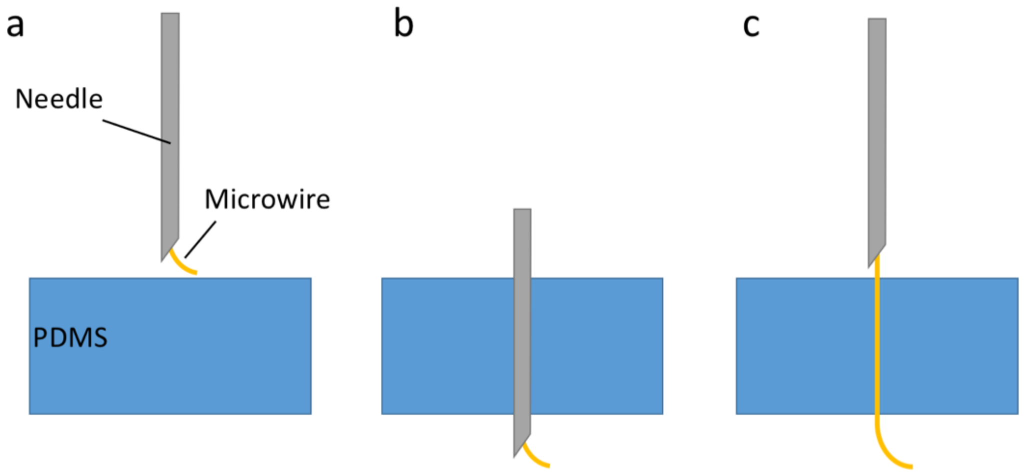

Figure 3.1 "Sewing" microwire integration process a. The microwire was threaded into the syringe needle. b. The syringe needle with microwire was punched through the PDMS. c. The syringe needle was withdrawn and the microwire was held inside the PDMS.

The process shown in Figure 3.1 is simple and the guiding slit can hold the microwire with sufficient friction. However, it is obvious that only straight vertical microwires can be integrated in this process.

An alternate process was developed as shown in Figure 3.2, where the needle is used to cut the substrate instead of penetrating through it. In this modified scheme, the microwire was threaded through the syringe needle. The syringe needle with the microwire was inserted vertically into the PDMS until the microwire was inserted into the PDMS. Then the needle was moved horizontally to cut an open slit on the PDMS surface. Ideally, the microwire electrode would be buried into the slit simultaneously. By cutting the guiding slits with the desired pattern, the microwire electrodes can be integrated with more complex patterns.

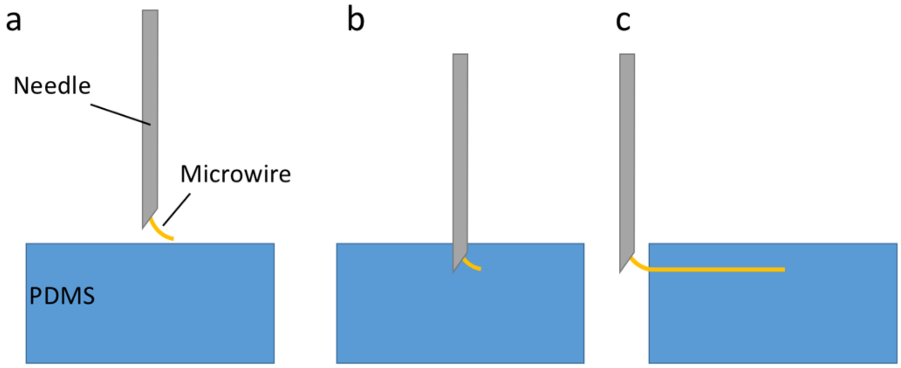

Figure 3.2 Needle-based microwire integration process a. The microwire was threaded into the syringe needle. b. The syringe needle with microwire was cut into the PDMS. c. The syringe needle was moved parallel to the PDMS surface cutting slits and writing the microwires into the slits.

In reality, the beveled edge of the syringe needle causes several issues. First, the sharp edge of the beveled tip is used as a blade to cut slits on PDMS. During cutting the reaction force on the beveled tip, it is often pushed away from the original path. Secondly, the guiding slit cut by the needle cannot be deeper than the vertical length of the beveled edge whereas it has to be close to it to inserted the microwire into the slit. As a result the vertical position of the microwire is not adjustable. Thirdly, the frictional force between the beveled edge and the microwire is far stronger than that between the PDMS and the microwire. As a result, the microwire was dragged along with the needle and withdrawn from the slit instead of being written into the slit. Therefore, an alternate mechanism was needed to replace the beveled edge as a cutting tool to cut the guiding slit with different depth into the PDMS substrate. In addition, a hollow tool with lower friction between the microwire and the tool itself is also needed to insert the microwire into the guiding slit.

In order to overcome these difficulties and to effectively cut guiding slits on PDMS, xurography technique using a cutting plotter was implemented. The plotter controls a rotary blade to cut guiding slits with complex patterns on PDMS. The insertion of microwires is performed by a customized pen consisting of a flat needle modified with a polymer tube. The pen can be installed on the cutting plotter to automate the microwire insertion process. Details about the xurographic microwire integration process are discussed in the next section. Combining these microwire patterning and insertion process with xurography based microfluidic device fabrication, a complete LOC device with integrated microelectrodes can be fabricated with a low-cost cutting plotter.

3.2 Microwire electrode integration process

The microfluidic channels were xurographically patterned on polymer films as previously described by Bartholomeusz et al. [6]. Figure 3.3 shows the detailed steps. The adhesive-backed polyethylene (PE) films (560 μm in thickness) were purchased from McMaster-Carr Supply Company. The PE films were fixed on the cutting mat of the cutting plotter (Cricut Explore, Provo Craft & Novelty, Inc.). Vector graph of the microchannel pattern was imported into the control software to cut the pattern on the PE film (Figure 3.3a). The microchannel pattern was transferred to a clean silicon wafer or glass slide with a transfer tape (M6-1F, Main Tape Company, Inc, US), which is laminated with an adhesive layer with low adhesion. The transfer tape was trimmed to a size smaller than the size of the PE film. The trimmed transfer tape was laminated on the PE film and peeled off together with the microchannel pattern (Figure 3.3b). The transfer tape with the microchannel pattern was then applied on the silicon/glass substrate (Figure 3.3c). The transfer tape was then peeled off leaving the adhesive-back PE film bonded to the substrate. The substrate with the master pattern was used as the master mold for micromolding of PDMS. The PDMS (Sylgard 184 kit, Dow Corning Corp., MI, USA) was prepared by mixing the silicone base and the curing agent at ratio of 10:1. The prepared prepolymer was poured onto the master mold and cured at 80 ºC for 1 hour (Figure 3.3d). The cured PDMS substrate with microchannel was then peeled off from the master mold for the subsequent microelectrode integration (Figure 3.3e).

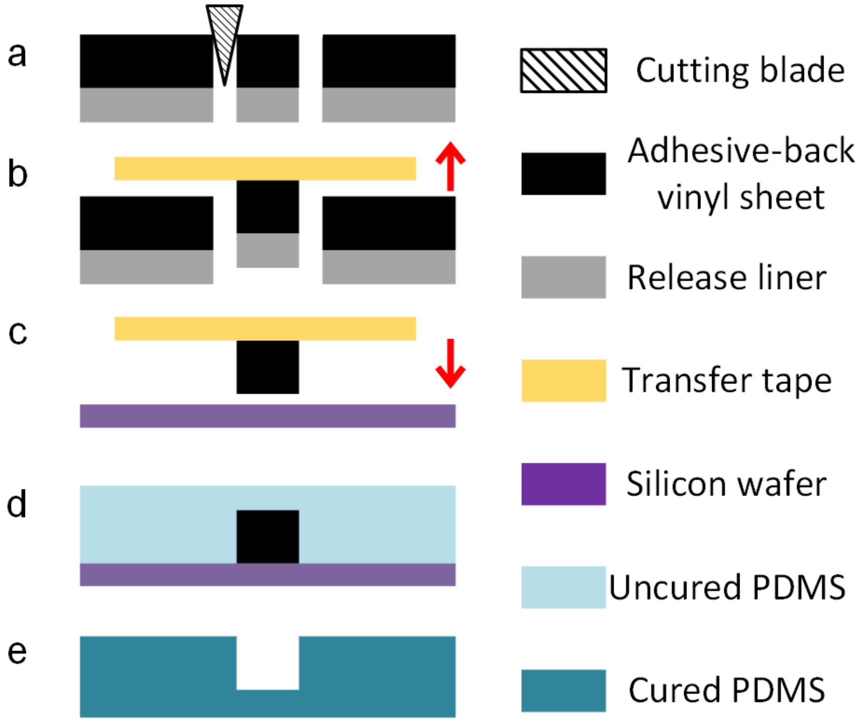

Figure 3.3 Schematic of xurographic microchannel fabrication process a. PE film patterning. b-c. Microchannel pattern transfer. d. PDMS molding. e. Cured PDMS peeled off for electrode integration.

Shallow slits were cut on the PDMS substrate to define the microwire electrode patterns. During cutting, the PDMS has to be firmly attached to the substrate or it would be peeled off under the cutting force. The original adhesive cutting mat doesn't have enough adhesion to PDMS and a 1 mm poly (methyl methacrylate) (PMMA) sheet was trimmed to the same size with the original cutting mat and used as a cutting mat appropriate to hold PDMS. The vector graph of the designed microelectrode pattern was imported into the control software to cut slits on the PDMS (Figure 3.4a). The microwire electrodes were "written" into these slits through a customized pen (Figure 3.4b). The PDMS microchannel with integrated microwire electrode was then bonded to another flat PDMS surface by wet bonding (Figure 3.4c). After the uncured PDMS adhesive was fully cured, the device became a monolithic PDMS LOC device with integrated microelectrodes (Figure 3.4d). When the microelectrode pattern is complicated or the spacing between the electrodes is too small, manual microwire writing become difficult. For easier microwire writing, the customized pen was also installed on the cutting plotter. Many commercial cutting plotters, such as Cricut Explore series (Provo Craft & Novelty, Inc.) and Silhouette Curio (QuicKutz, Inc., Lindon, UT, USA), are equipped with dual carriage multifunctional features for cutting, drawing, stripping, embossing. The dual carriage enables slit cutting and microwire electrode writing at the same time without changing the machine tool. (Figure 3.5).

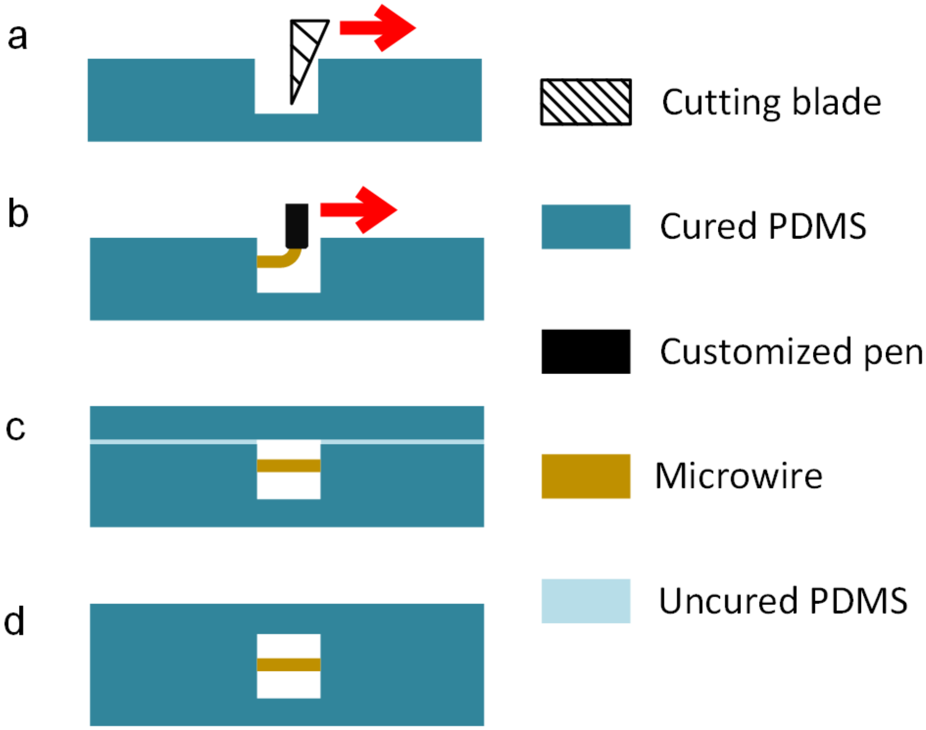

Figure 3.4 a. Slit patterning on the PDMS surface. b. Microwire electrodes written into the patterned slits. c. Device sealing and bonding with uncured PDMS adhesive. d. Curing of PDMS adhesive.

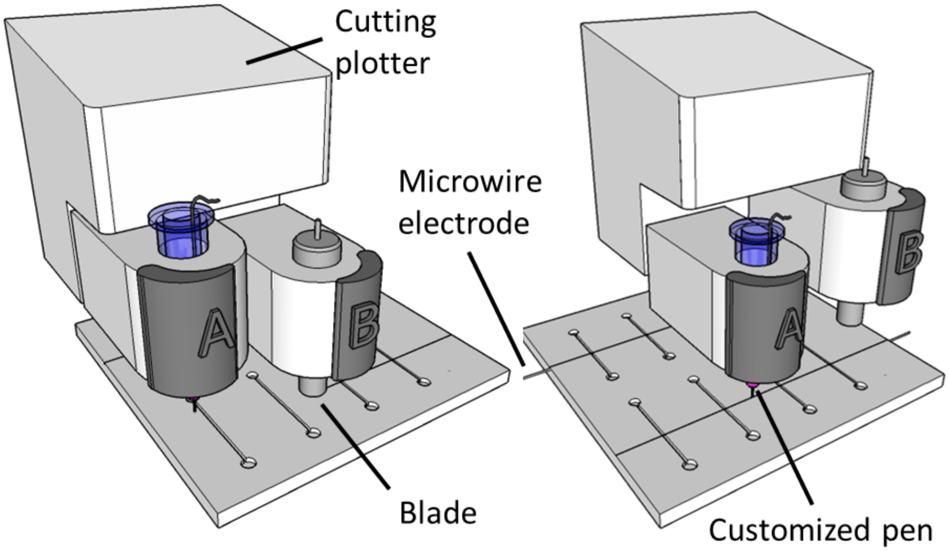

Figure 3.5 Cut-and-write integration process completed in the same cutting plotter.

3.2.1 Guiding slit cutting

The guiding slits cut on PDMS defines where the microwires would be integrated. In this section, the way to control the depth and pattern of the guiding slit and their effect on the position of the integrated microwire electrodes are discussed.

3.2.1.1 Controlling the depth of the PDMS slit

The depth of the slits is a significant feature to be controlled. The position of the microwire electrodes in the thickness direction is highly dependent on the depth of the slit. Characterization of the depth of the slits at different cutting parameters can enable development of a protocol to control the position of the microwire electrodes at different depths inside the microfluidic devices. Conventional planar microelectrodes can only be integrated at the bottom of the microchannel. Integrating microelectrodes other than at the bottom of the channel can improve the performance of these microelectrodes [108-110]. By controlling the depth of the slit within the height of the microchannel, the integrated microwire electrodes can be suspended in the microchannel. Such suspended microelectrodes have never been made in other microelectrode fabrication methods.

The cutting force of the Cricut cutting plotter was controlled in the control software using settings from 0 to 333. The settings number represents the level of force instead of the real force value. The real cutting force was measured by a spring scale (8011MN, Ohaus Scale Corp., NJ, USA). The hook of the spring scale was hooked on the cartridge without the blade on it to measure the force it applies to the blade during cutting. The cutting force was measured under various settings during the cutting process. The relationship between the real cutting force and these representative values is shown in Figure 3.6. The measurements show that the cutting force is between 60-160 mN and a single increase in the setting level results in an equivalent real cutting force increase of 2.33 mN.

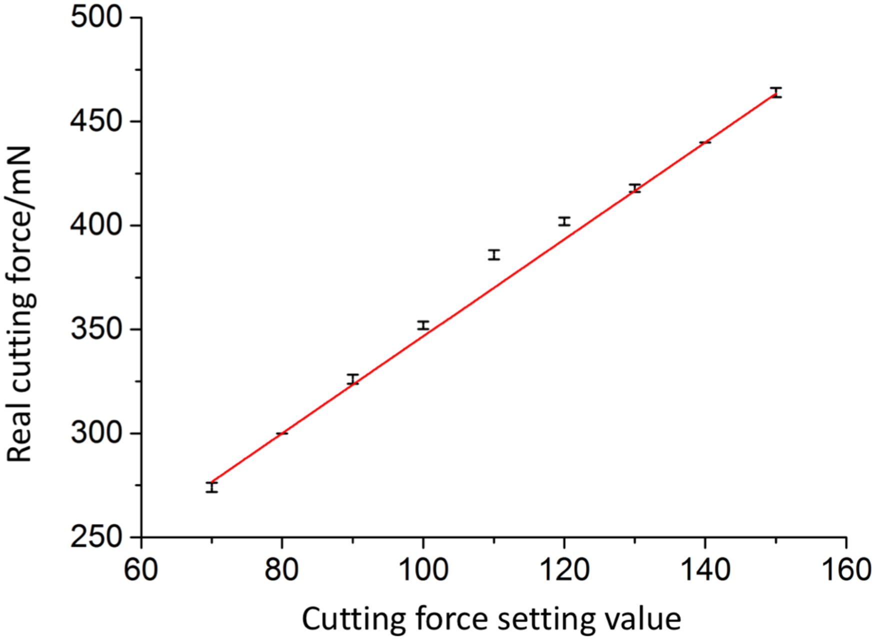

Figure 3.6 Real cutting force vs. cutting force setting value

The depth of the slits was simply characterized by measuring the depth of the slits cut under different cutting parameters using a microscope (S8AP0, Leica). Repetitive cuts can increase the depth of the slits. However, repetitive cuts at the same location resulted in removal of material around the existing slits due to the poor positional repeatability of the cutting plotter and the elastic deformation of the PDMS during cutting. Thus, repetitive cutting is not recommended. In the case of the Cricut cutting plotter, the only cutting parameter that can be controlled is the cutting force. In the case of the Silhouette SD cutting plotter both the cutting force and the blade length can be changed. For each parameter set, an array of 10 parallel slits was cut on a PDMS surface. The cross-section of the slits was obtained by cutting the PDMS with a razor blade. The cross-section was imaged by the microscope with a microscope scale.

The slit depths obtained under different cutting force are shown in Figure 3.7. The depth of the slit increased linearly with the cutting force. The minimum slit depth was about 200 μm at 18 mN cutting force. Further lowering the cutting force cause large variation of cut slit depth. Two linear regions were identified separated by a transition point around 270 mN. Before the transition point the slit depth increases with the cutting force with a slope of 2.76. After this transition point, the slope decreased to 1.39. The transition point is possibly the critical cutting force at which the blade holder first touches the PDMS surface. As shown in the schematic in Figure 3.7, before the transition point, only the sharp blade tip was in contact with the PDMS cutting it. After the transition point, the holder of the blade presses on the PDMS surface and the contact area between the blade, blade holder and the PDMS substrate was larger. The slit depth obtained after the transition point was found to be smaller than expected, likely because the area under the blade tip was pressed down during cutting which prevented the blade tip from extending completely into the PDMS. By further increasing the cutting force, the blade tip cut deeper into the PDMS, resulting in a deeper guiding slit.

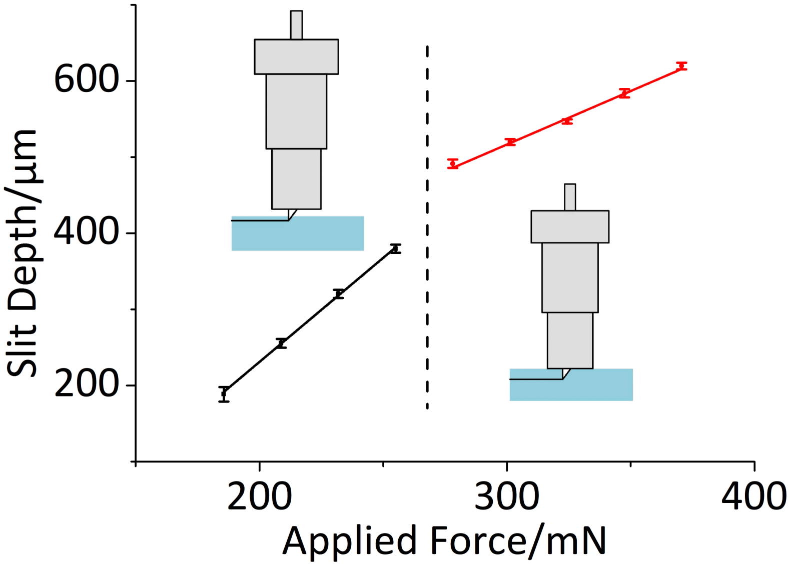

Figure 3.7 Slit depth dependence on cutting force with Cricut cutting plotter

The depth of the slits cut by another cutting plotter (Silhouette SD, QuicKutz, Inc., Lindon, UT, USA) was also characterized. The main difference between these two cutting plotters is that the silhouette SD cutting plotter was equipped with an adjustable blade, the length of which can be controlled in 10 levels. The blades of these two cutting plotters were shown in Figure 3.8.

Figure 3.8 Comparison of the cutting blade of Cricut explore cutting plotter (a) and Silhouette SD (b).

The characterization result of the Silhouette SD cutting plotter is shown in Figure 3.9. The depth of the slits increases linearly with the blade number. Also, the cutting force does not have a significant effect on the depth of the slit produced. The blade number basically represents the length of the blade used for cutting. The larger the blade number, the longer the blade length. The cutting force of the silhouette SD cutting plotter is higher than that of the Cricut one, but the resulting slits can be made much shallower by selecting a shorter blade length, possibly explained by the contact length between the blade holder and the

PDMS surface discussed above. The shallowest slit obtained was about 30 μm deep.

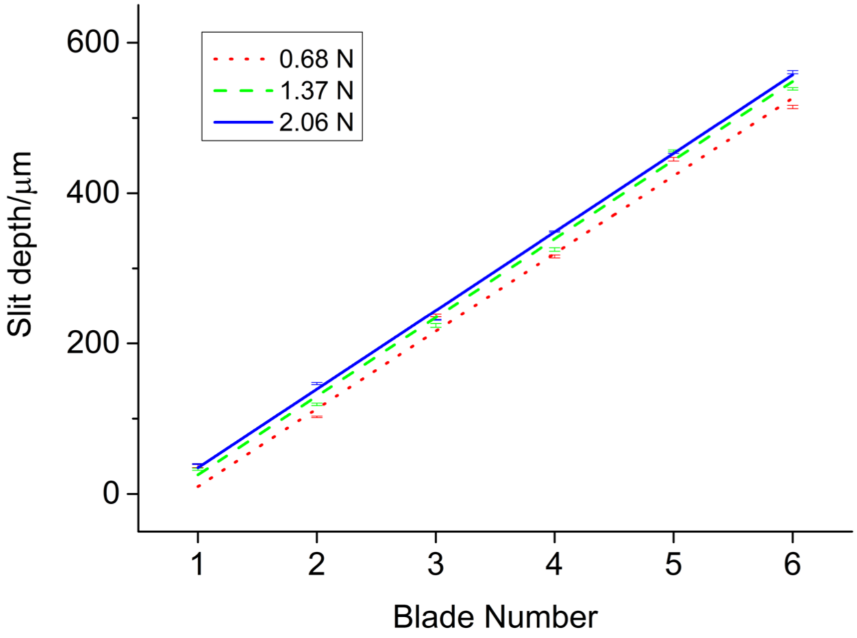

Figure 3.9 Depth of slits characterization on Silhouette SD cutting plotter

3.2.1.2 Slit spacing characterization

The size and dimensional accuracy of the microelectrodes depends on the diameter of the microwire chosen. However, the resolution and accuracy of the microelectrode pattern depends on the integration process. Because the microelectrode pattern is defined by the PDMS slits, the minimum spacing achievable between two slits determines the resolution of the microelectrode pattern.

The characterization of the spacing was similar to the slit depth characterization. Briefly, for each slit spacing an array of 10 parallel slits was cut on PDMS surface. The actual spacing was measured from the micrograph captured by the microscope. The measured results are shown in Figure 3.10. The actual spacing is linearly proportional to the setting spacing at spacing above 150 µm with slope of 0.9. The actual slit spacing is slightly smaller than the setting slit spacing, likely caused by the non-uniform deformation of the PDMS around a slit. The minimum spacing achievable by the Cricut cutting plotter was about 150 µm but occasional overlapping between the slits is to be expected and spacing larger than 150 µm would be recommended.

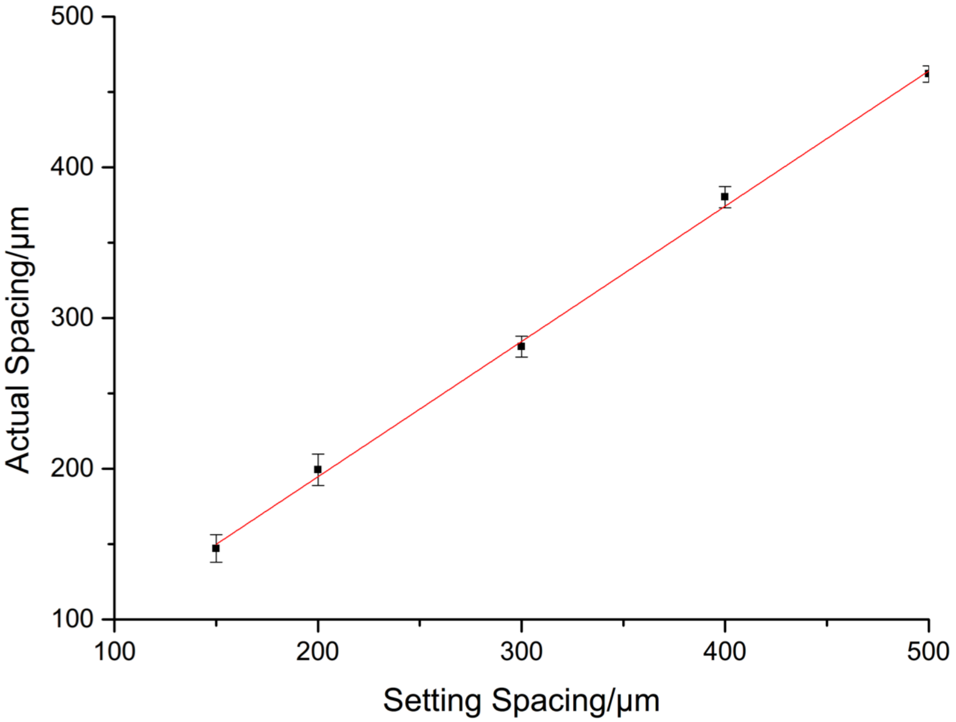

Figure 3.10 Actual slit spacing vs. setting slit spacing. The minimum spacing between two slits is 150 µm.

3.2.1.3 Flexible integration of microwire electrodes

The position of the microwire electrodes in the direction of the thickness of the microchannel can be controlled by the depth of the slits. The in-plane microelectrode pattern can be defined by the slit pattern. Therefore, these microwires can potentially be integrated into any position inside the PDMS device. Figure 3.11 shows three common microelectrode configurations used in many applications. The red microwire passes through the microchannel and is exposed to the content of it in a format that is suitable for in channel sensing or electrokinetic pumping. The blue microwire is integrated along the sidewall of the microchannel but is insulated from the channel in a format that is suitable for dielectrophoresis or magnetic particle manipulation. The yellow microwire was integrated into the PDMS substrate that underneath the microchannel layer. This format where the microwire is insulated from the microchannel is suitable for heating.

For a complete LOC device, these various configurations need to be integrated at various locations into the device. Due to limitations of existing fabrication methods, ideal configurations as depicted in Figure 3.11 are not possible or difficult to integrate and these designs have usually been patterned at the bottom surface of the microchannels. With the xurographic microwire electrode integration technique these microelectrodes can be easily integrated into any desired position inside the PDMS LOC device.

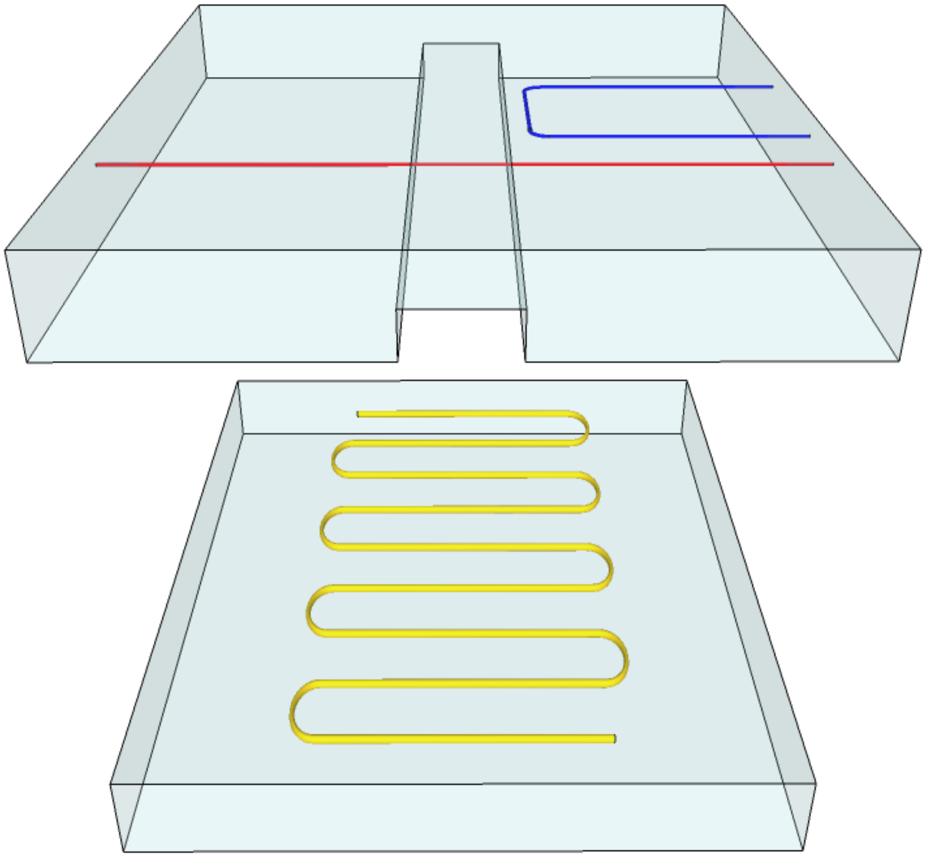

Figure 3.11 Schematic of 2.5D microwire electrode integration

3.2.1.4 In-channel microwire patterning

In other microelectrode fabrication techniques, the electrodes are either at the bottom of the channel or on the sidewalls of the channel, limited by the fabrication process. Microelectrodes integrated at the center of the microchannel can improve interaction between the electrode and the solution or enhance performance of functions such as heating, mixing.

The xurographic microwire integration process allows the integration of the microwire suspended in the middle of the channel. In order to integrate a suspended microwire electrode into a microchannel, the guiding slit was cut through the microchannel with depth shallower than the height of the microchannel. The microwire was then written into the guiding slit and as a result written across the middle microchannel. Figure 3.12 shows a suspended 50 μm copper microwire written across a 500 μm wide microchannel imaged by scanning electron microscope (SEM).

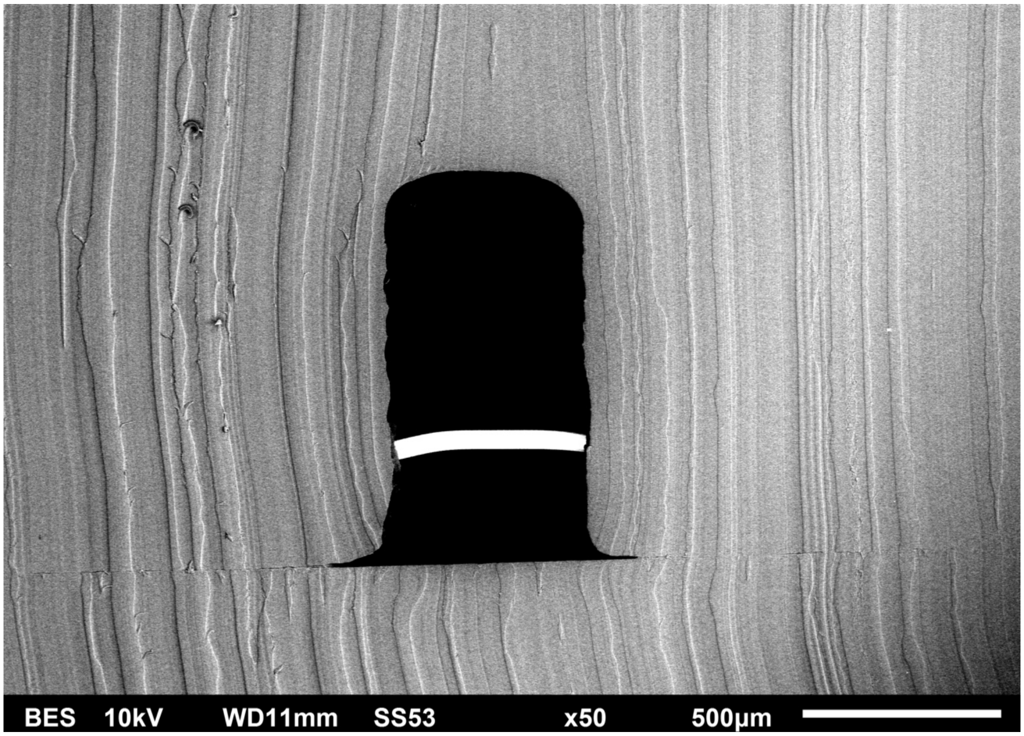

Figure 3.12 A suspended microwire in the middle of the microchannel.

The length of the microwire electrode exposed inside the microchannel determines the in-channel surface area of the electrode, which is an important parameter to control heating efficiency, sensor sensitivity, etc. Therefore, a fabrication scheme has been developed to precisely control the in-channel exposed length of the microwires. In this scheme, a series of parallel slits with 1 mm spacing was cut on the PDMS surface. Various in channel electrode length can be obtained by simply changing the pattern of writing the microwire into slits with different spacing between them (Figure 3.13a). Using the same scheme, multiple microwire electrodes of different in channel lengths can be integrated. For instance, three electrodes forming a electrochemical cell can be integrated using the same or different microwires on opposite sides of the microchannel by suitably designing the slits and then devising an appropriate pattern for microwire integration. (Figure 3.13b).

In some cases, such as in magnetic or electrical separations, the angle of the microelectrode with the microfluidic channel is important. Using the same scheme where the slit cutting pattern is decoupled from the microwire writing pattern, one can devise a scheme to create precise angles between the microwire electrode and the channel. For instance, when two slits are cut on both side of the microchannel and a microwire is written through them, both the length and the angle of the microwire can be controlled by adjusting the distance between these two slits along the microchannel. As shown in Figure 3.13c, three microwires were written into slits with 0, 1 and 2 mm spacing. The angle of the microwire electrode increased with enlarged spacing. These slanted microwire electrodes in the middle of the microchannel can be used to apply electric/magnetic field at defined and particular orientation.

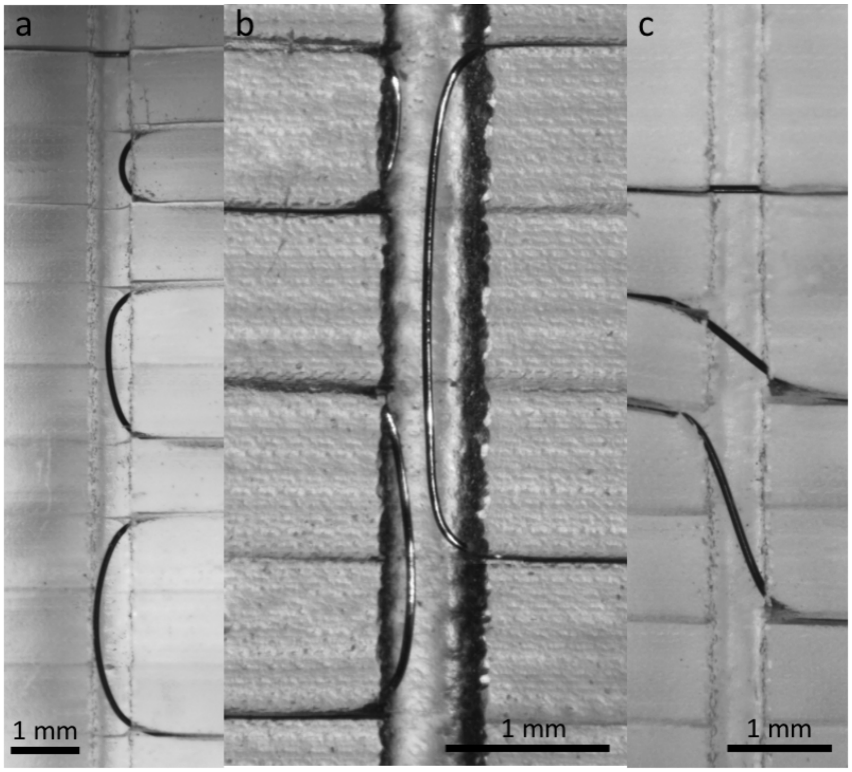

Figure 3.13 Microelectrodes of different length integrated into microchannel. a. Microwire electrodes with length of 0, 1, 2, 3 mm. b. Microwire electrodes with different spacing on both sides of the microchannel. c. Microwire electrodes with angle of 0, 45º, 80º.

3.2.2 Microwire electrode writing

3.2.2.1 Customized "pen" for microelectrode writing

The insertion process of the microwire into the guiding slit is similar to writing. During writing, the section of microwire written into the guiding slit was held in place by friction between the microwire and the PDMS slit which then enables the section of the wire coming out of the tip of the "pen" to be drawn out. In order for that to happen, the friction between the microwire and the pen tip in the writing direction should be small and lower than that between the microwire and the PDMS slit.

As mentioned in section 3.1, using a hard syringe needle to write the microwire into the guiding slits would drag the microwire out of the slit (due to high friction between the needle tip and the wire) or cut the microwire. Various substitutes for the guiding metal syringe needle such as plastic syringe needles, plastic pipette tips, stainless steel blunt tip syringe needles, were also tested by using them to write 50 μm copper microwires into the 500 μm deep guiding slits. The friction between the plastic needles or the plastic pipette tips and the microwires was found to be smaller than that between the microwire and the PDMS slit and the microwires can be successfully written into the PDMS slits. The outside diameter of 27 gauge plastic needle is about 410 μm making it suitable for insertion into the slits. However, its tip bent easily during writing process making it unsuitable for this purpose. Plastic pipette tips were stronger because their tips are conical in shape and larger. However, the larger tip outside diameter (about 800 μm) makes it difficult to insert the pipette tips into shallow slits.

Stainless steel blunt tip syringe needles are available in 30 gauge with outside diameter of about 300 μm. The stainless steel tip is also strong enough to write the microwires. However, the microwires were pulled out of the slits after “writing” because of the friction between the stainless steel tip and the microwires. To lower the friction, the stainless steel needle was sleeved with a miniature heat-shrink-tube (6699T11, McMaster–Carr, Inc., Atlanta, GA). The polyolefin heat-shrink-tube was slightly longer than the stainless steel needle and heated with a heat gun to shrink. The after-shrunk diameter of the heat-shrink-tube was similar to the inner diameter of the stainless steel needle, therefore forming a plastic tip at the stainless steel needle tip (Figure 3.14). The modified stainless steel needle was used to write the microwires into the slits. The stainless steel needle body and the small diameter make it easy to be inserted into the slits. With the plastic tip encapsulated at the stainless steel needle tip, the microwires were in contact with the polyolefin tube instead of the metal body and could be easily written into the patterned slits. The customized pen is shown under SEM (Figure 3.15) where it can be seen that after shrinkage the heat-shrink-tube forms a tip with similar inner diameter ahead of the stainless steel needle tip.

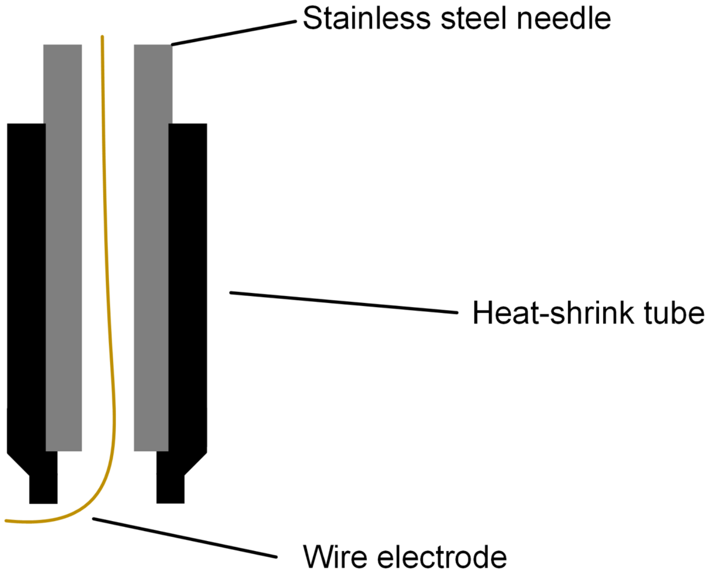

Figure 3.14 The schematic of the customized pen.

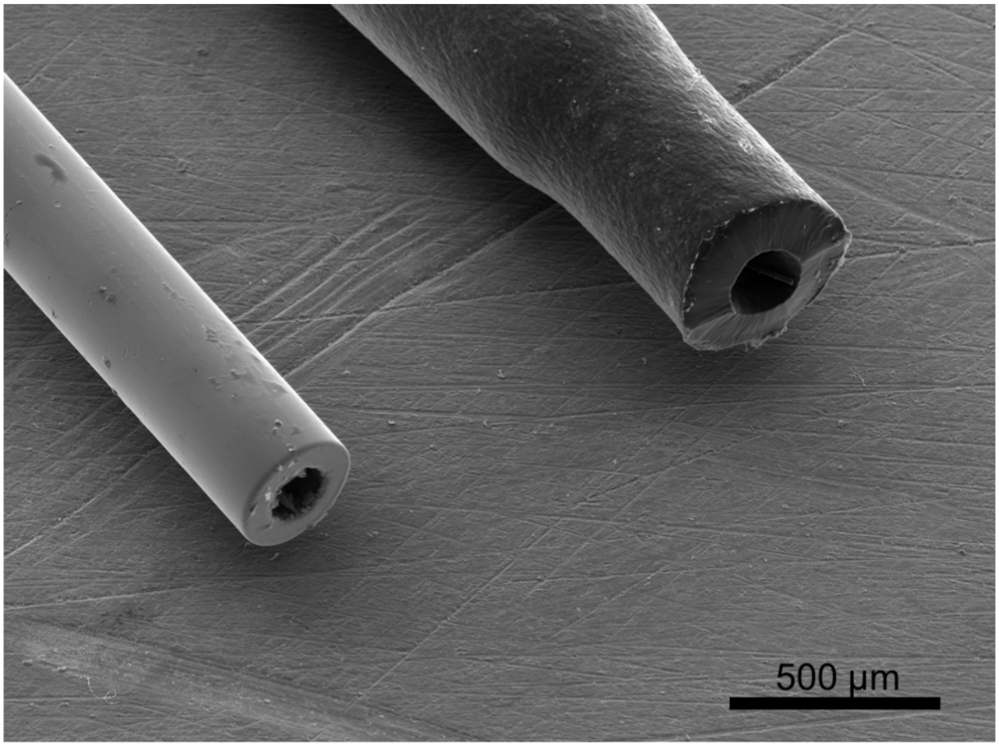

Figure 3.15 SEM image of a stainless steel needle with (right) and without (left) the heat-shrink-tube.

3.2.2.2 A diversity of microelectrode material choices

In order to demonstrate the versatility of the modified xurographic electrode integration process a variety of microwires with different materials and varied diameters such as a 250 µm unstriped optical fiber, a 125 µm glass capillary tube, a 50 µm copper microwire and a25 µm insulated copper wire were written into 500 µm deep slits and imaged under the scanning electron microscope (Figure 3.16). The optical fiber was not striped of the polymer coating as the striped fibers break easily during writing. It is clear that a variety of materials with various thicknesses and surface coatings can be easily integrated using this method. Optical fibers are useful as waveguides to route light or to collect it to various locations on the microfluidic chip. Similarly, microcapillaries are useful to route fluids from macroscale reservoirs to microfluidic devices. In addition, a variety of microwire types including bare metal/alloy wires as well as insulated wires are available which can be integrated directly. It is worthwhile to note that integration of insulation over microelectrodes deposited by other microfabrication methods require multiple steps that are often time consuming and expensive.

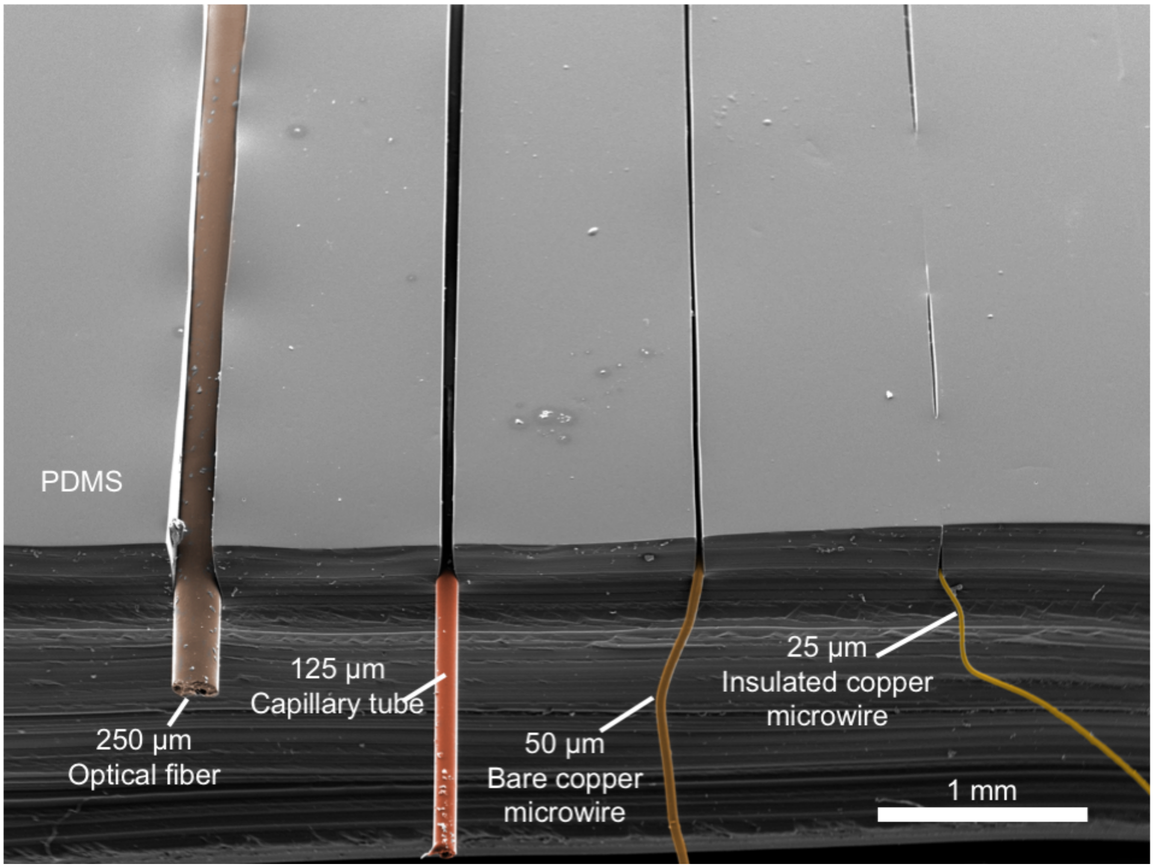

Figure 3.16 SEM image of microwires with different material and different diameter written into 500 µm slits

3.2.3 Simultaneous PDMS device bonding/sealing

The guiding slit into which the microwires are inserted is enlarged when large diameter microwires are inserted, as can be seen in Figure 3.16. This gap created due to the enlargement of the slit can be a source of leakage in microwire-integrated devices. In order to seal these gaps, droplets of sealants such as PDMS prepolymer can be added at the gap after bonding.

However, adding sealants is a post-processing step and not scalable. In order to efficiently bond the PDMS device and seal the gaps simultaneously, the microwire-integrated PDMS devices were bonded by the wet bonding technique [111]. Briefly, PDMS prepolymer was spin coated on a silicon wafer at 1300 rpm for 30 s to form a thin prepolymer layer. The PDMS slab with integrated microwires was then stamped on the spin-coated wafer and was coated uniformly with a thin layer of uncured pre-polymer only in the regions that were on the surface. The pre-polymer on the gaps wicked into the gaps effectively sealing it. The prepolymer-coated PDMS slab was aligned and bonded to another PDMS surface enclosing the microchannel. The aligned PDMS device was then baked to cure all the PDMS prepolymer.

Even with this process, the small gaps were observable by microscope and were not fully sealed by 10:1 PDMS prepolymer. Several modifications were made to the wet bonding procedure to enhance the wicking of prepolymer into the slits. Firstly, the viscosity of the prepolymer was lowered by addition of silicone oil to the pre-polymer in order to reduce the resistance during wicking. Secondly, the PDMS with integrated microwires kept on the silicon wafer with spin-coated pre-polymer for half an hour to leave enough time for wicking. Thirdly, the PDMS stamped on spin-coated prepolymer was placed in vacuum during this half an hour wicking.

A microchannel with integrated 25 μm insulated copper microwire was bonded with the modified wet bonding process. The cross-section along the microchannel was imaged with scanning electron microscope to observe the sealing performance. Before sealing, a gap above the integrated microwire can be observed (Figure 3.17a). Without proper sealing the fluids in the channel would leak from this gap. After sealing with the modified bonding process, the gap was completely sealed (Figure 3.17b). For microwires with larger diameter, the wicking time should be increased to ensure complete sealing.

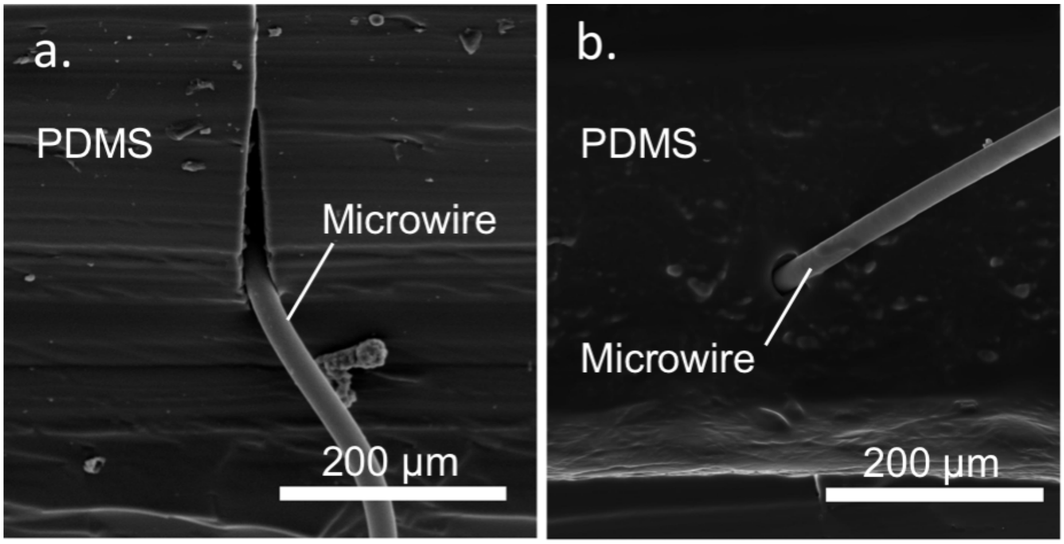

Figure 3.17 SEM image of a 25 μm integrated microwire before (a) and after (b) sealing

3.3 Application examples

In order to demonstrate the versatility of this method, various components requiring integrated metallic microelectrodes have been fabricated and their performance characterized in this section.

3.3.1 Microfluidic heater

The requirement for heating and temperature control for LOC applications such as PCR, mixing, digital microfluidics and cell culture necessitate the integration of heating element into the LOC devices. Early LOC devices employed external Peltier elements to control the temperature of the whole device [112]. The heating components were not integrated into the chip and the heating efficiency was low. Alternatively, in order to better control the temperature of the fluid inside the microchannel locally, a side channel was fabricated near the area to be heated/cooled. The temperature was controlled by injecting pre-heated fluid and pre-cooled fluid [113, 114] or fluids that generate heat through chemical reaction or adsorb heat by evaporation [115] into heater channel. Finally, metallic or conductive oxides resistors have been integrated using lithography based microfabrication methods to generate heat through Joule effect in LOC devices [22, 39]. In addition to the expensive microfabrication method, the need for an insulation layer between the heater necessitates further microfabrication steps.

Microwire heater integrated through xurographic process can overcome the limitations of the conventional methods as the heating microwires can be embedded into the PDMS substrates and therefore are insulated from the microchannel by the PDMS itself. As a demonstration, a microwire based heater design integrated into a PDMS microfluidic channel is shown in (Figure 3.18a). The device consists of a microchannel layer and a heater layer. In order to implement this design, a channel 1 mm in width and 20 mm in length was fabricated xurographically using the procedure as described in section 3.2. The reservoirs for inlet and outlet were punched out of the PDMS substrate with a 2 mm puncher. The 50 μm heating microwire electrode was made of Ni-Cr alloy. The serpentine heater microelectrode was designed with 2 mm spacing (Figure 3.18b). The heater microwire electrode was written into 250 μm deep slits cut on a flat PDMS surface and then bonded to the microchannel layer with uncured PDMS prepolymer. The prepolymer sealed the gap upon the heater microwire electrode and insulated it from solution in the microchannel.

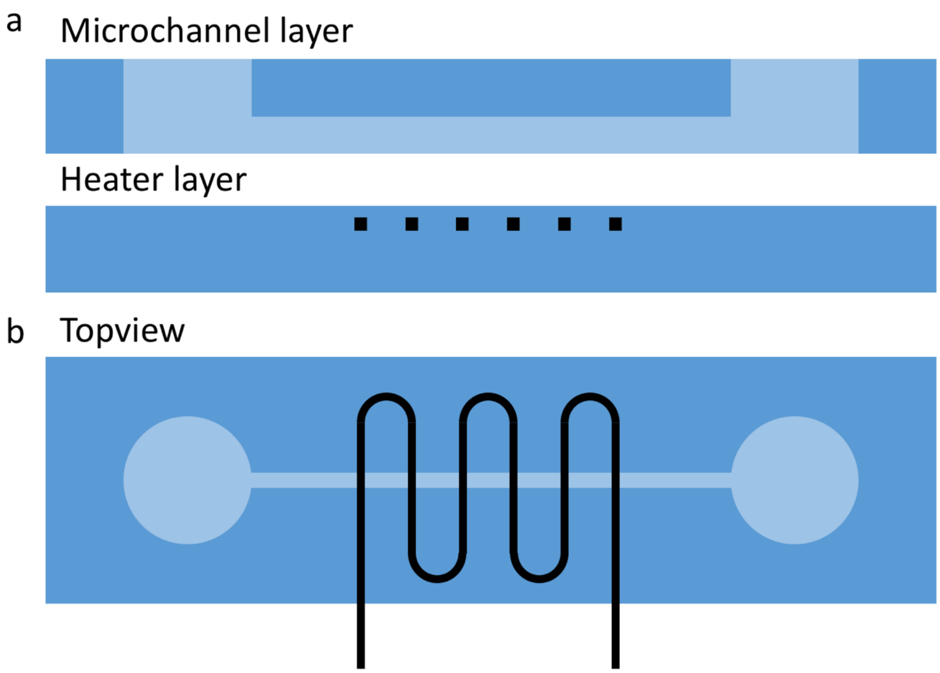

Figure 3.18 Design of the microfluidic heater pattern. Microchannel dimension: 1 mm in width, 20 mm in length, 125 µm in depth. The Ni-Cr microwire was written into a 250 µm deep slit.

The PDMS device with integrated heater microelectrode is shown in Figure 3.19a. The fabricated microwire heater under the microchannel was imaged using a microscope and is shown in Figure 3.19b.

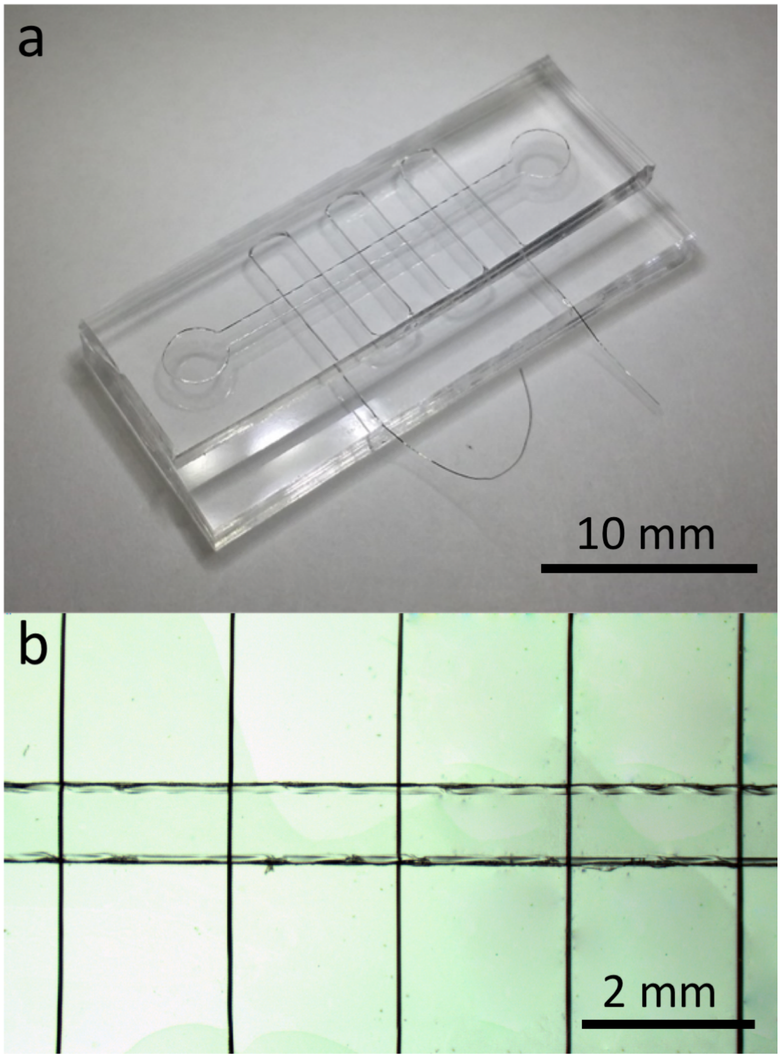

Figure 3.19 a. A PDMS device with integrated microwire heater. b. Micrograph of the microwire heater under the microchannel.

In order to test the performance of the fabricated heater, a thermocouple was introduced into the middle of the microchannel to monitor the temperature inside. The microchannel was filled with deionized water (DI water) and the heater was powered with a DC power source by applying voltage from 1 V to 4 V with 1 V interval. Temperature was monitored from the moment the voltage was applied. The experiment setup is showed in Figure 3.20.

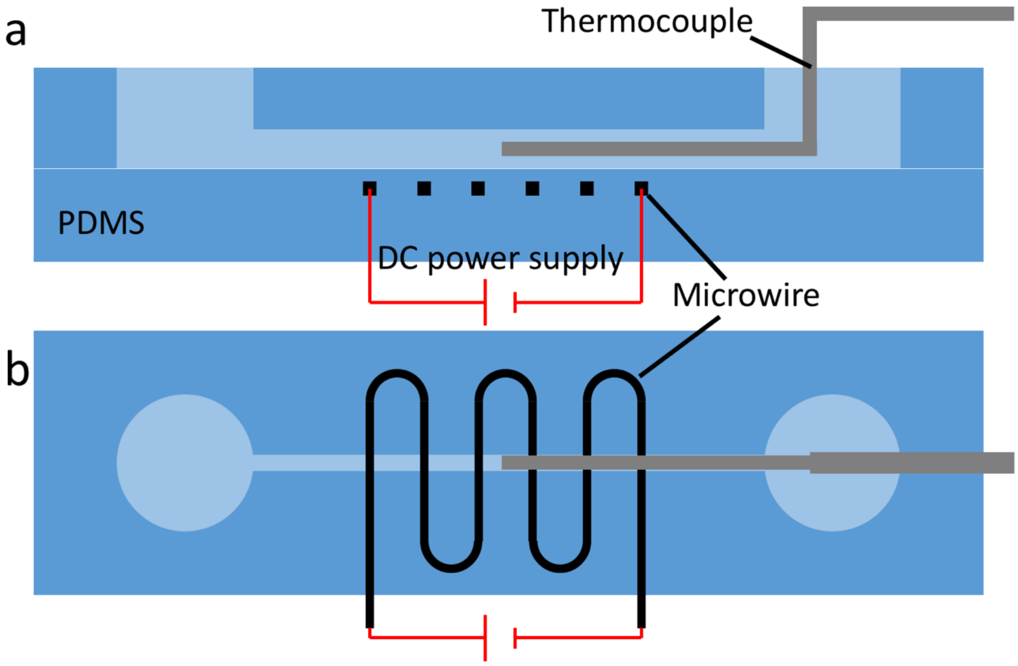

Figure 3.20 Cross-sectional view (a) and top view (b) of the experiment setup

The temperature inside the microchannel was recorded for 13 min until the temperature was steady, as shown in Figure 3.21. The heat generated by the microwire heater and that dissipated by the channel to its surroundings quickly reached an equilibrium and the temperature inside the channel reached steady state. The equilibrium temperature achieved when the operating voltage was 1, 2, 3, 4 V was 25.6, 33.3, 45.7 and 60 °C respectively.

The temperature also rose quicker with higher applied voltage. The higher voltage applied to the heater, the more heat the heater would generate and the higher the equilibrium temperature would be to dissipate more heat to the environment. The heating microwire in this design is sparsely distributed along the microchannel and the size of the channel is also large. The time required to reach the equilibrium is long but it provides a convenient way to maintain a certain temperature with minimum instrumentation. Higher heating efficiency can be achieved by optimizing the heater microwire distribution and the depth at which the microwire heater was integrated. By integrating insulated heating microwires into the middle of the microchannel it would be possible to obtain even more rapid heating of the solution in the microchannels.

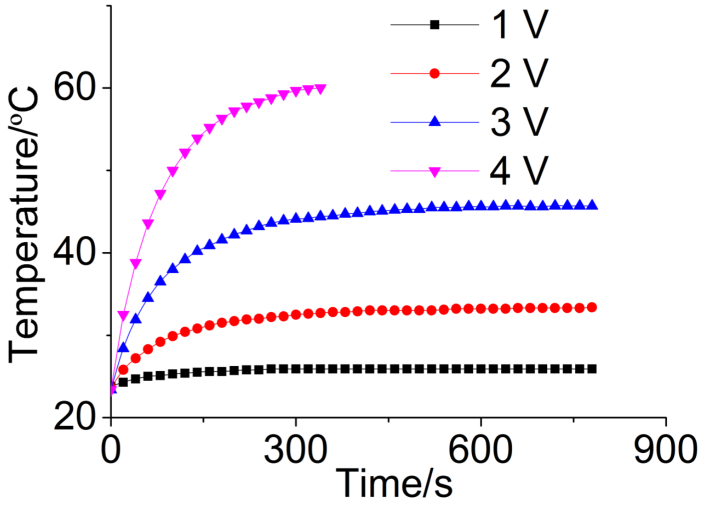

Figure 3.21 Water temperature changes in the microchannel at different applied voltage.

3.3.2 Electrochemical sensor

Electrochemical sensors have been integrated in some early LOC devices for on-chip detection as an alternative to expensive laser-induced fluorescence [24]. Electrochemical detection is sensitive, selective, inexpensive and the electrical signal can be processed by conventional electronics. These electrochemical sensors are also highly compatible with microfabrication techniques and can be integrated into LOC devices easily. Most of the electrochemical microelectrodes are planar electrodes deposited by PVD or nanoparticle sintering. These planar microelectrodes can only be integrated on the bottom or the top of the microchannel. However, the response of these sensors are dependent on transport of the analyte to the sensor surface which in the planar electrodes embedded at the bottom of the channel will take significant amount of time [4]. Therefore, the capacity to integrate the microelectrodes at different positions in the height direction can be useful.

With the xurographic microwire integration technique, microwire electrodes for electrochemical sensing can be integrated at various positions at the height direction. As a demonstration, an electrochemical sensor was fabricated with three electrode setup as shown in Figure 3.22. The three electrodes setup includes a 15 μm diameter carbon nanotube microwire working electrode, a silver/silver chloride electrode and a platinum counter electrode from left to right in the figure. The silver/silver chloride reference electrode was inserted in close proximity to the carbon nanotube working electrode to reduce the effect of solution resistance. These microwire electrochemical electrodes were integrated at a depth of 250 μm into a PDMS microchannel which has a height of 560 μm and width of 500 μm. The PDMS microchannel with integrated electrochemical electrodes was bonded to a flat PDMS surface with uncured PDMS prepolymer. The silver/silver chloride electrode was modified from a 50 μm silver microwire electrochemically in a similar fashion as reported previously [116]. The microchannel was filled with 1 M KCl solution and then 2 V anodic DC potential was applied to grow silver chloride on the silver microwire electrode. After silver microwire modification, the microchannel was washed with DI water.

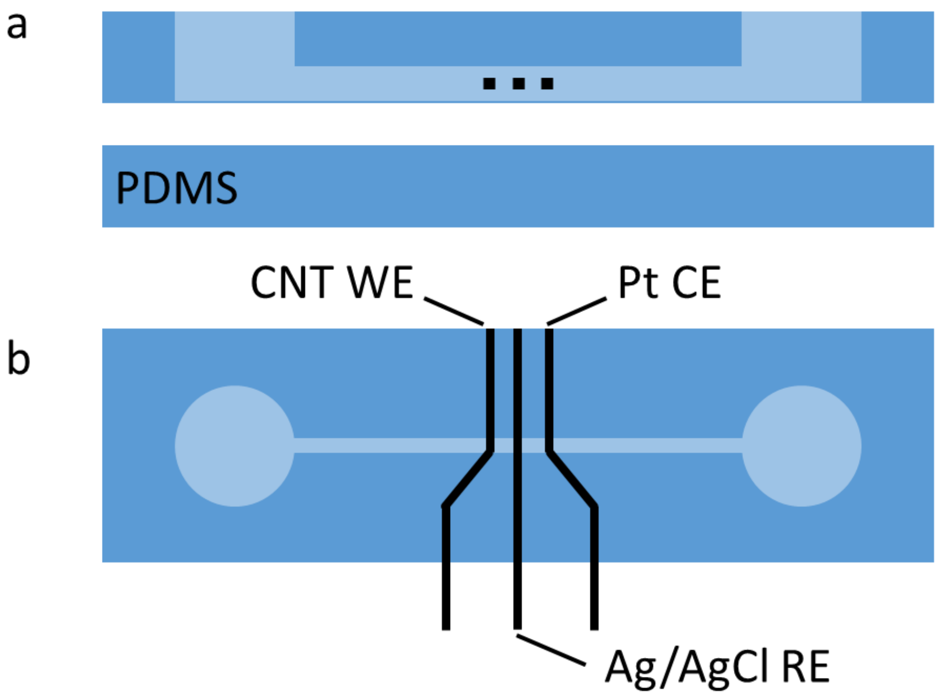

Figure 3.22 Schematic of the electrochemical sensor design. a. Cross-section view of the electrochemical sensor. b. Top view of the electrochemical sensor.

The fabricated electrochemical sensor was tested using cyclic voltammetry of ferricyanide. Potassium Ferricyanide (1 mM) in 1 M KCl was injected into the microchannel. The applied potential was cycled between 0.2 V to 1.2 V with step voltage of 5 mV was applied to the working and counter electrodes using a EmStat potentiostat (PalmSens Inc.) at scan rates of 50, 100, 200, 300, 400 mV/s. The cyclic voltammetry was run 10 times for each scan rate and the results were found to be repeatable. Electrochemical sensors with microelectrode of 1 mm and 10 mm respectively were made for comparison. The result is shown in Figure 3.23. Much higher signal strength was acquired with the electrochemical sensor with 10 mm microelectrodes.

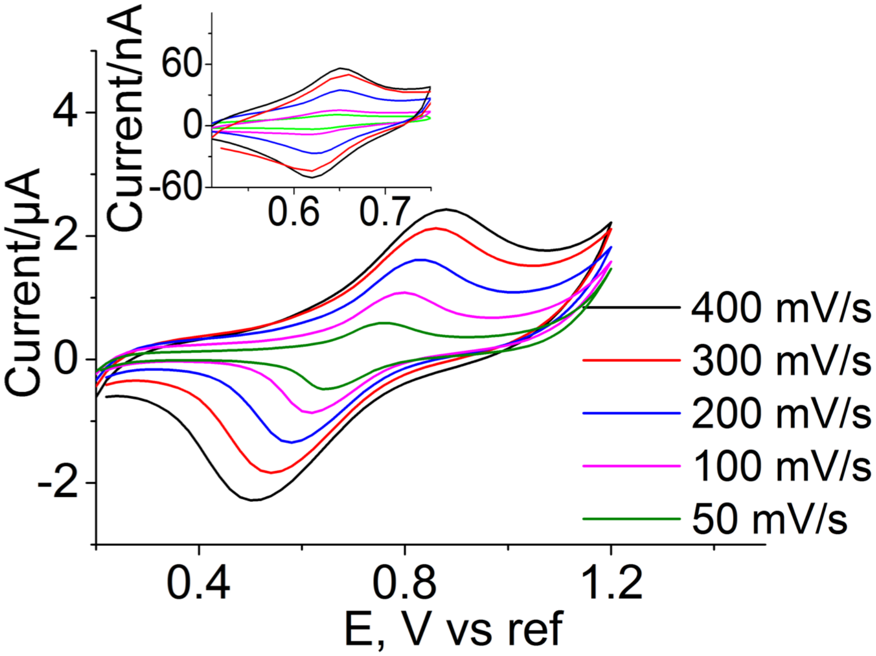

Figure 3.23 Cyclic voltammetry of ferricyanide in electrochemical sensor with different microwire electrode length. The insert is results for device with 1 mm electrode.

3.3.3 Electro-osmotic Micromixer

Mixing is challenging in microfluidics due to the low Reynolds number flow in microchannels. In laminar flows, mixing is achieved by diffusion, which is slow and requiring a long mixing length. Complicated microchannel features such as grooves and 3D serpentine structure can introduce chaotic advection which increases contact area and contact time between two fluids and enhance mixing. However, the mixing efficiency is low resulting in a long mixing length. In contrast, active mixing employs external forces to mix the fluids. Electro-osmosis, which drives the motion of fluid by applying potential across the microchannel, is a type of electrokinetic phenomenon and also a common active microfluidic mixing technique. The potential is commonly applied through planar electrodes integrated on the bottom of the microchannel. The mixing only occurs on the surface of these planar electrodes and therefore cannot induce sufficient mixing especially for high aspect ratio microchannels. Integrating microwire electrodes into the middle of the microchannel can possibly induce better mixing in the middle of the microchannel.

The concept of the alternative current (AC) microwire induced charged electro-osmosis (ICEO) mixer is shown in Figure 3.24. When a conductive microwire is placed in an electric field, a double layer charge would be induced around the microwire. The electrical double layer would then be driven to move under the electric field (Figure 3.24a). Bulk fluid motion is also induced due to the viscosity of fluid. At reverse electric field direction, electrical forces and the surface charge poles are reversed, resulting in unchanged fluidic motion direction (Figure 3.24b).

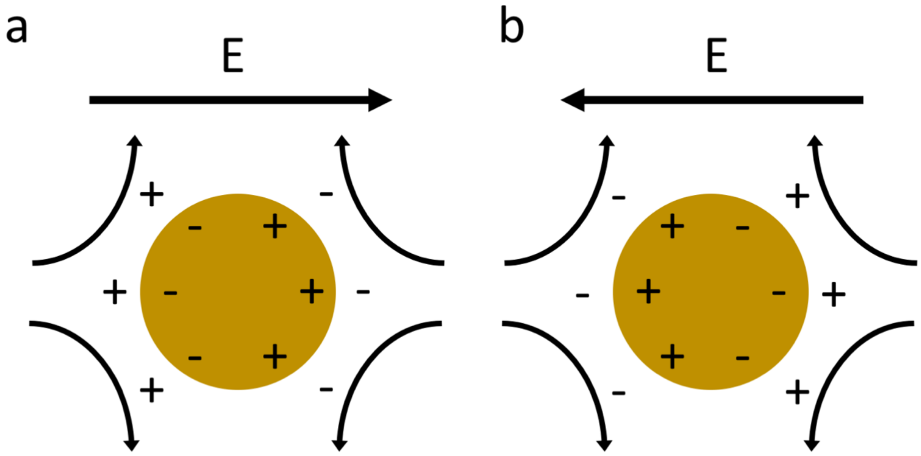

Figure 3.24 AC electro-osmosis around a microwire

The design of the ICEO microfluidic mixer is shown in Figure 3.25 The top layer is a Y-shape microfluidic channel with width of 500 µm and height of 560 µm. Three 50 µm copper microwire electrodes were integrated into 250 deep of the microchannel with 1 mm spacing between them. The middle microwire electrode was left with no external electrical connection. The PDMS Y-shape microchannel with integrated mixer microelectrodes was bonded to a flat PDMS surface by wet bonding.

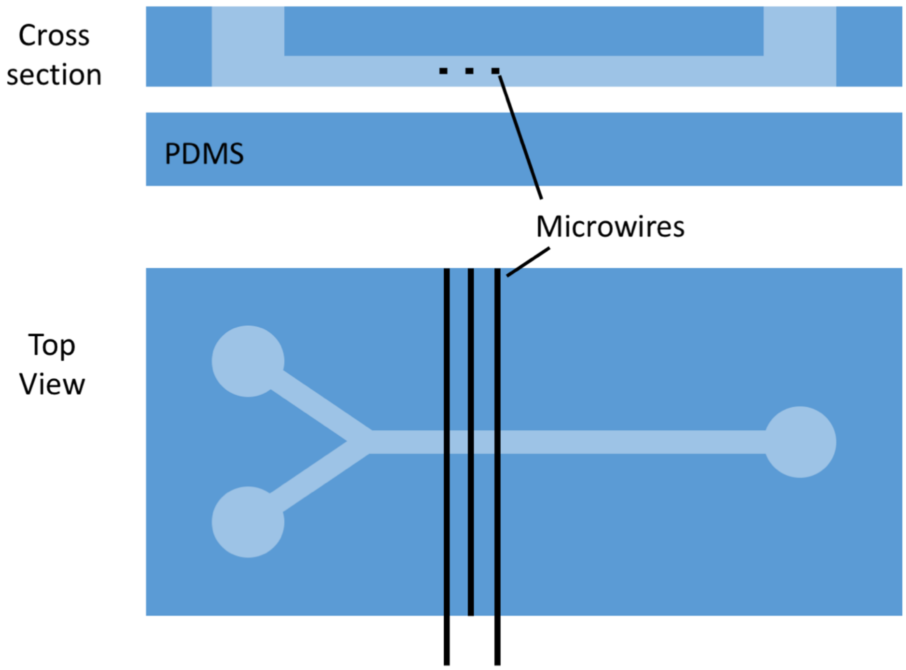

Figure 3.25 A microfluidic electro-osmotic mixer design

DI water dyed with green and red food color respectively was continuously injected and mixed in the two inlets of the Y-shape microchannel with flow rate of 5 µl/min. AC voltage of 10 kHz from 50 to 200 V was applied to the two microwire electrodes on both sides to generate electric field from 250 V/cm to 1000 V/cm to the region in between. The electric field induced electro-osmotic flow around the microwire and mix the two dyed solution.

The mixing of these two dyed solution in the mixing region was imaged with the microscope (Figure 3.26). It was observed that higher voltage led to greater mixing. It could also be seen that the electro-osmotic mixing only occurred in the mixing region. Since the electrodes for the mixer is confined within a few mm's, the strong electric field applied for mixing does not interfere with other parts of the device. Increase of electric field strength to 750 V/cm by applying 150 V was sufficient to induce complete electrokinetic mixing of the two solutions.

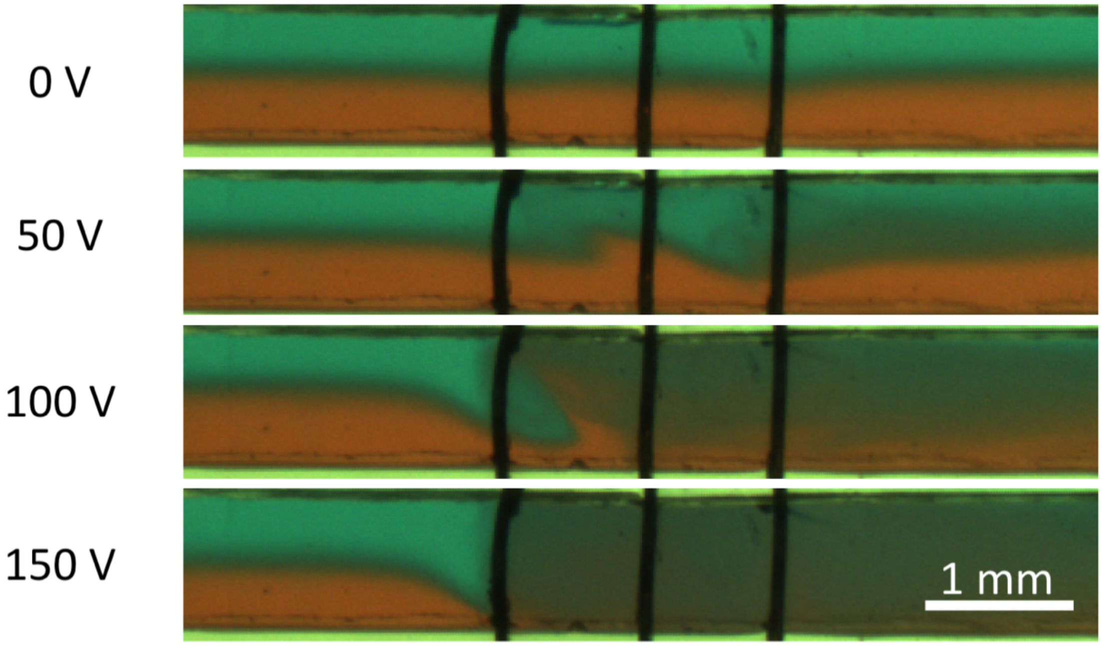

Figure 3.26 Mixing of DI water dyed with green and red food color at different applied voltage.

3.3.4 Optical waveguide

LOC devices with integrated light-emitting diode (LED), optical fibers, photodiodes and other optical components have been fabricated to miniaturize traditional optical sensing systems with high resolution microscope. These optical devices are highly sensitive with low limit of detection. Optical fiber is useful for light transmission into specific location. These optical fibers have been used externally for illumination and detection [117]. However, it is difficult to align the external optical fibers to the microchannel accurately. To accurately integrate the optical fiber into the LOC device, a technique similar to the microwire integration technique discussed in section 2.2.7 was used. A fiber channel was fabricated in the LOC device with the same dimension of the optical fiber. The optical fiber was inserted into the fiber channel for illumination [118] or detection [119]. The insertion process is manual and the optical fiber would come out of the fiber channel easily.

As shown in Figure 3.16, the xurographically patterned slit can hold the optical fiber in the PDMS. In this section, an optical fiber was integrated into a 1 mm wide microchannel as a optical waveguide for external light source. A 250 µm optical fiber (FG105UCA, Thorlabs, Newton, NJ, USA) was integrated in the same manner of microwire electrode integration. About 5 mm of the optical fiber end was striped and cleaved to a final glass end of about 1 mm. The fiber is stripped only at the tip in order to prevent it from breaking when written using the modified xurographic process. The optical fiber was written with a pipette tip (AD10EK, Diamed Lab Supplies Inc., Mississauga, Ontario) with inner diameter of 800 µm. In order to demonstrate the versatility and the accuracy of this approach, the optical fiber was written into a slit crossing the microchannel leaving the cleaved tip suspended in the microchannel (Figure 3.27a). The device was then bonded by wet bonding. The written optical fiber was held by the guiding slit and stayed in position during subsequent alignment, bonding and sealing.

The integrated fiber was used to illuminate the fluorescence dye to determine DNA concentration. Lambda DNA samples with different concentration from 1 ng/ml to 1 μg/ml in 1X TE buffer (10 mM Tris-HCl, 1 mM EDTA, pH 7.5) was dyed with picogreen (200-fold dilution of the original reagent) and injected into the microchannel. Excitation light of 490 nm Nominal wavelength from a fiber-coupled LED (M490F2, Thorlabs, Newton, NJ) was guide through the optical fiber into the microchannel. The emission light was detected with fluorescence microscope (Figure 3.27b).

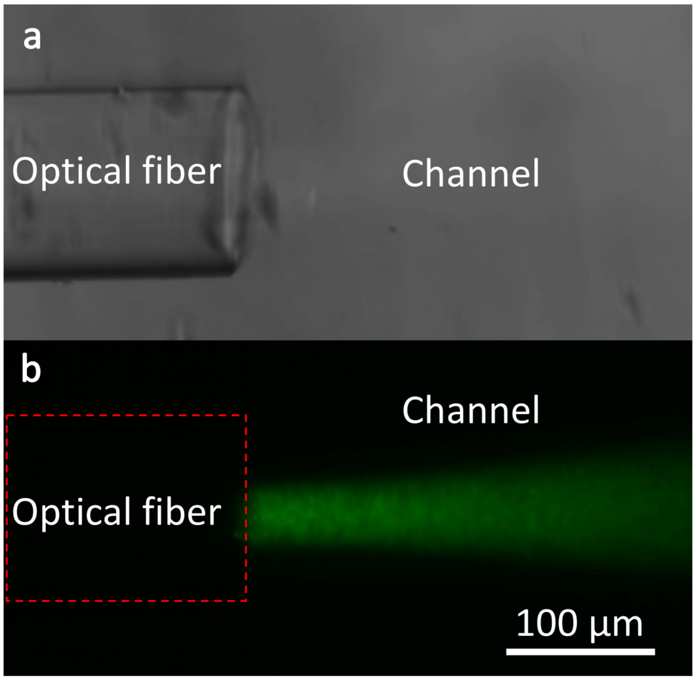

Figure 3.27 a. An optical fiber written into the microchannel. b. Emission light from dyed DNA sample.

The emission light was imaged with the fluorescence microscope. Before turning on the LED, no emission light was seen and the image is dark (data not shown). After turning on the LED, a light beam can be seen coming from the tip of the optical fiber, indicating that the dyed DNA sample along the excitation light beam was ignited. The fluorescence intensity was measured in the image from the mean brightness of the beam. The fluorescence is linear to the DNA concentration (Figure 3.28). The result is in consistent with the quantification curve of picogreen reagent [120].

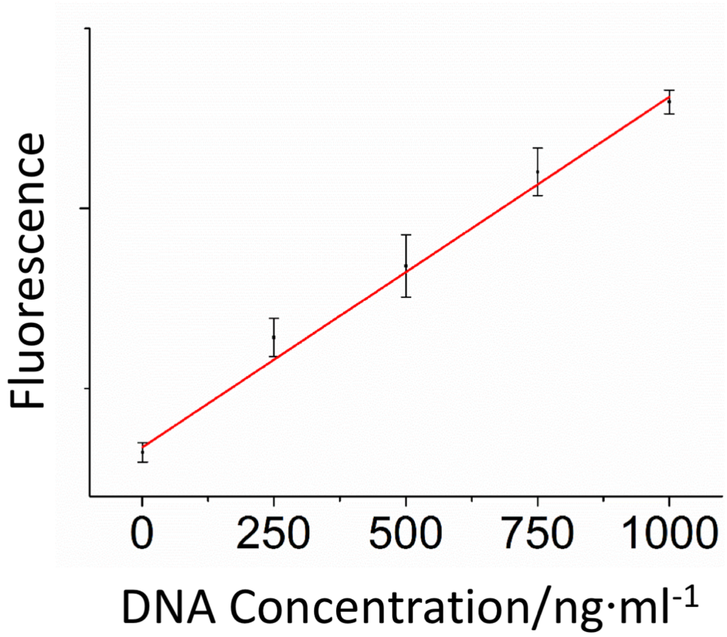

Figure 3.28 Fluorescence intensity vs. DNA concentration

3.4 Summary

A modified xurographic microwire electrode integration technique was described in this chapter. The microchannel fabrication and microelectrode integration was performed using a low-cost (US$200) cutting plotter. A cutting plotter is more affordable than the equipment required in other microelectrode integration techniques and can be implemented without any special clean room facilities.

In addition to reducing the cost of microelectrode integration significantly, this technique demonstrated many advantageous features. First, micro-electrodes down to 25 μm in size has been successfully integrated in PDMS LOC devices. Secondly, the position of these 2D microelectrodes in thickness direction can be controlled, which is a useful feature that the other microelectrode fabrication techniques lack. This feature permit integration of microelectrodes into almost any position inside the PDMS device. Integrating microwire electrodes suspended inside the microchannel with locally controlled pattern was also demonstrated. These suspended microwire electrodes enables better interaction with the solution. Different microfluidic components including a microfluidic heater, an electrochemical sensor, an electro-osmosis mixer and an optical waveguide were integrated into PDMS microfluidic devices to demonstrate the versatility of the modified xurographic method as well as the advantage of the additional microelectrode position control.

Despite the many advantages, the xurographic technique established in this chapter can only be used to integrate microwire electrodes into PDMS LOC devices. In the next chapter, another xurographic process would be developed to integrate microwire electrodes into most of the polymeric LOC devices based on wet bonding.

Chapter 4: Xurographic microwire electrode integration for rigid polymers

In chapter 3, a xurographic microwire electrode integration method to integrate microwire electrodes into elastomers microfluidic devices, typically PDMS LOC devices, was established. In the integration process, the compressive force from the deformed elastomeric slits and the resulting static friction between the microwire and the elastomer holds the microwires in the slit. This method is only applicable for elastomers and not for rigid polymers such as polyethylene terephthalate (PET), Polycarbonate (PC), PE and PMMA. During mechanical cutting, the rigid polymers deform more plastically than elastically. As a result, the resulting shape of the cut is an open V-shape grooves [105] instead of closed slits. Microwires written into these open grooves are not held by friction and would come out easily, in a fashion similar to the electrode microchannel used to integrate microwires discussed in 2.2.7 [4]. Thus the mechanism described in 3.1 is not applicable to materials other than elastomers. In order to solve this problem, a more universal microwire electrode integration technique was developed and is characterized in this chapter.

4.1 Mechanism

As discussed above, an alternate mechanism to integrate the microwire in a defined position is needed in the case of rigid polymeric substrates. Adhesives can be introduced between the microwire and the rigid polymer to bond the microwire on the polymer. Considering that adhesive bonding has also been used widely in polymeric LOC device fabrication, the microwire integration can be completed together with device fabrication process.

Adhesive bonding is a bonding technique where two substrates are bonded with an adhesive layer in between. Two types of adhesives are available: liquid adhesive and pressure sensitive adhesive (PSA) tape. Liquid adhesives can be cured by evaporation of solvent, mixing base material (such as epoxy or acrylate) with curing agent, or external ultraviolet source. PSA is a viscoelastic polymeric material (e.g. acrylics and rubber) coated on a supporting substrate and is commercially available in various sizes. After removal of the supporting substrate, the PSA can be laminated between two substrates and bond them together. A pressure would be applied on the substrates to force the adhesive to wet the substrate and improve the bonding strength.

The mechanism for the integration of microwire electrodes into rigid polymer based microfluidic devices is shown in Figure 4.1. First, the microwire is written on top of the adhesive film (Figure 4.1a). The microwire can be written as complex pattern because of the adhesion from the adhesive layer which hold the microwire once it is written on it. Then a rigid polymer substrate would be laminated on the adhesive film and the microwire is partly pressed into the adhesive layer (Figure 4.1b). However, a gap would exist above the microwire as shown in Figure 4.1b. Further application of bonding pressure on the polymer film would force the adhesive to reflow and fill the gaps around the microwire and strengthen the bonding between the substrates (Figure 4.1c).

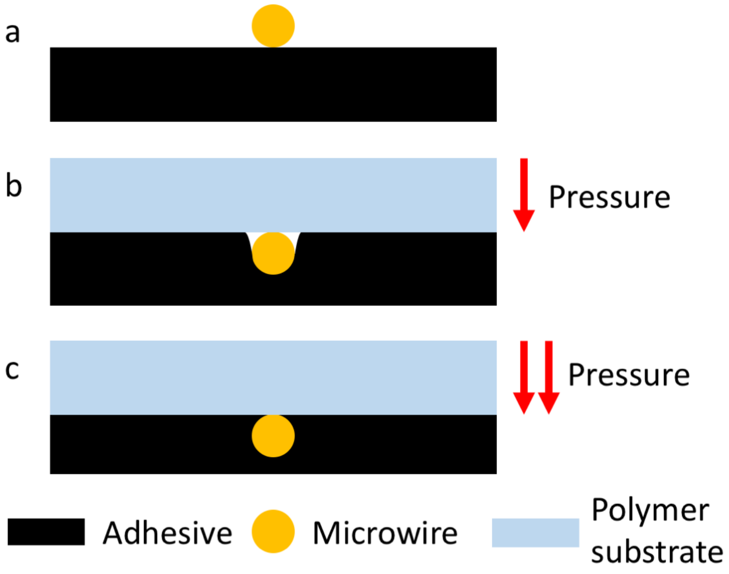

Figure 4.1 Principle of adhesive-based microwire electrode integration. a. A microwire is written on the PSA film. b. A polymer substrate is pressed on the PSA film and the microwire was pressed into the PSA film. c. Further applying bonding pressure forces the adhesive into the gaps.

A complete microwire integration process based on PSA is shown in Figure 4.2. The PSA films are laminated on the polymer film for the microchannel (Figure 4.2a). The polymer film with laminated PSA was then patterned with the cutting plotter to obtain the microchannel features (Figure 4.2b). The protective liner of the PSA is then removed to expose the PSA film (The liner is not shown in the figure). The microwire electrode is embedded on the PSA film by writing with a customized pen (Figure 4.2c). The microchannel with integrated microwire electrode is then sealed with two other polymer film (Figure 4.2e), one at the top and another at the bottom to form a closed LOC device (Figure 4.2f).

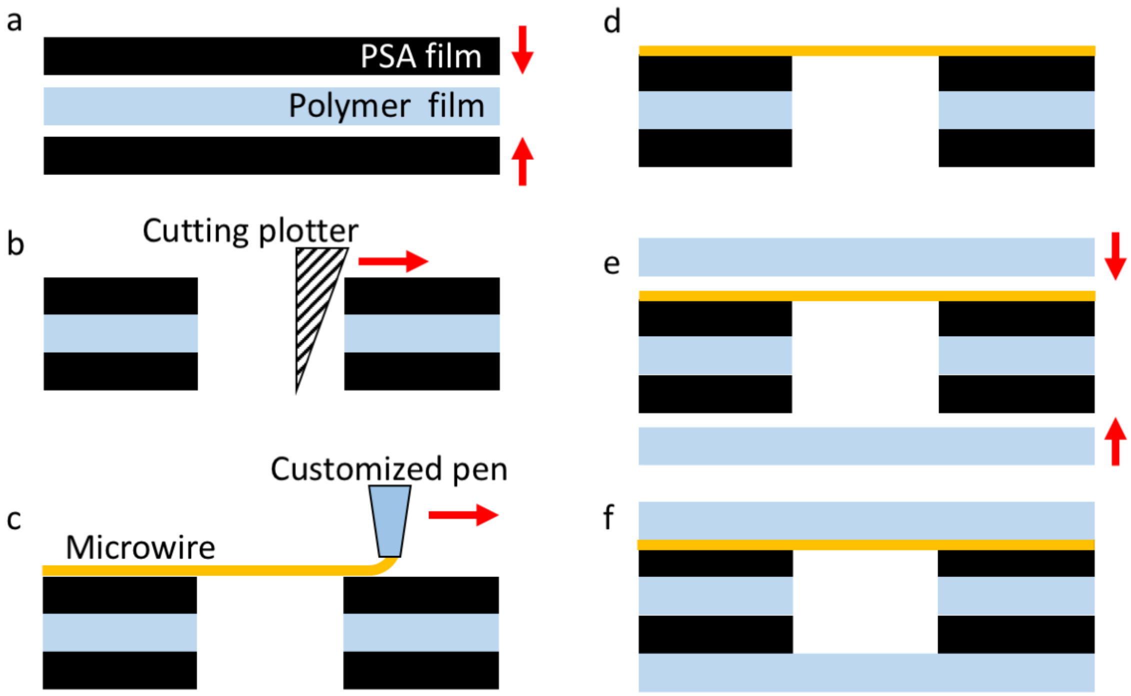

Figure 4.2 A simple example of PSA-based microwire integration process.

The embedding of microwires in the PSA film was further characterized by scanning electron microscope. First, a PSA film patterned with a reservoir and bonded to a glass slide and a 50 µm copper microwire was written across the reservoir. A PDMS substrate was use to apply pressure on the PSA film. Because of the weak adhesion between the PDMS and the PSA film, it can be easily removed without peeling off the adhesive film. The resulting microwire-integrated PSA film was imaged under the SEM (Figure 4.3). It can be seen that the microwire written on the PSA surface was pressed and sealed into the PSA. The microwire written into the reservoir was suspended in the reservoir.

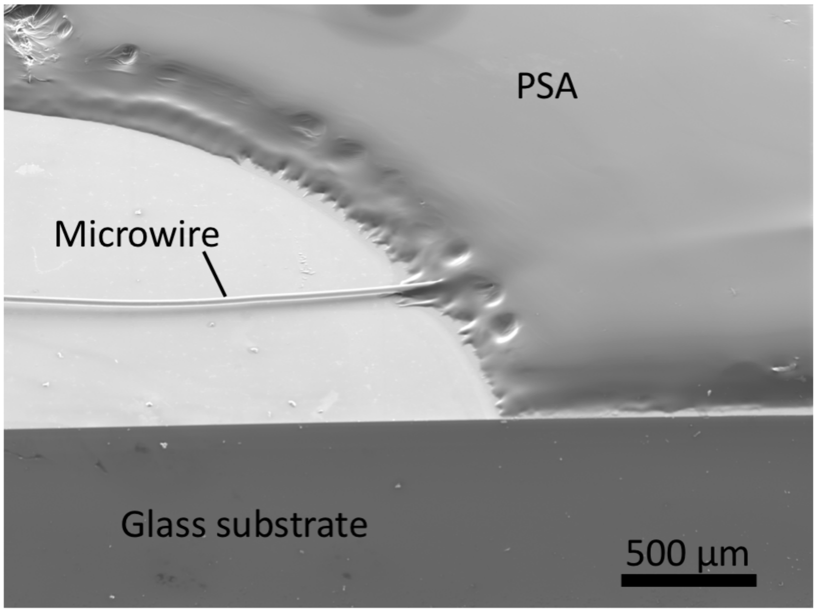

Figure 4.3 Microwire-adhesive interface imaged with SEM

4.1.1 Partially cured liquid adhesive

The integration method above can also be applied to liquid adhesives. Liquid adhesive can be partially cured into high viscous layer, e.g. B-stage epoxy and partially cured PDMS adhesive. The partially cured adhesive is equivalent to the adhesive films and can be used for microwire direct writing.

An example of a process flow using PDMS prepolymer adhesive is shown in Figure 4.4. First, the uncured PDMS prepolymer was spin-coated on a silicon wafer at 1500 rpm for 30s to obtain a thin film with thickness about 50 µm (Figure 4.4a) and baked at 60 ºC for 3 min to partially cure the prepolymer to a highly viscous film (Figure 4.4b). Next, a 50 µm copper microwire was written on the partially cured prepolymer film (Figure 4.4c). Subsequently, the partially cured prepolymer film with integrated microwire electrodes was used to seal a PDMS microchannel. The PDMS microchannel was aligned and stamped on the partially cured prepolymer film (Figure 4.4d). The microwires were embedded into the prepolymer film except the region under the microchannel (Figure 4.4e). Finally, the assembled device was then baked at 80 ºC for half an hour to cure the prepolymer (Figure 4.4f).

The adhesive layer can also be selectively coated on the substrate with microchannel features through microcontact printing. The substrate would be stamped on the partially cured PDMS adhesive and the adhesive would only be coated on the areas to be bonded excluding the microchannel regions. The microwire would be then written on this adhesive layer.

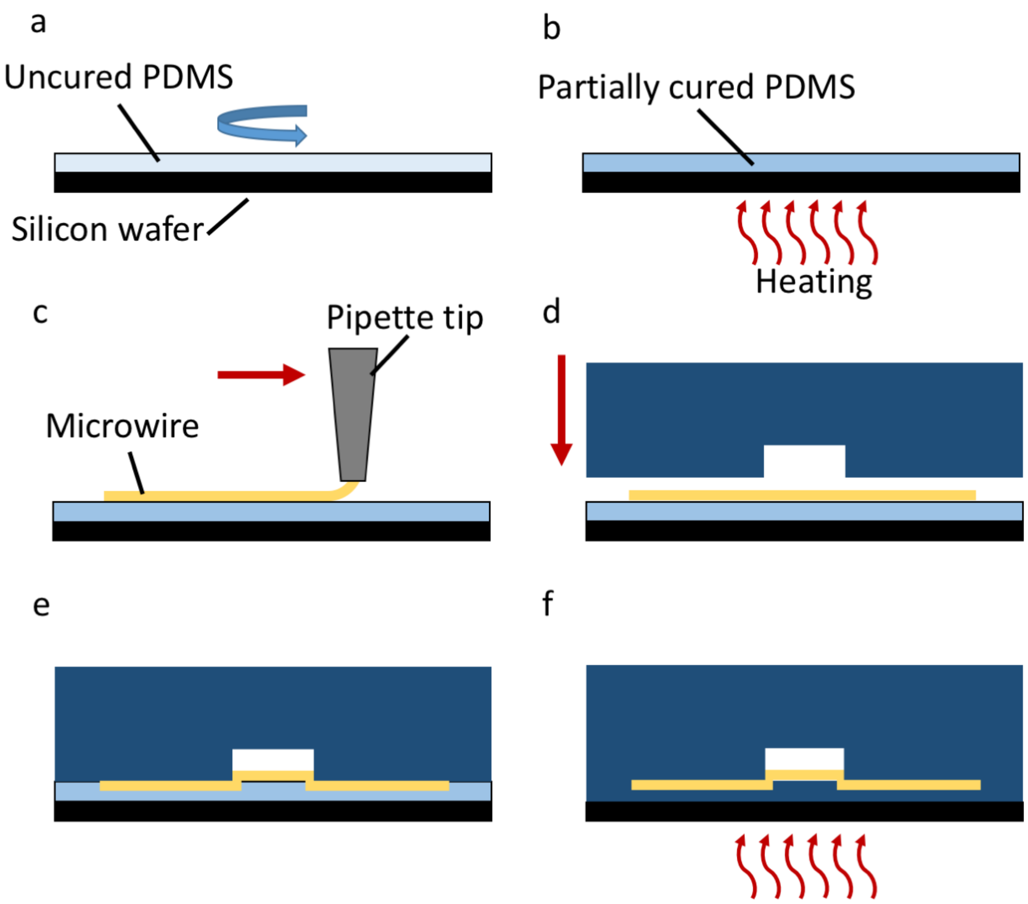

Figure 4.4 Partially cured PDMS adhesive-based microwire integration

A resulting microwire-integrated PDMS microchannel was imaged with microscope (Figure 4.5). The thin PDMS adhesive was cured as a membrane on top of the microchannel. The microwire was integrated between the membrane and the PDMS channel. The region inside the microchannel was exposed to the microchannel.

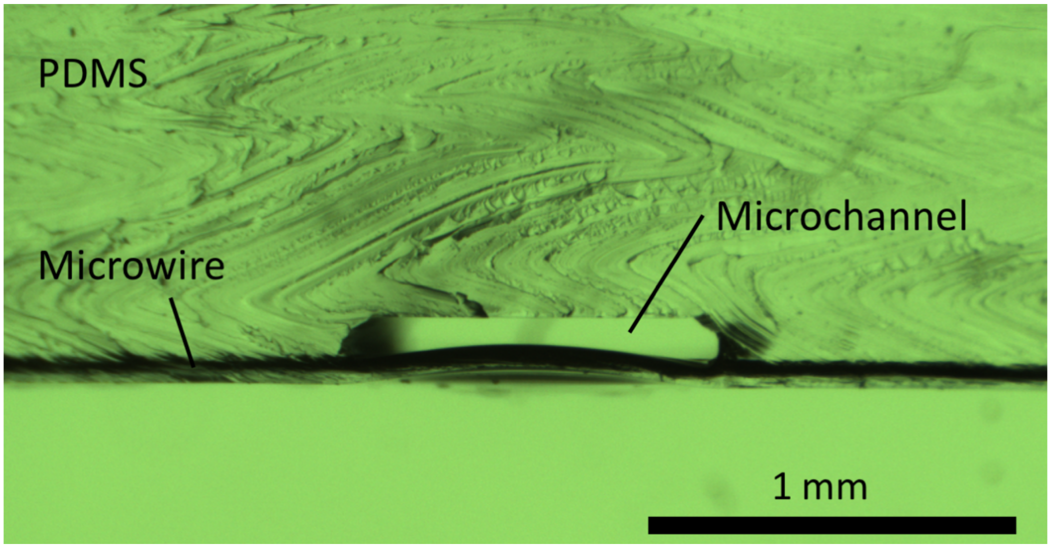

Figure 4.5 Micrograph of a 50 μm copper microwire integrated into a PDMS microchannel through partially cured PDMS.

4.1.2 Microwire writing

In chapter 3, the customized pen is a stainless steel syringe needle encapsulated with a heat-shrink-tube to insert and write the microwire into the originally closed slits. To write the microwires on adhesive surface, however, a stiff pen is not necessary. Instead, plastic pipette tip (AD10EK, Diamed Lab Supplies Inc., Mississauga, Ontario) is used in this chapter.

Microwires were first written on the adhesive manually for preliminary test. When the pipette tip got in contact with the adhesive, it peeled off the adhesive easily. When the pipette tip got too far from the adhesive film, the microwire wasn't in contact with the adhesive and cannot be written on it. Therefore, the distance between the pipette tip and the adhesive needed to be controlled.

Therefore, in order to control the position of the writing tip to the substrate as well as the writing force, various designs for the pen were considered. The initial design of the pen is shown in Figure 4.6. The pen body and the lid were 3D printed with thread on them for assembly. A spring (9657K81, McMaster-Carr) with outside diameter of 4.75 mm and spring constant of 0.03 N/m was placed into the chamber in the pen body with diameter of 5 mm. The pipette tip was subsequently inserted into the chamber and supported by the spring. The lid was then screwed into the pen body and the spring pushed the pipette tip against the lid and the position of the pipette tip can be adjusted by screwing the lid in and out. Before writing the microwire electrode, the pipette tip in the customized pen was adjusted down to be close to the adhesive layer with gap smaller than the diameter of the microwire.

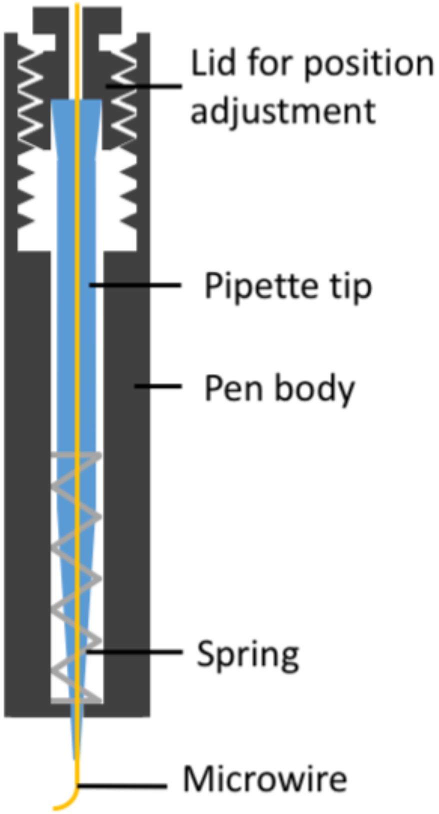

Figure 4.6 Customized pen with adjustable pipette tip position.

However, the result of writing using a pen of this configuration was not repeatable when the pipette tip position was fixed with respect to the substrate. This may be due to several factors. The film thickness may be non-uniform. Alternatively, the cutting mat may not be perfectly flat or the cutting machine may not have a smooth motion leading to vibration or wobble of the tip. The distance between the pipette tip and the adhesive should be such that it should not come in contact, but should be smaller than the diameter of the wire to embed the wire firmly. If the pipette tip touches the adhesive during writing, the adhesive film it traverses through would stick with the tip and be peeled off. If the pipette tip is too far from the adhesive film, the microwire cannot be embedded on the adhesive. Instead of adding precise position control components to the machine, this problem was solved by a modification to the customized pen with two springs on both side of the pipette tip (Figure 4.7a). The second spring provides room for the pipette tip to move up during writing. The stiffness of the spring is small enough to lower the possible pressure on the adhesive film. During writing, the force balance on the pipette tip would be $F_{spring1} + F_{spring2} + F_{writing} = 0$ as shown in Figure 4.7b. $F_{spring1} = k\Delta x$ and $F_{spring2} = -k\Delta x$ where k is the stiffness of the springs and Δx is the variation of the position of pipette during writing. With the soft spring used in the design (k = 0.03 N/m) and a large variation of 1 mm ($\Delta x = 1\,mm$), the pressure on the film would be $F_{writing} = 60$ µN. The actual pressure would be smaller as the whole film thickness is normally several hundred microns. Therefore, the initial position of the pipette tip can be closer to the adhesive film to ensure the contact between the microwire and the adhesive film. The pipette tip adjusts its position automatically and the writing force generated is very small.

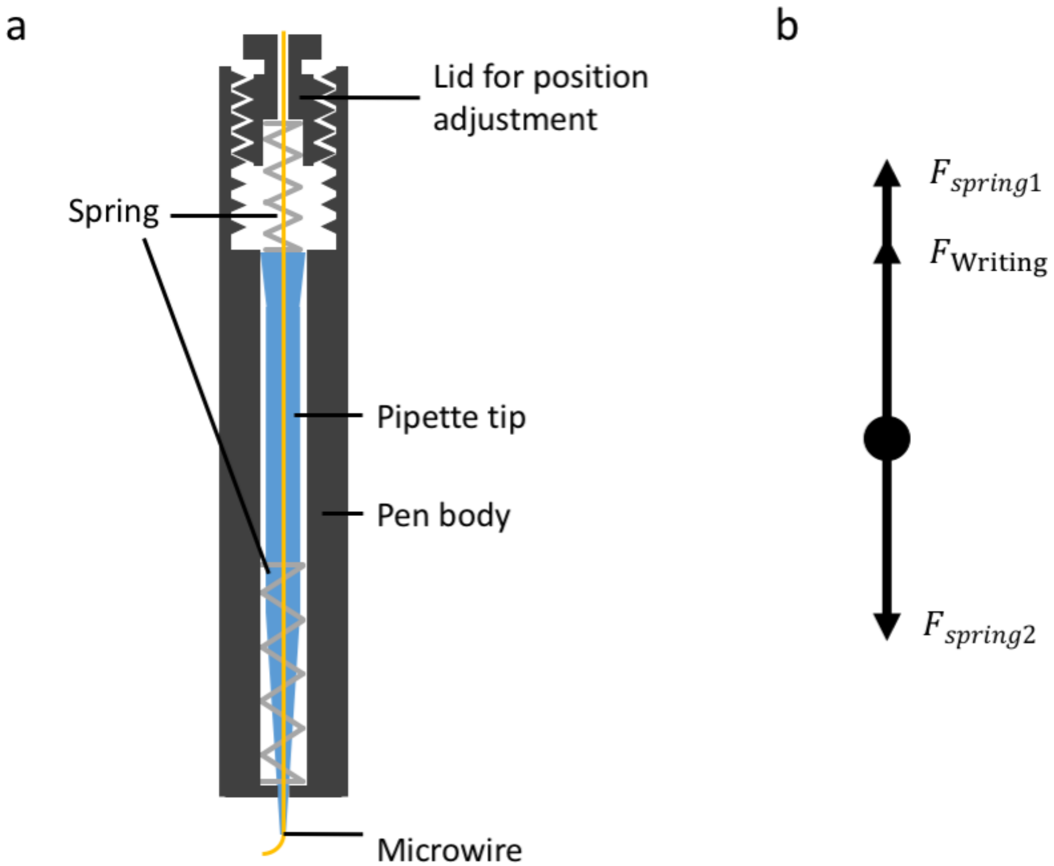

Figure 4.7 a) Modified customized pen design with two springs. b) Force balance on the pipette tip during writing.

4.1.3 Resolution

The resolution of the microwire writing was defined as the smallest spacing between two parallel lines. Silver microwires (50 µm in diameter) were written into serpentine microelectrode patterns with spacing of 100 to 500 µm between the lines on a PSA film. Micrographs of the written microwires with spacing from 100 to 300 µm are shown in

Figure 4.8. The adjacent lines of the serpentine pattern overlapped with each other when the spacing was 100 or 200 µm. At 250 µm spacing the microwires were not overlapping with each other but the spacing between the wires varies significantly from that in the design pattern. The spacing between the microwires become uniform and accurately reproduced the design pattern above 300 µm.

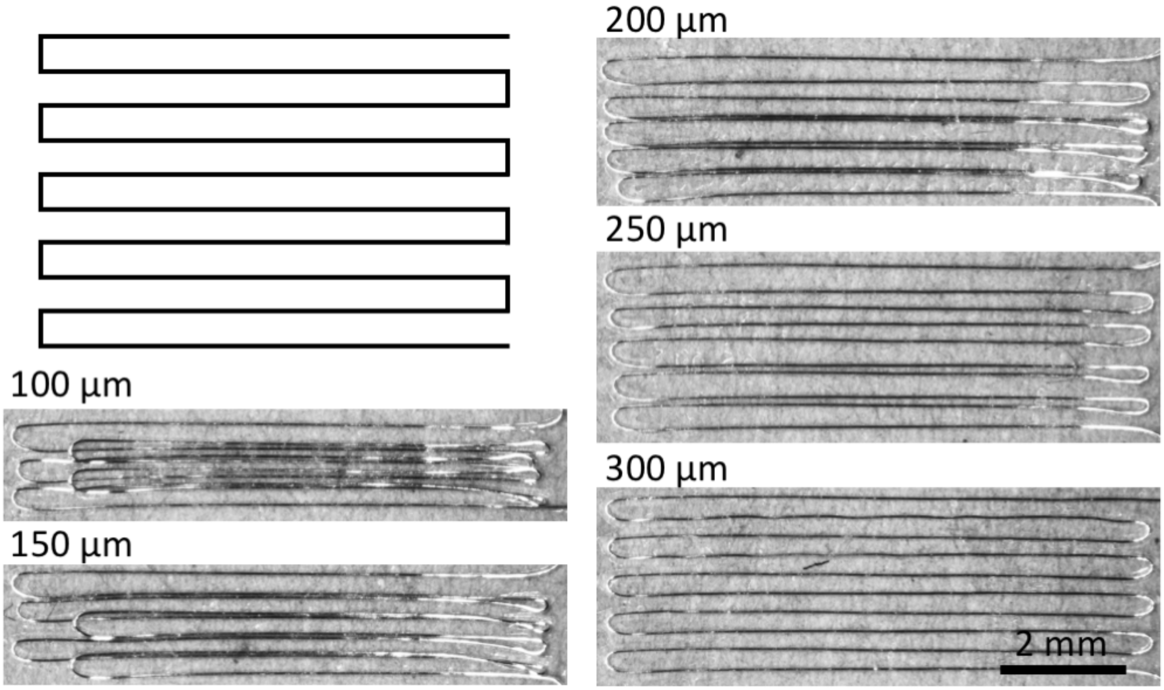

Figure 4.8 Characterization of resolution of microwire writing. The pattern used to characterize resolution (upper left) and the micrograph of microwires with different spacing.

The quantitative measure of the spacing between the microwire electrodes were measured from the micrographs as shown in Figure 4.9. The spacing equal to or larger than 300 µm is repeatable and linear with slope of 1.04. Even though the microwires are not overlapping with pattern designed with 250 μm spacing, the variation of the spacing is very large and the average spacing of 281 μm is also significantly different from the linear fitting. High resolution cutting plotter or reducing pen nozzle size can help improve the resolution of microwire writing.

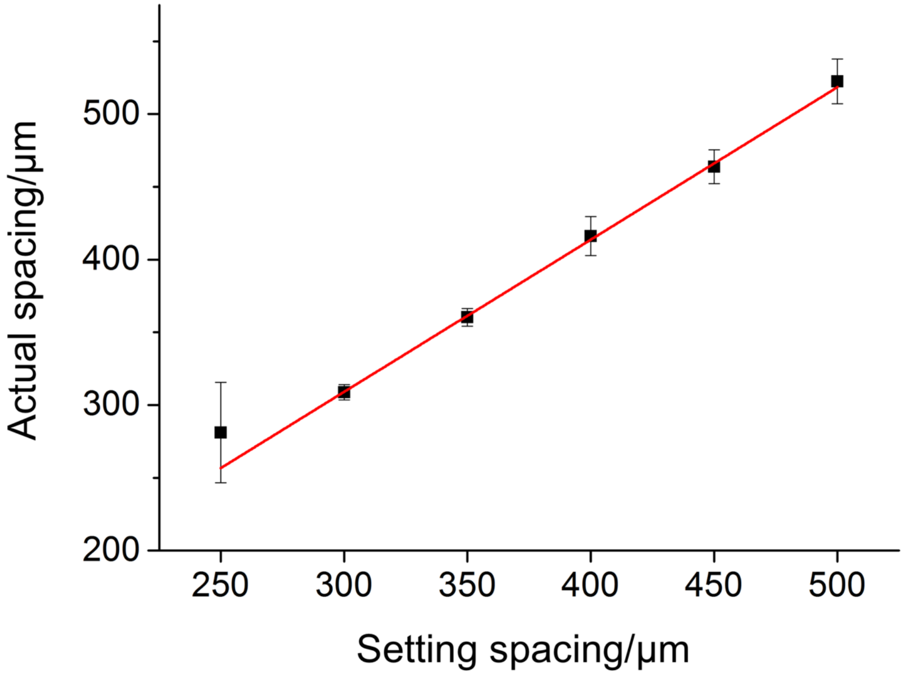

Figure 4.9 Actual microwire spacing vs. designed spacing in the microelectrode pattern

4.1.4 Writing electrode patterns with turning

It can be observed from Figure 4.8 that the designed right angle turnings are written as circular turnings. The reason for this transformation can be possibly explained by the movement of the wire inside the writing tip as shown in Figure 4.10. The dotted red line in this figure shows the intended path of the pipette tip at a sharp corner. During the writing process, the microwire whose size is smaller than the nozzle of the pipette tip, is positioned at the edge of the nozzle opposite to the moving direction. During a turn, the position of the wire changes from the 9^{o} clock position to the 12^{o} clock position as the pipette tip does not rotate. This translocation of the wire inside the pipette tip leads to a change in its trajectory on the adhesive which is different from that of the pipette tip itself.

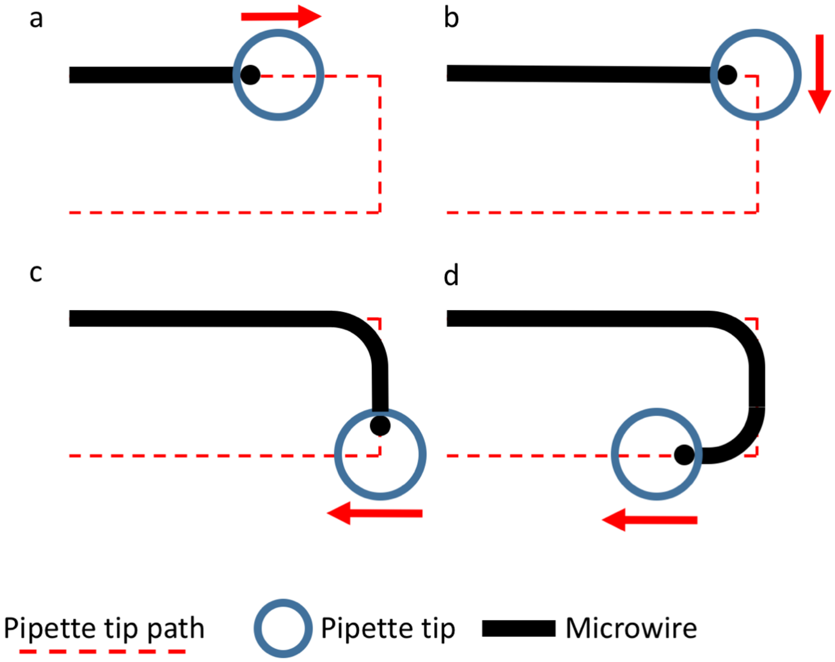

Figure 4.10 Formation of circular corner

4.1.5 Multiple microwire electrode integration

As the microwires are written continuously, only one continuous microwire electrode can be written at a time. However, for flexible LOC devices which are thin enough to be cut, multiple independent microwire electrodes can be obtained by drawing a continuous pattern with turns at a common region which can be subsequently cut to isolate the individual electrodes from one another. As shown in Figure 4.11a, a microwire electrode was first integrated as a continuous serpentine pattern. After integration, the turnings of the serpentine pattern were trimmed, leaving an array of parallel microwire electrodes (Figure 4.11b). The image of the trimmed surface shows that the array of integrated microwires (Figure 4.11c).

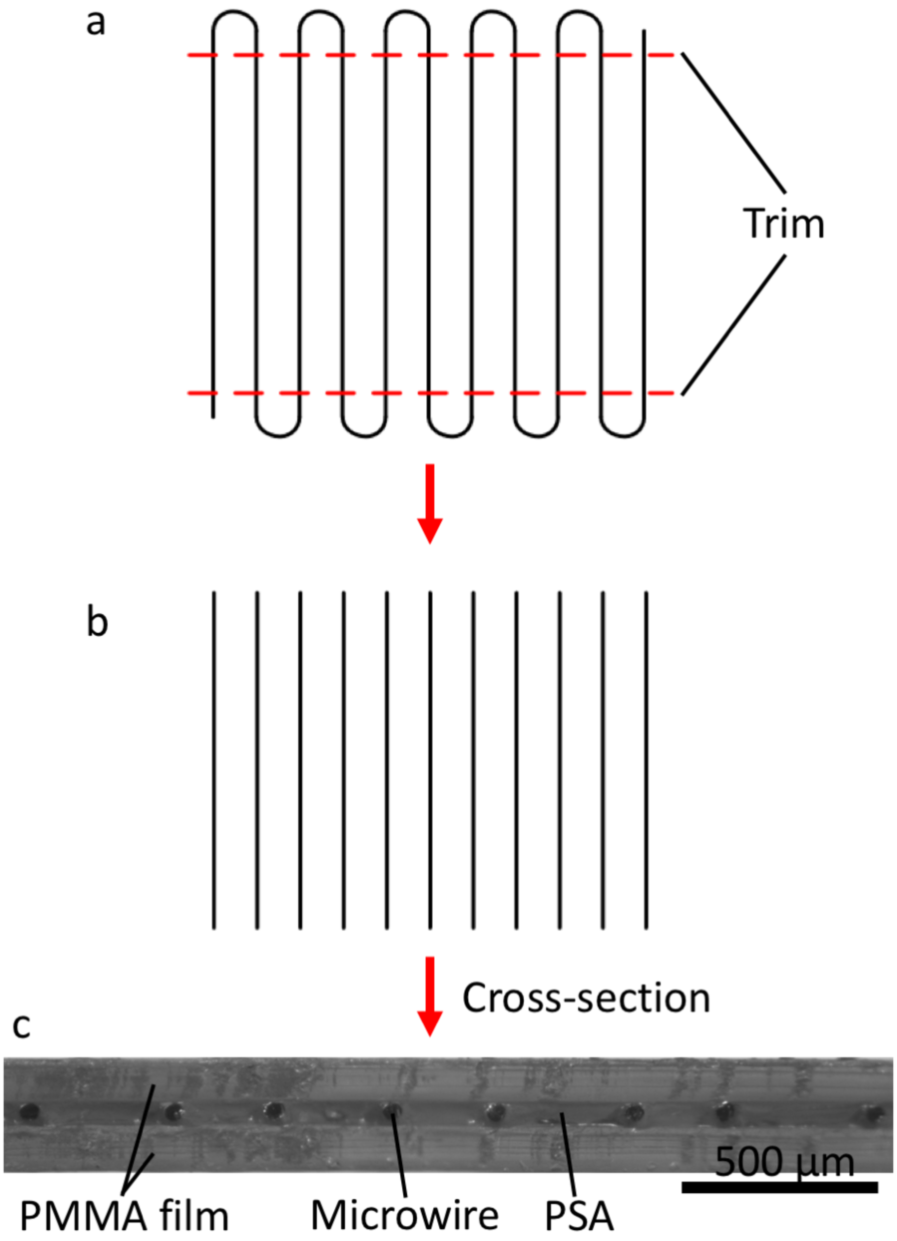

Figure 4.11 An array of microwire electrodes obtained by trimming the continuous microwire electrode. a. The pattern of the written microwire electrode (Black) and the path for trimming (Red). b. The microwire electrode pattern after trimming. c. Cross-section of the trimmed multiple microwire electrodes.

Multiple microwires can also be obtained at different positions in the height direction. Three 50 μm silver microwires were written into three 125 μm PMMA films with laminated PSA and assembled together. The microwires were aligned to be at the same location along the microchannel but at different height (Figure 4.12a&b). The device was trimmed perpendicular to the microwires to further show their relative positions (Figure 4.12c). These microwire electrodes are useful for integrating multiple electrodes at the same position or further enhancement of interaction between the electrodes and the solution.

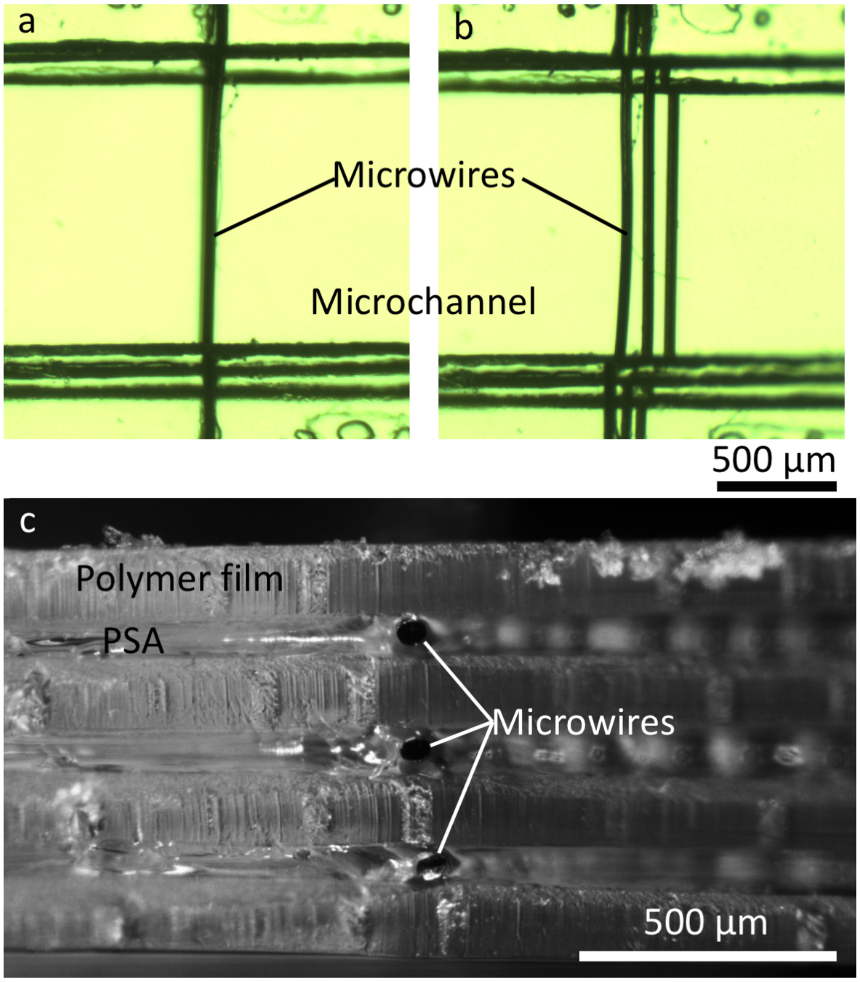

Figure 4.12 Three silver microwires integrated into the same location along the microchannel but different layers of a multilayer device. a. Top view of the integrated microwires. b. Tilt-view of the integrated microwires. c. Cross-section of the multilayer device with three integrated microwires.

4.1.6 Effect of microwire hardness

Other than diameter and material, the hardness of the microwire should also be considered when selecting the microwire to be integrated. The hardness of the microwire represents its resistance to bending. Microwires that can be easily integrated using the xurographic process generally have low hardness. As the microwire would be bent by the tip of the pen during the writing process, soft microwires with low resistance to bending, would be easily bent and embedded to the adhesive film and remain adhered to it (Figure 4.13a). For hard microwires, the writing process was not strong enough to completely bend the microwire and the adhesive force when it is embedded was in sufficient to retain it in its shape (Figure 4.13b). Commercially available wires do not have defined hardness values, therefore one should select annealed microwire as opposed to hard microwires.

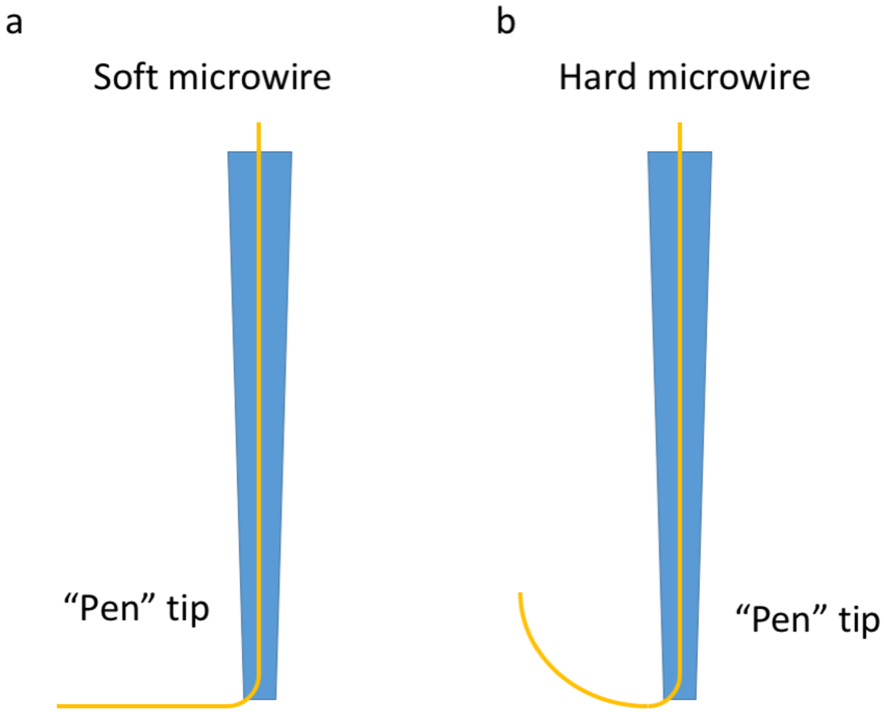

Figure 4.13 Soft microwire (a) vs. hard microwire (b) during microwire writing.

4.2 Application examples

4.2.1 Microfluidic heaters

As discussed in 3.3.1, microfluidic heaters are important in many applications such as PCR and cell culture. With the adhesive-based microwire integration technique, heater can be integrated directly at the bottom or top of a closed microchannel.

A microfluidic heater was designed with a multilayer structure as shown in Figure 4.14a. All the polymer film used in this design was 125 μm thick PMMA. PSA films were laminated on the PMMA film before patterning as shown in the figure. From top to bottom, it contains 4 layers. The first layer is the reservoir layer which is a PMMA/PSA film that has been patterned with two circular reservoirs with diameter of 2 mm. The second layer is the microchannel layer which is a PMMA/PSA film patterned with a U-shape microchannel with width of 500 μm. The third layer is the heater layer which is a PMMA/PSA film with a 50 μm silver microwire heater written on the PSA film. The bottom layer is the electrical connection layer which is a PMMA film with two conductive tape (76555A711, McMaster-Carr) on it. After assembly, both ends of the silver microwire was pressed on the conductive tape and embedded into the PSA film.

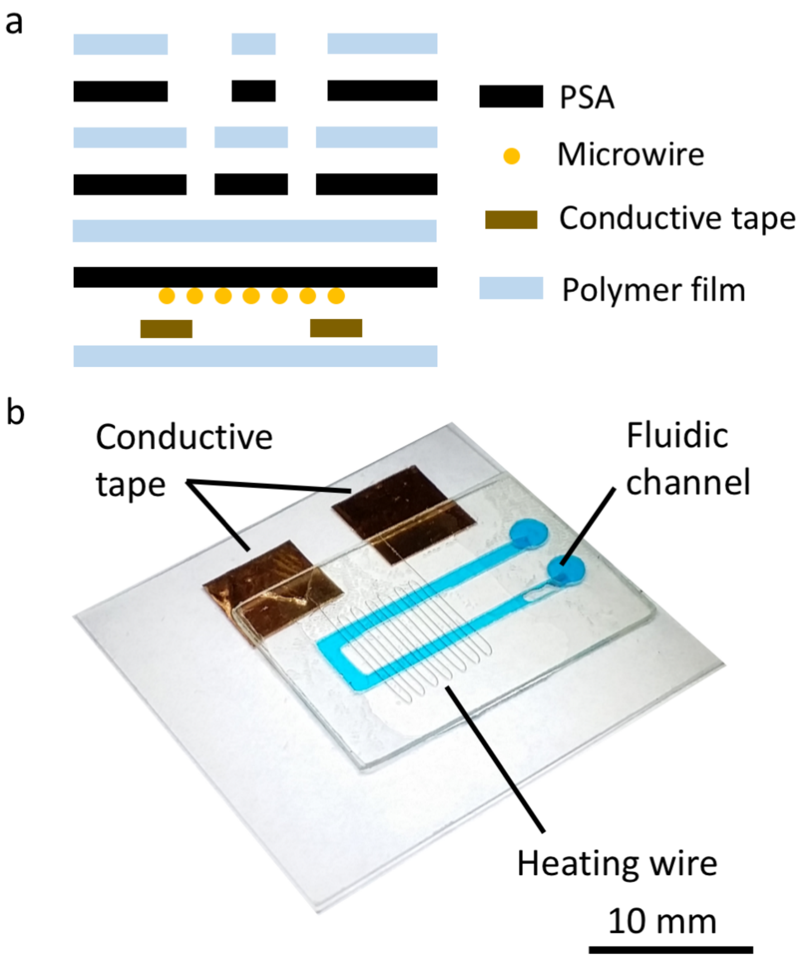

Figure 4.14 An assembled microfluidic heater.

Before experiment, the resistance of the microwire was measured to be 2 Ω with MultiMate. A DC power supply was connected to the two conductive tape to power the heater through two alligator clips (Figure 4.15a). The temperature was measured with a thermal imaging camera (Flir ONE, FLIR® Systems, Inc.). Before heating, the temperature in the heater area is about 25 ºC (Figure 4.15b). The heater was powered with 0.5 V voltage with current of 0.25 A. After about 3 min when the temperature variation was within 0.5 ºC, the temperature was measured again (Figure 4.15c). The highest temperature of 60.6 ºC was measured at the heater area. The color in the heater area was roughly uniform, indicating a relatively uniform temperature distribution. The average temperature on the heater area is 58.4 ºC with standard deviation of 0.84 ºC.

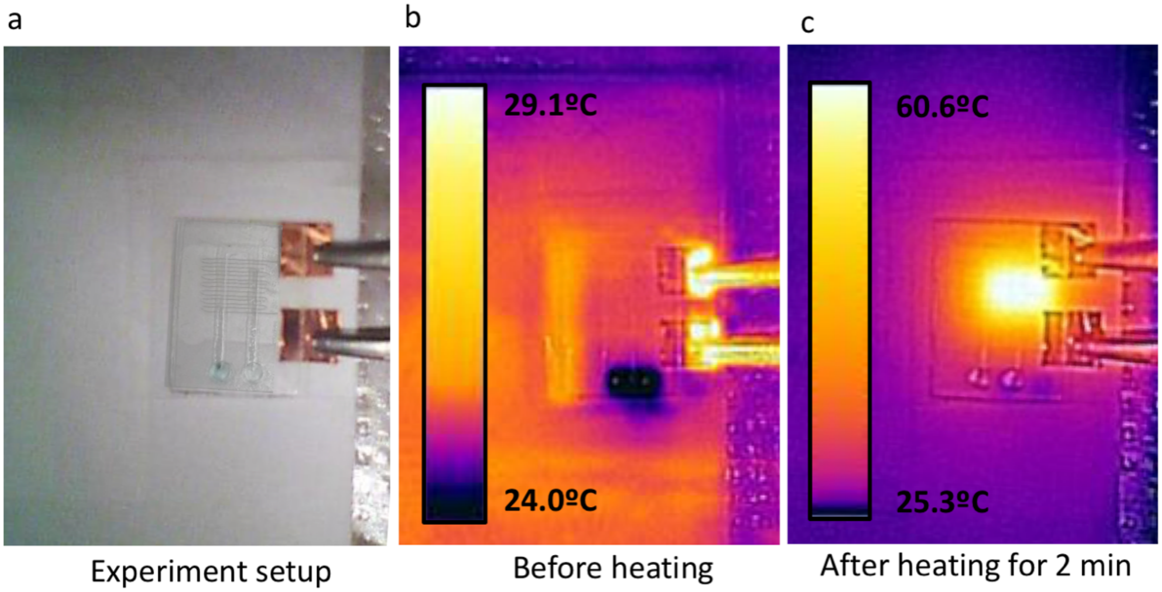

Figure 4.15 a) Experiment setup to test the integrated heater. b) Thermograph before heating. c)Thermograph after heating.

4.2.2 Electro-osmosis mixer

An electro-osmosis mixer with the same principle in Figure 3.24 is designed as Figure 4.16a. The mixer contains a reservoir layer, two microchannel layer and a bottom layer. Similarly, the polymer films used in the design were 125 µm PMMA films. On top was the reservoir layer with two circular reservoirs (diameter: 2 mm) patterned on a PMMA/PSA film. The microchannel layers were 500 µm wide Y-shape microchannels pattern on two PMMA/PSA film. The electro-osmotic electrodes were written on the PSA of the first microchannel layer. The bottom layer was a PMMA film with no pattern. After assembly (Figure 4.16b), the microwires were embedded into the middle of the two microchannel layers (Figure 4.16c).

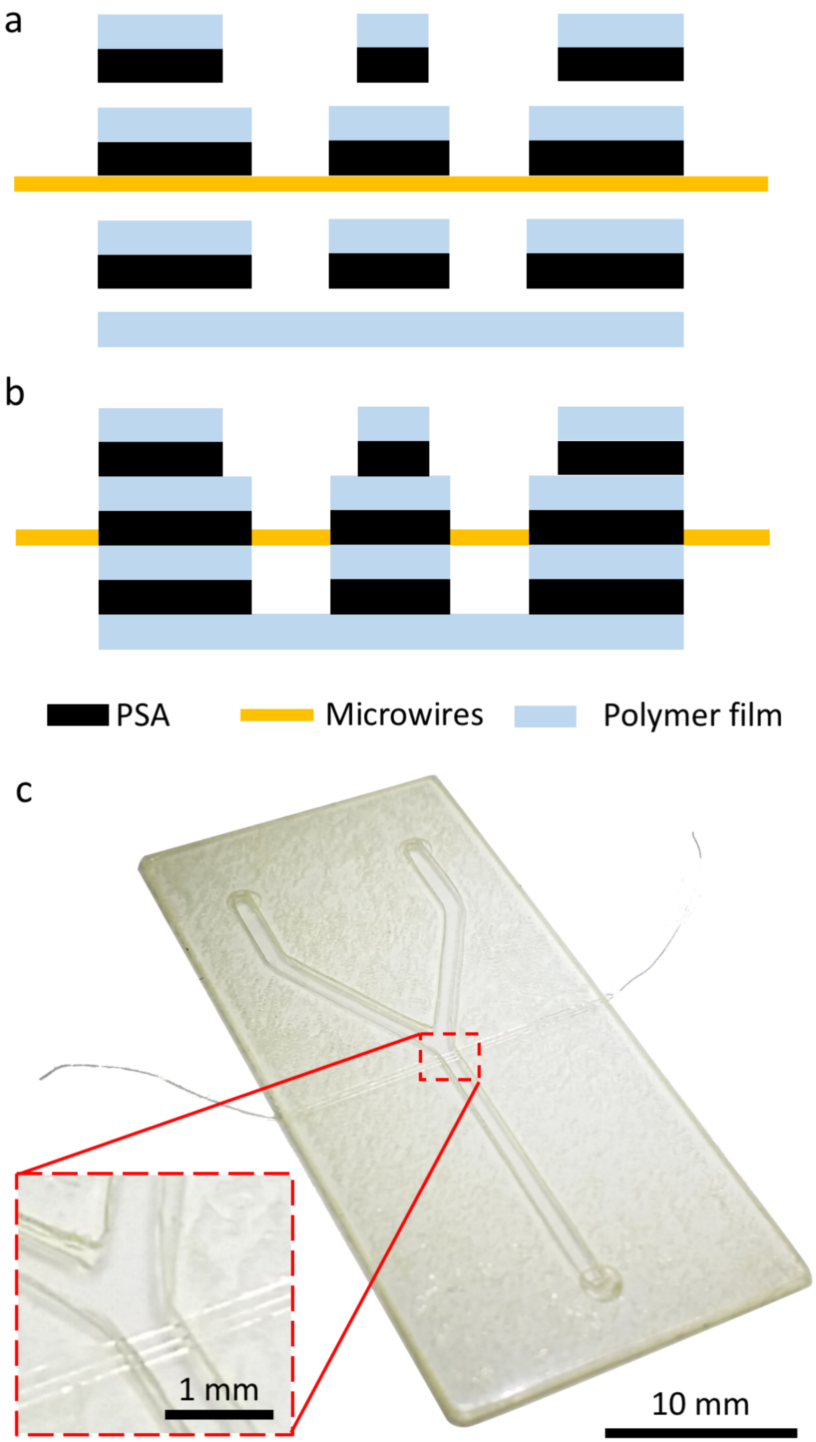

Figure 4.16 Design of an electro-osmosis mixer with microwire electrodes integrated based on PSA.

DI water with red and green food color were injected into the Y-shape microchannel and mixed. 10 kHz AC voltage from 50 V to 200 V was applied to the microwire electrodes at both ends. The mixing was observed with microscope (Figure 4.17). The observed result is similar to the result in 3.3.3. The dyed water solutions tended to be fully mixed with increased applied voltage. The boundary between the red and green solution was not observable when the applied voltage increased to 200 V.

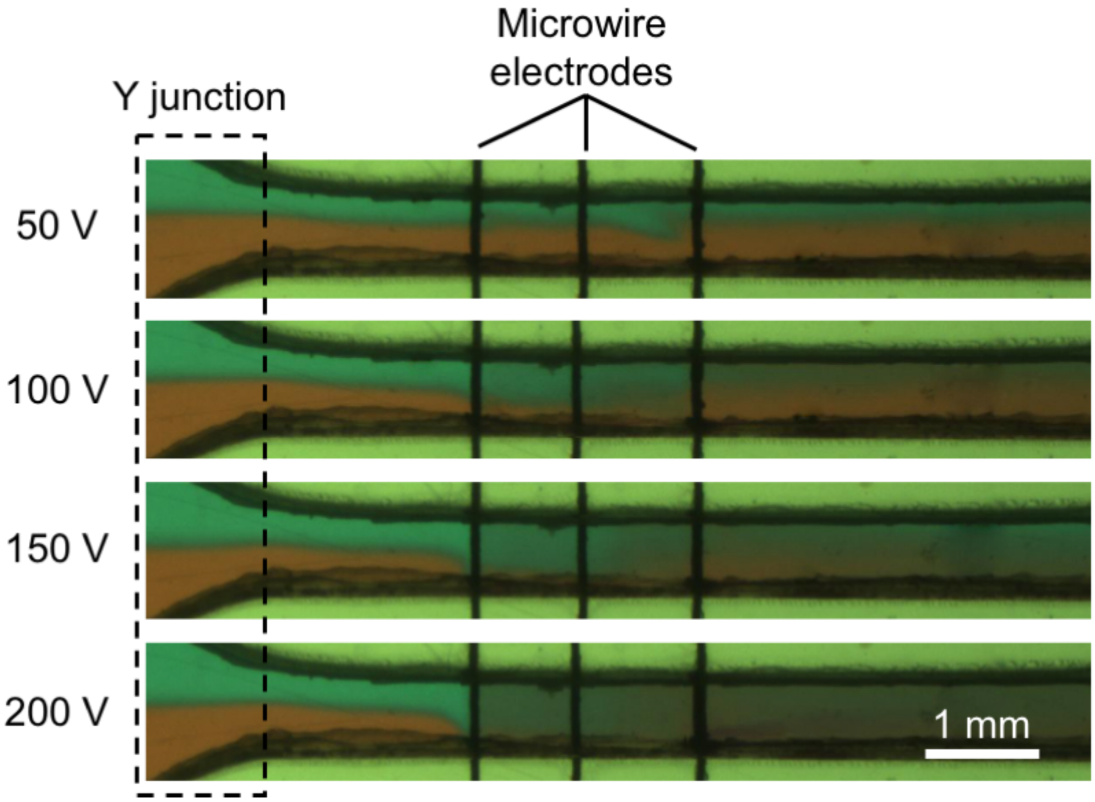

Figure 4.17 Electro-osmosis mixing under different voltage

4.2.3 Electrochemical sensor

Electrochemical detection is low-cost, sensitive and can be easily integrated into microfabrication processes. In 3.3.2 a microwire-based electrochemical sensor integrated into PDMS LOC device was presented. In this section a microwire-based electrochemical sensor is integrated into rigid polymeric device.

The design of the three electrode electrochemical sensor is shown in Figure 4.18a. From top to bottom, it contains a reservoir layer, a microchannel layer and an electrical connection layer. The reservoir layer was a PMMA film patterned with two circular reservoirs with diameter of 2 mm. The microchannel layer was a PSA/PMMA/PSA film patterned with a microchannel with width of 1 mm and length of 20 mm. A carbon nanotube microwire working electrode, a 50 μm silver microwire reference electrode and a 50 μm platinum microwire counter electrode were written on the bottom PSA film with spacing of 500 μm between them. The electrical connection layer was a PMMA film 5 mm wider than the other films. Three conductive tape was taped on the edge of the PMMA film to provide electrical connection to the microwire electrodes. After assembly (Figure 4.18b), the microchannel was filled with 1 M KCl solution and then 2 V DC anodization was applied to grow silver chloride on the silver microwire electrode. After silver microwire modification, the microchannel was rinsed with DI water.

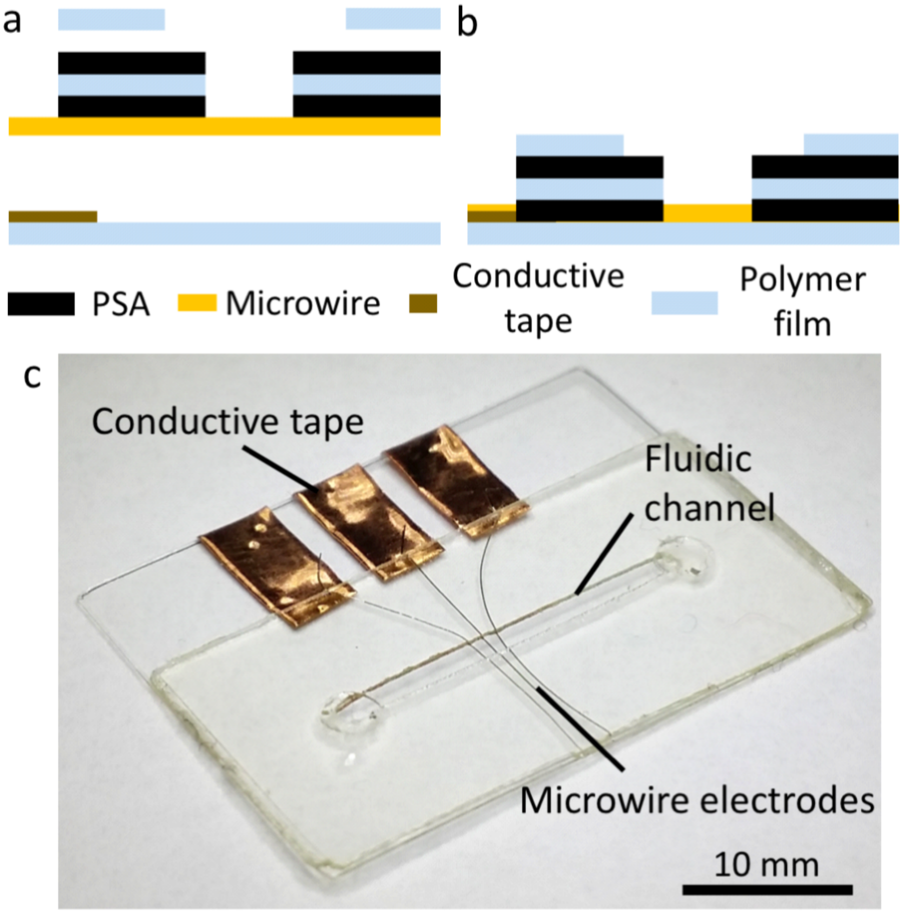

Figure 4.18 Design of the electrochemical sensor a) Before assembly. b) After assembly. c) Photography of an assembled electrochemical sensor.

The electrochemical sensor was tested with cyclic voltammetry of ferricyanide. Potassium ferricyanide (1 mM) in 1 M KCl was injected into the microchannel. Cyclic voltage between 0 to 0.5 V with step voltage of 5 mV was applied to the working and counter electrodes. The cyclic voltammetry was completed with EmStat potentiostat (PalmSens

Inc.). The cyclic voltammetry was run at different scan rate of 50, 100, 200, 300, 400, 500 mV/s. The result is shown in Figure 4.19. The redox current increases with increased scan rate as expected. For each scan rate the cyclic voltammetry was repeated 10 times with similar results.

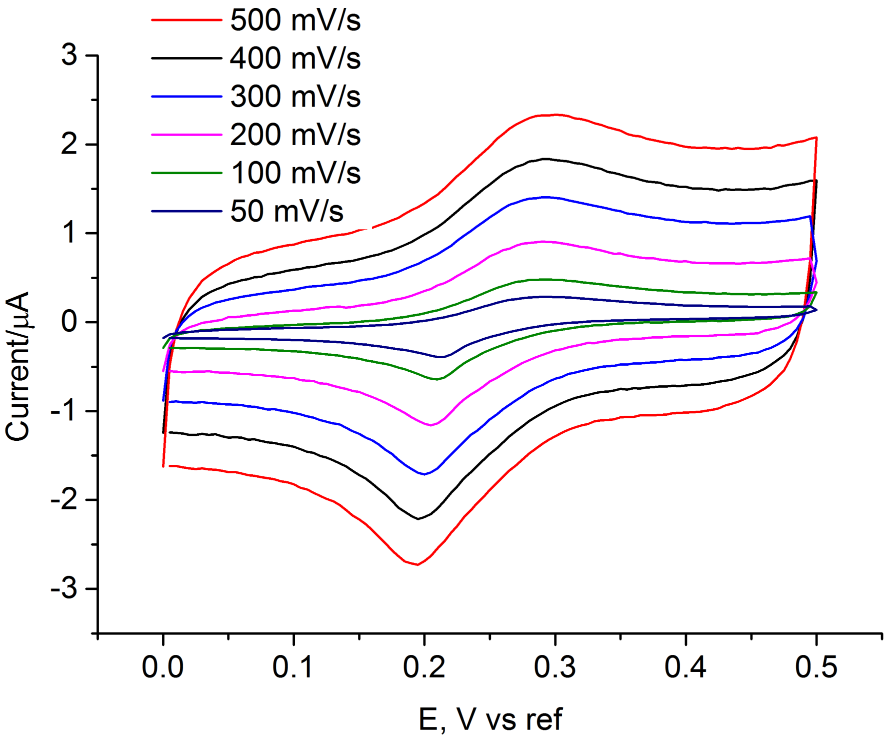

Figure 4.19 Cyclic voltammetry of ferricyanide with the three electrode electrochemical sensor.

4.3 Conclusion

In this chapter an adhesive-based xurographic process for microwire electrode integration for most of the polymer material was established. The microwires were written on the adhesive layer and integrated into the LOC device during adhesive bonding. The minimum spacing between two microwires is 300 μm. The position of the microwire in the height direction can be controlled by overlapping multiple microchannel layers. Multiple microwire electrode can be obtained by trimming a continuous microwire electrode.

The xurographic microwire electrode integration process established in this chapter can be incorporated with original xurography techniques to fabricate microelectrode-integrated, flexible, low-cost, polymeric LOC devices. Application examples including an integrated heater, electro-osmosis mixer and electrochemical sensor were demonstrated.

Chapter 5: Conclusion and future work

5.1 Conclusion

Integration of metallic microelectrodes into LOC devices has always been a challenging issue. A diversity of techniques has been developed for microelectrode integration, such as PVD, electroplating, electroless plating, and metallic nanoparticle sintering, which has been briefly reviewed in chapter 2. These techniques, however, either require expensive facilities, labor-intensive operation, time-consuming process or have limitations on material and dimension of the microelectrodes. Microwires are promising candidates for microelectrodes but the existing integration techniques for microwires can only integrate a straight microwire into a LOC device. In this thesis, xurography was modified and used to integrate the microwire electrodes into elastomers and rigid polymers. Low-cost cutting plotter was used to fabricate the microfluidic channels and integrate the microwire electrodes into the microfluidic devices. Microwires down to 15 μm have been successfully integrated. Microwires of smaller diameter are commercially available and can be possibly integrated into LOC devices. Numerous materials choices for the microelectrode are commercially available with uniform diameter and purity. For the first time, suspended microelectrode with controllable position in the height direction can be integrated into polymeric LOC devices.

Implementation of microwire solved many problems typical of other microelectrode fabrication techniques. First, microwires with diameter from 4 μm to hundreds of μm are commercially available, which eliminated the need for expensive lithography based fabrication methods for define high quality microelectrodes. Secondly, the quality of these microwires, including purity and diameter, are well controlled and standardized, which makes them of better quality as compared to some of the more experimental microelectrode fabrication techniques that require careful parametric control to produce consistent high quality microelectrodes. Thirdly, these microwire electrodes are manufactured by wire drawing and subsequent annealing with excellent mechanical properties, e.g. tensile strength comparable to bulk material. In contrast, the microelectrodes fabricated by other microelectrode fabrication techniques especially on polymeric substrates are fragile because they cannot be annealed at high temperatures.

The xurographic process for microchannel fabrication and microwire electrode integration is both completed with a cutting plotter, whose price can be as low as 200 USD to about 4000 USD for high resolution. A 200 USD cutting plotter has been used in our experiment and demonstrated sufficient capability to complete these two process, which is affordable to any laboratories, especially those without access to cleanroom facilities, PVD machine and other equipment.

However, the xurographic process can only be used to integrate microwire/fiber components into LOC devices. Because of the shape of the microwires, it is not easy to have a microwire electrode with a large surface area. Increasing the diameter of the microwire might partially or completely block the microchannel. Alternatively, a large surface might be obtained by integrating a dense serpentine pattern. Nevertheless, a more efficient technique is needed to provide electrical connection to the microwire electrodes, especially when a number of microwire electrodes has been integrated or the microwire electrodes are integrated closely. Furthermore, the xurographic process is based on adhesive bonding but adhesive bonding might not be a good option for applications requiring high bonding strength. The adhesive layer would also introduce unwanted material to the microchannel wall.

5.2 Future work

Even though the versatility of the xurographic microwire integration process has been demonstrated in the previous chapters, the fidelity of the microwire electrode pattern can be further improved. Using higher resolution cutting plotter such as Graphtec professional cutting plotters (FC5100A-75, Graphtec America, Irvine, CA, USA) can significantly improve the resolution. Besides upgrading the cutting plotter, there are some aspects to be optimized to further improve the fidelity of microelectrode pattern. In the case of microwire integration into PDMS, the microelectrode pattern is defined by the slit pattern on PDMS. The large deformation of PDMS during slit cutting, however, affects the fidelity of the slit pattern. It can be solved by hardening the PDMS, i.e. increasing the ratio of silicone base. The increased hardness can reduce the deformation of PDMS during slit cutting. In the case of adhesive-based microwire integration, the microelectrode pattern is determined by the direct writing process and the adhesion between the adhesive layer and the microwire that kept the microwire at the written position. Therefore, optimization of the distance between the pen nozzle and the adhesive layer as well as choosing the right adhesive type can help improve the fidelity of the written microwire electrode pattern.

The xurographic process enables integration of suspended microwire electrodes inside the microchannel for the first time. These suspended microwire electrodes enables better interaction with the fluid inside the microchannel. These suspended microelectrodes can be used to drive electrokinetic flow in the middle of the microchannel, which has been demonstrated in the electro-osmostic mixer in previous chapters. The microwire electrodes in these designs can be optimized, e.g. by altering the direction of the middle polarizable microwire electrode. A slanted microwire electrode can induce electro-osmotic flow perpendicular to the boundary between the two solutions to be mixed and improve mixing efficiency. The mixing efficiency can be further improved by integrating multiple microwire electrodes at different height in the microchannel.

Moreover, as multi-layer microwire electrodes can be integrated, connecting these multi-layer microwire electrodes and building 3D microwire electrodes with these xurographic process would be one of the future work. One possible solution would be via holes. For a multilayer device with integrated microwire electrodes on multiple layers, small holes would be cut on all the layers at the location where the microwires in different layers should be connected. After alignment and assembly, these small holes stack together to be a via hole, with the microwires to be connected exposed inside the via hole. A small drop of solder paste or low melting point metal would then be added to the via hole and soldered/cooled down, connecting all the microwires in the via hole. This technique can be used to fabricate 3D microelectrodes such as 3D microcoils for NMR [121].

Appendix A: Xurographic microwire integration process for PDMS

A.1 Xurographic PDMS microchannel fabrication

1) Laminate the adhesive-back polymer film with desired thickness on the cutting mat.

2) Feed the cutting mat into the cutting plotter.

3) Convert the designed microchannel pattern to vector format (usually .def. or .svg) and import it into the control software of the cutting plotter.

4) Place the microchannel pattern at the position to be cut. If an array of microchannel is wanted, duplicate it and array them correctly.

5) Set the cutting parameters and run the cutting plotter to cut the pattern on the adhesive-back polymer film.

6) Trim a transfer tape to a size that covers all the microchannel patterns and laminate it

on the microchannel patterns. Apply pressure to bond the transfer tape to the patterns firmly.

7) Peel off the transfer tape and the microchannel patterns should be peeled off together with the transfer tape.

8) Laminate the transfer tape on a clean glass/silicon substrate. Apply pressure to bond the microchannel pattern to the substrate then remove the transfer tape, leaving the microchannel pattern (array) on the substrate as the master mold for PDMS micromolding.

9) Prepare PDMS by mixing silicone base and curing agent with ratio of 10:1, pour it on the polymer film master mold and degas it for 30 min.

10) Cured the PDMS in oven at 80 ºC for 1 h.

11) Peel off the PDMS slab from the master mold.

A.2 Xurographic microwire electrode integration

1) Laminate the fabricated PDMS with/without microchannel on the PMMA sheet trimmed to the size the same with the original cutting mat.

2) Convert the designed microelectrode pattern to vector format and import it into the control software of the cutting plotter. Duplicate and center the microelectrode pattern. One of the pattern would be set to be written.

3) Align the microelectrode pattern to the position of the PDMS slab. The microelectrode

pattern can be aligned by cutting an alignment mark on the PMMA sheet.

4) Set the cutting parameter according to the desired slit depth and run the cutting plotter to cut the slit pattern on the PDMS slab.

5) Thread the microwire electrode into the customized pen with assistance of a capillary tube. The microwire is adhered to the tip of the capillary tube with a small amount of adhesive (or wiring the microwire electrode around the capillary tube). After inserting the capillary tube through the customized pen, detach the microwire from the capillary tube and withdraw the capillary tube from the customized pen.

6) Install the customized pen on the cutting plotter. If cutting plotter with 1 cartridge is used, replace the cutting blade with the customized pen.

7) Run the writing microelectrode pattern to write the microwire into the slit pattern.

8) Cut the excess portion of the microwire outside the slit pattern.

9) Remove the PDMS slab with integrated microwire electrode from the PMMA sheet.

For cutting plotter with one cartridge, replace the cutting blade with the customized pen replace after slit cutting. The microwire writing is completed by repeating the cutting path.

A.3 Device assembly

1) Prepare uncured PDMS adhesive by mixing silicone base, silicone oil and curing agent

with ratio of 5:5:1.

2) Spin-coat the uncured PDMS adhesive on a silicon wafer or glass slide at 1300 rpm for 30 s.

3) Stamp the PDMS slab with integrated microelectrode on the spin-coated uncured PDMS adhesive for 30 min.

4) Place the PDMS slab with coated adhesive on another PDMS slab.

5) Cure the PDMS adhesive on a hot plate at 150 °C for 10 min.

Appendix B Adhesive-based microwire integration process

B.1 Xurographic polymer film microchannel fabrication

1) Choose the desired polymer film and PSA film with desired property and thickness.

2) Laminate the films with the same pattern together to avoid unnecessary alignment. It could be a pure polymer film, a polymer/PSA film, PSA/polymer/PSA film, polymer/PSA/polymer film according to the design of the microfluidic device.

3) Laminate the polymer film on a flat table. Remove the liner on one side of the PSA

film from one of its corner and laminate it on the polymer film carefully (use a handheld roller or laminator if available). Make sure no visible bubble is trapped between the polymer film and the PSA film which would affect the flatness of the film. Laminate other films in the same way if applicable.

4) Cut small pieces from each of the prepared film with a size of 10 cm x 10 cm. Laminate them on the cutting mat. Feed the cutting mat into the cutting plotter.

5) Draw a rectangle with size of 0.5" x 0.5" and place it in the film area. Set the cutting force at the value recommended by the manufacturer to cut vinyl films.

6) Run the cutting plotter to cut the rectangle on the film. If the blade fails to cut through the film, increase the cutting force by 10 and cut another rectangle in a different location. Repeat until the film is cut through. If the film cannot be cut through even with the highest cutting force, increase the times the machine cuts. Test all the prepared films and record the cutting parameters for each of them. The cut pressure setting in Cricut design space (Provo Craft & Novelty, Inc.) is 333 for a 125 μm PMMA film with laminated PSA film (Scotch 7951, 3M, Inc., Minneapolis, MN) on both side and 311 for a 125 μm PMMA film with laminated PSA film on one side.

7) Trim the prepared film to the size of the cutting mat (12" x 12") if the size of the film exceeds the size of the cutting mat. Laminate the trimmed film on the cutting mat and feed

the cutting mat into the cutting plotter.

8) Convert the designed microchannel pattern to vector format and import it into the control software of the cutting plotter.

9) Arrange all the microchannel patterns to the position to be cut. If an array of microchannel is wanted, duplicate it and align them correctly.

10) Set the cutting parameters as recorded in step 5. Run the program to cut the microchannels on the film.

11) Peel off the pattern polymer film and remove the unwanted area with tweezers.

B.2 Adhesive-based microwire integration process

1) Thread the microwire into the customized pen as described previously and install it on the cutting plotter.

2) Laminate an PSA film (or PSA laminated on polymer film) on the cutting mat and feed the cutting mat into the cutting plotter. Remove the liner of the PSA film facing up.

3) Adjust the lid of the customized pen to the highest position.

4) Draw a simple line pattern and place it on the region with laminated film on it. Set it to be writing pattern.

5) Run the writing pattern and pause the program once the pen goes down to write.

6) Adjust the lid to lower the pipette tip until it touches the film. Exit the program.

7) Convert the microchannel pattern and microelectrode pattern to vector format and import it into the control software of the cutting plotter. Set the microelectrode pattern to be writing pattern.

8) Align the microchannel pattern and microelectrode pattern correctly and place them at the desired position. It is recommended to run the cutting and writing in one project to avoid alignment between cutting and writing.

9) Set the cutting parameter as recorded in Appendix B.1. Run the cutting pattern and cut the pattern on the PSA film. Remove the unwanted area with tweezers.

10) Run the writing pattern to write the microwire electrode on the PSA film.

11) Protect the PSA film with integrated microwire with the liner removed in step 9).

12) Peel off the PSA film with integrated microwire.

B.3 Device assembly

1) Remove the liners of all the films. Align them correctly and apply pressure on top to bond them together. For device requiring accurate alignment between layers, alignment holes with diameter of a syringe needle should be cut on all the films. The patterned films would be aligned together by the syringe needle inserted through these alignment holes.

The films are taped together and the syringe needle would then be withdrawn from the alignment holes.

2) For better bonding, the aligned films can be sent into a laminator. Alternatively, place a heavy weight on it for 30 min.

LIST OF REFERENCES

1. Terry, S.C., *A gas chromatography system fabricated on a silicon wafer using integrated circuit technology.* 1975.

2. Terry, S.C., J.H. Jerman, and J.B. Angell, *A gas chromatographic air analyzer fabricated on a silicon wafer.* IEEE Transactions on Electron Devices, 1979. **26**(12): p. 1880-1886.

3. Gawron, A.J., R.S. Martin, and S.M. Lunte, *Fabrication and evaluation of a carbon-based dual-electrode detector for poly (dimethylsiloxane) electrophoresis chips.* Electrophoresis, 2001. **22**(2): p. 242-248.

4. García, C.D. and C.S. Henry, *Direct Determination of Carbohydrates, Amino Acids, and Antibiotics by Microchip Electrophoresis with Pulsed Amperometric Detection.* Analytical Chemistry, 2003. **75**(18): p. 4778-4783.

5. Douville, N.J., et al., *Fabrication of two-layered channel system with embedded electrodes to measure resistance across epithelial and endothelial barriers.* Analytical chemistry, 2010. **82**(6): p. 2505-2511.

6. Bartholomeusz, D.A., R.W. Boutté, and J.D. Andrade, *Xurography: rapid prototyping of microstructures using a cutting plotter.* Microelectromechanical Systems, Journal of, 2005. **14**(6): p. 1364-1374.

7. Cosson, S., et al., *Ultra-rapid prototyping of flexible, multi-layered microfluidic devices via razor writing.* Lab on a Chip, 2015. **15**(1): p. 72-76.

8. Kim, J., R. Surapaneni, and B.K. Gale, *Rapid prototyping of microfluidic systems using a PDMS/polymer tape composite.* Lab on a Chip, 2009. **9**(9): p. 1290-1293.

9. Yuen, P.K. and V.N. Goral, *Low-cost rapid prototyping of flexible microfluidic devices using a desktop digital craft cutter.* Lab on a Chip, 2010. **10**(3): p. 384-387.

10. Widmer, H., J. Erard, and G. Grass, *Automated monitor systems for the continuous surveillance of environmental samples.* International journal of environmental analytical chemistry, 1984. **18**(1-2): p. 1-10.

11. Garn, M., et al., *A flow injection analysis system for fermentation monitoring and control.* Biotechnology and bioengineering, 1989. **34**(4): p. 423-428.

12. Lintel, H.v., F. Pol, and S. Bouwstra, *A piezoelectric micropump based on micromachining of silicon.* Sensors and actuators, 1988. **15**(2): p. 153-167.

13. Shoji, S., M. Esashi, and T. Matsuo, *Prototype miniature blood gas analyser fabricated on a silicon wafer.* Sensors and Actuators, 1988. **14**(2): p. 101-107.

14. Manz, A., et al., *Design of an open-tubular column liquid chromatograph using silicon chip technology.* Sensors and Actuators B: Chemical, 1990. **1**(1): p. 249-255.

15. Manz, A., N. Graber, and H.M. Widmer, *Miniaturized total chemical analysis systems: A novel concept for chemical sensing.* Sensors and Actuators B: Chemical, 1990. **1**(1): p. 244-248.

16. Martynova, L., et al., *Fabrication of Plastic Microfluid Channels by Imprinting Methods.* Analytical Chemistry, 1997. **69**(23): p. 4783-4789.

17. Roberts, M.A., et al., *UV laser machined polymer substrates for the development of microdiagnostic systems.* Analytical chemistry, 1997. **69**(11): p. 2035-2042.

18. McCormick, R.M., et al., *Microchannel electrophoretic separations of DNA in injection-molded plastic substrates.* Analytical Chemistry, 1997. **69**(14): p. 2626-2630.

19. Effenhauser, C.S., et al., *Integrated capillary electrophoresis on flexible silicone microdevices: analysis of DNA restriction fragments and detection of single DNA molecules on microchips.* Analytical Chemistry, 1997. **69**(17): p. 3451-3457.

20. Xia, Y. and G.M. Whitesides, *Soft lithography.* Annual review of materials science, 1998. **28**(1): p. 153-184.

21. Duffy, D.C., et al., *Rapid prototyping of microfluidic systems in poly (dimethylsiloxane).* Analytical chemistry, 1998. **70**(23): p. 4974-4984.

22. Stoeber, B., et al., *Flow control in microdevices using thermally responsive triblock copolymers.* Journal of Microelectromechanical Systems, 2005. **14**(2): p. 207-213.

23. Harrison, D.J., et al., *Micromachining a miniaturized capillary electrophoresis-based chemical analysis system on a chip.* SCIENCE-NEW YORK THEN WASHINGTON-, 1993. **261**: p. 895-895.

24. Woolley, A.T., et al., *Capillary electrophoresis chips with integrated electrochemical detection.* Analytical Chemistry, 1998. **70**(4): p. 684-688.

25. Wang, J., et al., *Voltammetry on microfluidic chip platforms.* Analytical chemistry, 2000. **72**(21): p. 5285-5289.

26. Lu, H., M.A. Schmidt, and K.F. Jensen, *A microfluidic electroporation device for cell lysis.* Lab on a Chip, 2005. **5**(1): p. 23-29.

27. Zong, X., R. Zhu, and X. Guo, *Nanostructured gold microelectrodes for SERS and EIS measurements by incorporating ZnO nanorod growth with electroplating.* Scientific reports, 2015. **5**.

28. Wang, L., et al., *Dielectrophoresis switching with vertical sidewall electrodes for microfluidic flow cytometry.* Lab on a Chip, 2007. **7**(9): p. 1114-1120.

29. Hao, Z., H. Chen, and D. Ma, *Preparation of Micro Gold Devices on Poly(dimethylsiloxane) Chips with Region-Selective Electroless Plating.* Analytical Chemistry, 2009. **81**(20): p. 8649-8653.

30. Lee, H.-H., K.-S. Chou, and K.-C. Huang, *Inkjet printing of nanosized silver colloids.* Nanotechnology, 2005. **16**(10): p. 2436.

31. Fuller, S.B., E.J. Wilhelm, and J.M. Jacobson, *Ink-jet printed nanoparticle microelectromechanical systems.* Journal of Microelectromechanical systems, 2002. **11**(1): p. 54-60.

32. Siegel, A.C., et al., *Cofabrication of Electromagnets and Microfluidic Systems in Poly(dimethylsiloxane).* Angewandte Chemie, 2006. **118**(41): p. 7031-7036.

33. Siegel, A.C., et al., *Microsolidics: Fabrication of Three‐Dimensional Metallic Microstructures in Poly (dimethylsiloxane).* Advanced Materials, 2007. **19**(5): p.

727-733.

34. Cong, H. and T. Pan, *Photopatternable conductive PDMS materials for microfabrication.* Advanced Functional Materials, 2008. **18**(13): p. 1912-1921.

35. Brun, M., et al., *Nanocomposite Carbon‐PDMS Material for Chip‐Based Electrochemical Detection.* Electroanalysis, 2011. **23**(2): p. 321-324.

36. Trouillon, R. and M.A.M. Gijs, *Delayed voltammetric with respect to amperometric electrochemical detection of concentration changes in microchannels.* Lab on a Chip, 2014. **14**(16): p. 2929-2940.

37. Bowden, N., et al., *Spontaneous formation of ordered structures in thin films of metals supported on an elastomeric polymer.* Nature, 1998. **393**(6681): p. 146-149.

38. Franssila, S., *Introduction to microfabrication*. 2010: John Wiley & Sons.

39. Jha, S.K., et al., *An integrated PCR microfluidic chip incorporating aseptic electrochemical cell lysis and capillary electrophoresis amperometric DNA detection for rapid and quantitative genetic analysis.* Lab on a Chip, 2012. **12**(21): p. 4455-4464.

40. Hsieh, K., et al., *Rapid, Sensitive, and Quantitative Detection of Pathogenic DNA at the Point of Care through Microfluidic Electrochemical Quantitative Loop‐Mediated Isothermal Amplification.* Angewandte Chemie, 2012. **124**(20): p. 4980-4984.

41. Li, Y., et al., *Micro electrochemical sensor with copper nanoclusters for nitrate determination in freshwaters.* Micro & Nano Letters, 2012. **7**(12): p. 1197-1201.

42. Pereira Rodrigues, N., Y. Sakai, and T. Fujii, *Cell-based microfluidic biochip for the electrochemical real-time monitoring of glucose and oxygen.* Sensors and Actuators B: Chemical, 2008. **132**(2): p. 608-613.

43. Kuo, C.-T. and C.-H. Liu, *A novel microfluidic driver via AC electrokinetics.* Lab on a Chip, 2008. **8**(5): p. 725-733.

44. Du, X., et al., *Microfluidic pumps employing surface acoustic waves generated in ZnO thin films.* Journal of Applied Physics, 2009. **105**(2): p. 024508.

45. Castillo-León, J. and W.E. Svendsen, *Lab-on-a-Chip Devices and Micro-Total Analysis Systems: A Practical Guide*. 2014: Springer.

46. Graff, M., et al., *Microstenciling: a generic technology for microscale patterning of vapor deposited materials.* Journal of microelectromechanical systems, 2004. **13**(6): p. 956-962.

47. Xu, Y., et al., *Low cost fabrication of microelectrodes on plastic substrate.* Microsystem technologies, 2011. **17**(3): p. 361-366.

48. Charles, A.H., *Electroplating and Deposited Metallic Coatings*, in *Electronic Materials and Processes Handbook, Third Edition*. 2004, McGraw Hill Professional, Access Engineering.

49. Dini, J. *An Electroplater's View of PVD Processing*. in *AESF Sur/Fin*. 1992. Citeseer.

50. Do, J. and C.H. Ahn, *A polymer lab-on-a-chip for magnetic immunoassay with on-chip sampling and detection capabilities.* Lab on a Chip, 2008. **8**(4): p. 542-549.

51. Smistrup, K., et al., *On-chip magnetic bead microarray using hydrodynamic focusing in a passive magnetic separator.* Lab on a Chip, 2005. **5**(11): p. 1315-1319.

52. Vulto, P., et al., *A full-wafer fabrication process for glass microfluidic chips with integrated electroplated electrodes by direct bonding of dry film resist.* Journal of Micromechanics and Microengineering, 2009. **19**(7): p. 077001.

53. Tomkiewicz, M., *Environmental aspects of electrodeposition.* Modern Electroplating, Fifth Edition, 2010: p. 555-571.

54. Wang, Y., et al., *In-channel modification of biosensor electrodes integrated on a polycarbonate microfluidic chip for micro flow-injection amperometric determination of glucose.* Sensors and Actuators B: Chemical, 2010. **145**(1): p. 553-560.

55. Wang, Y., et al., *A high‑performance polycarbonate electrophoresis microchip with integrated three‑electrode system for end‑channel amperometric detection.* Electrophoresis, 2008. **29**(9): p. 1881-1888.

56. Kong, Y., et al., *Fabrication of a gold microelectrode for amperometric detection on a polycarbonate electrophoresis chip by photodirected electroless plating.* Electrophoresis, 2006. **27**(14): p. 2940-2950.

57. Watson, M.W., et al., *Microcontact printing-based fabrication of digital microfluidic devices.* Analytical chemistry, 2006. **78**(22): p. 7877-7885.

58. Allen, P.B., et al., *Selective electroless and electrolytic deposition of metal for applications in microfluidics: Fabrication of a microthermocouple.* Analytical chemistry, 2003. **75**(7): p. 1578-1583.

59. Cho, Y.-K., T.-h. Kim, and J.-G. Lee, *On-chip concentration of bacteria using a 3D dielectrophoretic chip and subsequent laser-based DNA extraction in the same chip.* Journal of Micromechanics and Microengineering, 2010. **20**(6): p. 065010.

60. Lee, H., et al., *Mussel-Inspired Surface Chemistry for Multifunctional Coatings.* Science, 2007. **318**(5849): p. 426-430.

61. Buffat, P. and J.P. Borel, *Size effect on the melting temperature of gold particles.* Physical review A, 1976. **13**(6): p. 2287.

62. Kawahara, Y., et al., *Instant inkjet circuits: lab-based inkjet printing to support rapid prototyping of UbiComp devices*, in *Proceedings of the 2013 ACM international joint conference on Pervasive and ubiquitous computing*. 2013, ACM: Zurich, Switzerland. p. 363-372.

63. Perelaer, J., et al., *Printed electronics: the challenges involved in printing devices, interconnects, and contacts based on inorganic materials.* Journal of Materials Chemistry, 2010. **20**(39): p. 8446-8453.

64. Medina-Sanchez, M., et al., *On-chip electrochemical detection of CdS quantum dots using normal and multiple recycling flow through modes.* Lab on a Chip, 2012. **12**(11): p. 2000-2005.

65. Dong, H., et al., *Screen-printed microfluidic device for electrochemical immunoassay.* Lab on a Chip, 2007. **7**(12): p. 1752-1758.

66. Perelaer, J., B.J. de Gans, and U.S. Schubert, *Ink‐jet printing and microwave sintering of conductive silver tracks.* Advanced materials, 2006. **18**(16): p. 2101-

2104.

67. Bieri, N., et al., *Manufacturing of nanoscale thickness gold lines by laser curing of a discretely deposited nanoparticle suspension.* Superlattices and Microstructures, 2004. **35**(3): p. 437-444.

68. Kim, H.-S., et al., *Intense pulsed light sintering of copper nanoink for printed electronics.* Applied Physics A, 2009. **97**(4): p. 791-798.

69. Reinhold, I., et al., *Argon plasma sintering of inkjet printed silver tracks on polymer substrates.* Journal of Materials Chemistry, 2009. **19**(21): p. 3384-3388.

70. Allen, M.L., et al., *Electrical sintering of nanoparticle structures.* Nanotechnology, 2008. **19**(17): p. 175201.

71. Magdassi, S., et al., *Triggering the Sintering of Silver Nanoparticles at Room Temperature.* ACS Nano, 2010. **4**(4): p. 1943-1948.

72. Wyzkiewicz, I., et al., *Self-regulating heater for microfluidic reactors.* Sensors and Actuators B: Chemical, 2006. **114**(2): p. 893-896.

73. Pabst, O., et al., *All inkjet-printed piezoelectric polymer actuators: Characterization and applications for micropumps in lab-on-a-chip systems.* Organic Electronics, 2013. **14**(12): p. 3423-3429.

74. Zhu, H., et al., *Screen-printed microfluidic dielectrophoresis chip for cell separation.* Biosensors and Bioelectronics, 2015. **63**: p. 371-378.

75. Kim, Y., et al., *Direct inkjet printing of micro-scale silver electrodes on polydimethylsiloxane (PDMS) microchip.* Journal of Micromechanics and Microengineering, 2014. **24**(11): p. 115010.

76. Lee, S.H., et al., *Fabrication of a 3 dimensional dielectrophoresis electrode by a metal inkjet printing method.* Micro and Nano Systems Letters, 2013. **1**(1): p. 1-7.

77. Grouchko, M., et al., *Conductive Inks with a "Built-In" Mechanism That Enables Sintering at Room Temperature.* ACS Nano, 2011. **5**(4): p. 3354-3359.

78. Sjostrom, S.L., et al., *High-throughput screening for industrial enzyme production*

hosts by droplet microfluidics. Lab on a Chip, 2014. **14**(4): p. 806-813.

79. Agresti, J.J., et al., *Ultrahigh-throughput screening in drop-based microfluidics for directed evolution.* Proceedings of the National Academy of Sciences, 2010. **107**(9): p. 4004-4009.

80. Mazutis, L., et al., *Single-cell analysis and sorting using droplet-based microfluidics.* Nat. Protocols, 2013. **8**(5): p. 870-891.

81. Li, S., et al., *A novel method to construct 3D electrodes at the sidewall of microfluidic channel.* Microfluidics and Nanofluidics, 2013. **14**(3-4): p. 499-508.

82. Richards, A., et al., *Design and demonstration of a novel micro-Coulter counter utilizing liquid metal electrodes.* Journal of Micromechanics and Microengineering, 2012. **22**(11): p. 115012.

83. Hallfors, N., et al., *Integration of pre-aligned liquid metal electrodes for neural stimulation within a user-friendly microfluidic platform.* Lab on a Chip, 2013. **13**(4): p. 522-526.

84. So, J.-H. and M.D. Dickey, *Inherently aligned microfluidic electrodes composed of liquid metal.* Lab on a Chip, 2011. **11**(5): p. 905-911.

85. Sherman, R., L. Middleman, and S. Jacobs, *Electron transport processes in conductor ‐filled polymers.* Polymer Engineering & Science, 1983. **23**(1): p. 36-46.

86. Pavesi, A., et al., *How to embed three-dimensional flexible electrodes in microfluidic devices for cell culture applications.* Lab on a Chip, 2011. **11**(9): p. 1593-1595.

87. Deman, A.-L., et al., *Characterization of C-PDMS electrodes for electrokinetic applications in microfluidic systems.* Journal of Micromechanics and Microengineering, 2011. **21**(9): p. 095013.

88. Liu, C.-X. and J.-W. Choi, *Patterning conductive PDMS nanocomposite in an elastomer using microcontact printing.* Journal of Micromechanics and Microengineering, 2009. **19**(8): p. 085019.

89. Niu, X., et al., *Characterizing and patterning of PDMS‐based conducting composites.* Advanced Materials, 2007. **19**(18): p. 2682-2686.

90. Ahuja, T. and D. Kumar, *Recent progress in the development of nano-structured conducting polymers/nanocomposites for sensor applications.* Sensors and Actuators B: Chemical, 2009. **136**(1): p. 275-286.

91. Ali, M.A., et al., *Highly efficient bienzyme functionalized nanocomposite-based microfluidics biosensor platform for biomedical application.* Scientific reports, 2013. **3**.

92. Castaño‐Álvarez, M., M.T. Fernández‐Abedul, and A. Costa‐García, *Poly(methylmethacrylate) and Topas capillary electrophoresis microchip performance with electrochemical detection.* ELECTROPHORESIS, 2005. **26**(16): p. 3160-3168.

93. Safari, S., P.R. Selvaganapathy, and M.J. Deen, *Microfluidic Reference Electrode with Free-Diffusion Liquid Junction.* Journal of The Electrochemical Society, 2013. **160**(10): p. B177-B183.

94. Martin, R.S., et al., *In-channel electrochemical detection for microchip capillary electrophoresis using an electrically isolated potentiostat.* Analytical chemistry, 2002. **74**(5): p. 1136-1143.

95. Garcí, C.D. and C.S. Henry, *Enhanced determination of glucose by microchip electrophoresis with pulsed amperometric detection.* Analytica chimica acta, 2004. **508**(1): p. 1-9.

96. Lee, W.G., et al., *An impulsive, electropulsation-driven backflow in microchannels during electroporation.* Lab on a Chip, 2008. **8**(2): p. 224-226.

97. ASTM Standard F72, 2006, "Standard Specification for Gold Wire for Semiconductor Lead Bonding," ASTM International, West Conshohocken, PA, 2006, 10.1520/F0072-06, www.astm.org

98. Novak, R., N. Ranu, and R.A. Mathies, *Rapid fabrication of nickel molds for prototyping embossed plastic microfluidic devices.* Lab on a chip, 2013. **13**(8): p. 1468-1471.

99. Hwang, H., et al., *Three dimensional multicellular co-cultures and anti-cancer drug assays in rapid prototyped multilevel microfluidic devices.* Biomedical microdevices, 2013. **15**(4): p. 627-634.

100. de Santana, P.P., et al., *Fabrication of glass microchannels by xurography for electrophoresis applications.* Analyst, 2013. **138**(6): p. 1660-1664.

101. Taylor, D., et al., *Shrink film patterning by craft cutter: complete plastic chips with high resolution/high-aspect ratio channel.* Lab on a Chip, 2010. **10**(18): p. 2472-2475.

102. Atencia, J., G.A. Cooksey, and L.E. Locascio, *A robust diffusion-based gradient generator for dynamic cell assays.* Lab on a Chip, 2012. **12**(2): p. 309-316.

103. Lafleur, J.P., et al., *Miniaturised centrifugal solid phase extraction platforms for in-field sampling, pre-concentration and spectrometric detection of organic pollutants in aqueous samples.* Talanta, 2010. **81**(1): p. 722-726.

104. Sundberg, S.O., et al., *Spinning disk platform for microfluidic digital polymerase chain reaction.* Analytical chemistry, 2010. **82**(4): p. 1546-1550.

105. Do, J., J.Y. Zhang, and C.M. Klapperich, *Maskless writing of microfluidics: Rapid prototyping of 3D microfluidics using scratch on a polymer substrate.* Robotics and Computer-Integrated Manufacturing, 2011. **27**(2): p. 245-248.

106. Kanakamedala, S.K., et al., *A simple polymer based electrochemical transistor for micromolar glucose sensing.* Sensors and Actuators B: Chemical, 2011. **157**(1): p. 92-97.

107. González-Guerrero, M.J., et al., *Membraneless glucose/O 2 microfluidic enzymatic biofuel cell using pyrolyzed photoresist film electrodes.* Lab on a Chip, 2013. **13**(15): p. 2972-2979.

108. Senousy, Y. and C. Harnett, *Fast three dimensional ac electro-osmotic pumps with nonphotolithographic electrode patterning.* Biomicrofluidics, 2010. **4**(3): p. 036501.

109. Numthuam, S., et al., *Synergistic effects of micro/nano modifications on electrodes for microfluidic electrochemical ELISA.* Sensors and Actuators B: Chemical, 2011. **156**(2): p. 637-644.

110. Lu, K.-Y., et al., *Three dimensional electrode array for cell lysis via electroporation.* Biosensors and Bioelectronics, 2006. **22**(4): p. 568-574.

111. Satyanarayana, S., R.N. Karnik, and A. Majumdar, *Stamp-and-stick room-temperature bonding technique for microdevices.* Microelectromechanical Systems, Journal of, 2005. **14**(2): p. 392-399.

112. Yang, J., et al., *High sensitivity PCR assay in plastic micro reactors.* Lab on a Chip, 2002. **2**(4): p. 179-187.

113. Casquillas, G.V., et al., *Fast microfluidic temperature control for high resolution live cell imaging.* Lab on a chip, 2011. **11**(3): p. 484-489.

114. Mao, H., T. Yang, and P.S. Cremer, *A microfluidic device with a linear temperature gradient for parallel and combinatorial measurements.* Journal of the American Chemical Society, 2002. **124**(16): p. 4432-4435.

115. Guijt, R.M., et al., *Chemical and physical processes for integrated temperature control in microfluidic devices.* Lab on a Chip, 2003. **3**(1): p. 1-4.

116. Safari, S., et al., *Electrochemical growth of high-aspect ratio nanostructured silver chloride on silver and its application to miniaturized reference electrodes.* Nanotechnology, 2011. **22**(31): p. 315601.

117. Malcik, N., et al., *The performance of a microchip-based fiber optic detection technique for the determination of Ca 2+ ions in urine.* Sensors and Actuators B: Chemical, 2005. **107**(1): p. 24-31.

118. Ishimatsu, R., et al., *An organic thin film photodiode as a portable photodetector for the detection of alkylphenol polyethoxylates by a flow fluorescence-immunoassay on magnetic microbeads in a microchannel.* Talanta, 2013. **117**: p. 139-145.

119. Miyaki, K., et al., *Fabrication of an integrated PDMS microchip incorporating an LED-induced fluorescence device.* Analytical and bioanalytical chemistry, 2005. **382**(3): p. 810-816.

120. Blotta, I., et al., *Quantitative assay of total dsDNA with PicoGreen reagent and real-time fluorescent detection.* ANNALI-ISTITUTO SUPERIORE DI SANITA, 2005.

41(1): p. 119.

121. Kong, T.F., et al., *Adhesive-based liquid metal radio-frequency microcoil for magnetic resonance relaxometry measurement.* Lab on a Chip, 2012. **12**(2): p. 287-294.